AD_____

Award Number: DAMD17-97-1-7340

TITLE: Molecular Mechanisms of Glial Abnormalitites in Neurofibromatosis

PRINCIPAL INVESTIGATOR: Michael G. Rosenfeld, Ph.D.

CONTRACTING ORGANIZATION: University of California, San Diego
La Jolla, California 92093-0934

REPORT DATE: October 2000

TYPE OF REPORT: Final

PREPARED FOR: U.S. Army Medical Research and Materiel Command
Fort Detrick, Maryland 21702-5012

DISTRIBUTION STATEMENT: Approved for Public Release;
Distribution Unlimited

1. AGENCY USE ONLY (Leave blank)	2. REPORT DATE	3. REPORT TYPE AND DATES COVERED
	October 2000	Final (19 Sep 97 - 17 Sep 00)

4. TITLE AND SUBTITLE
Molecular Mechanisms of Glial Abnormalitites in Neurofibromatosis

5. FUNDING NUMBERS
DAMD17-97-1-7340

6. AUTHOR(S)
Michael G. Rosenfeld, Ph.D.

7. PERFORMING ORGANIZATION NAME(S) AND ADDRESS(ES)
University of California, San Diego
La Jolla, California 92093-0934

E-MAIL:
mrosenfeld@ucsd.edu

8. PERFORMING ORGANIZATION REPORT NUMBER

9. SPONSORING / MONITORING AGENCY NAME(S) AND ADDRESS(ES)
U.S. Army Medical Research and Materiel Command
Fort Detrick, Maryland 21702-5012

10. SPONSORING / MONITORING AGENCY REPORT NUMBER

11. SUPPLEMENTARY NOTES
This report contains colored photos

12a. DISTRIBUTION / AVAILABILITY STATEMENT
Approved for public release; distribution unlimited

12b. DISTRIBUTION CODE

13. ABSTRACT ***(Maximum 200 Words)***

Schwann cells proliferation appears to be controlled by cAMP, implicating CREB, and the CREB-binding protein. CBP specifically modulate cAMP and *ras*-dependent growth events in glia. This is likely to underlie the misregulation in Schwann cell proliferation associated with neurofibromatosis type 1, in which two copies of the NF1 gene are functionally in active. The characterization of CBP as an integrator of cAMP and *ras*-related growth factor responses, together with the observation that limiting CBP can result in AP-1 inhibiting events, has led us to explore the role of CBP, transcriptional coactivators, and associated transcription factors in these events. Representational difference analysis has been modified to determine the gene traits responsible for ordered and abnormal transcriptional responses in genetic models designed to alter cAMP- and *ras*-dependent signaling pathways, permitting identification and characterization of factors which contribute to the etiology of neurofibromatosis type 1. We have succeeded in perfecting a method that identified bona fide targets, as experimentally demonstrated. We have investigated the cooperative nature of regulatory interfaces between transcriptional coactivators and transcription factors, and find that specific interactions of transcriptional coactivators with CBP act to dictate the choice between transcriptional activation and quiescence under conditions of elevated second messenger signaling mechanisms.

14. SUBJECT TERMS
Neurofibromatosis

15. NUMBER OF PAGES
100

16. PRICE CODE

17. SECURITY CLASSIFICATION OF REPORT	18. SECURITY CLASSIFICATION OF THIS PAGE	19. SECURITY CLASSIFICATION OF ABSTRACT	20. LIMITATION OF ABSTRACT
Unclassified	Unclassified	Unclassified	Unlimited

MOLECULAR MECHANISMS OF GLIAL ABNORMALITIES IN NEUROFIBROMATOSIS

FINAL REPORT

PART 3

Table of Contents

LIST OF TABLES

PART 4

INTRODUCTION

Neurofibromin, the product of the neurofibromatosis type I gene, appears to inhibit *ras* function, a cytoplasmic proto-oncogene gene product abnormally up-regulated in many models of unrestricted cellular growth. This protein is normally associated with the control of cellular growth and proliferation, but abnormal expression of this protein often results in the misregulation of additional signaling pathways. Abnormal proliferation in neurofibromatosis type I is limited to a few cell types, including Schwann cells. Because Schwann cells have unusual regulation of growth, including stimulation of proliferation by the intracellular signaling molecule cAMP, the opportunity to devise a cell-specific strategy to investigate alternative modes of regulation of cAMP-directed signaling is possible through the comparison of regulatory factors that stimulate or repress cellular proliferation in response to cAMP. cAMP related effects are manifested primarily through the activation of gene expression, specifically via the transcription factor referred to as cAMP response element binding protein (CREB). Based on the nature of the unusual elements of growth control in Schwann cells, we have hypothesized that specific factors associated with CREB, and the CREB-binding protein, CBP, serve to specifically modulate cAMP and *ras* - dependent growth events in glia, and underlie the NF1 mutation induced Schwann cell component proliferation. The role of CBP as a fundamental component of the transcriptional complex mediating responses of cAMP, growth factors, and nuclear receptors together with experimental evidence demonstrating that the transcriptional effects of different signalling pathways are integrated at the level of the nucleus, inhibiting effects on AP-1 activation, this has led us to the dissection of the molecular events by which diverse signaling pathways coverage to translate into specific differentiation and proliferative consequences for cellular phenotype.

PART 5

BODY

Our efforts in this Grant involve the investigation of molecular mechanisms underlying the development of glial abnormalities as manifested by improper developmental regulation of transcriptional events mediating the growth and proliferation of Schwann cells. Underlying our investigation is the hypothesis, described in detail together with supporting data in the main body of the Grant, that rate-limiting distributions and/or actions of the nuclear integrator CBP made available for transcriptional output are dictated by the combinatorial overlay of competing and synergistic externally-derived signaling modes, which in turn determine the selective recruitment of specific cohorts of coregulatory and are factors subsequently required and responsible for ultimately regulating cellular phenotype through the determination of specific programs of transcriptional activation.

As outlined in Specific Aims II and III, the characterization of signaling pathways and the nature of the relative availability and abundance of CBP coregulators recruited through converging signals in normal development for cell types that proliferate in response to elevated levels of cAMP compared to cell types that do not proliferate in response to elevated intracellular cAMP form the basis of an objective framework by which to judge the expression and recruitment of coregulators under circumstances during which the standard cellular program of signal integration is altered, such as is the case when excessive activation of one or more cellular response pathways is effectively upregulated. During this review period, we have evaluated molecular determinants required for recruitment of coregulators and their interactions relative to CBP under diverse applications of external stimuli. In the context of Specific Aims II and III, Tasks 10-15, the molecular determinants regulating CBP and CBP-associated coregulatory molecules have been investigated, permitting assessment of the extent to which these interactions determine the relative divergence of transcriptional throughput. The interface of transcription factors with CBP including ligand-dependent activation of nuclear receptor-mediated gene transcription relies upon recruitment of coactivators including members of the N-CoA family. Members of this group, p/CIP, NCoA-1, and NCoA-2, contain critical LXXLL core motifs. The LXXLL is a small helix that is oriented and positioned by conserved glutamic acid and lysine residues in helix 2 (AF2) and helix 3, respectively, permitting packing into the hydrophobic pocket found by receptor helices 4, 5, 6. Differential usage of molecular interfaces between members of the nuclear receptor superfamily and the coactivator N-CoA-1 are dictated by discrete combinatorial differences in ligand and receptor availability and usage that determine specific interactions between combinations of spatially distinct LXXLL consensus sequences with helices 1 and 3 of the nuclear receptor family members (ref.1 and appendix 1, part A) and result in distinct transcriptional output. These findings have identified the nature of molecular determinants between transcription factors and transcriptional coregulators required to determine potential transcriptional outputs relative to the availability of interacting transcription factors, including members of the nuclear receptor superfamily. Subsequently, we discovered that a similar, but larger helix LXXXIXXXI/L is present in corepressors, such as N-CoR, permitting binding into the same hydrophobic pocket in the unliganded receptor.

The effects of extrinsic signaling pathways have been further investigated in an effort to determine the molecular determinants of nature the interactions of transcriptional

coregulators with CBP that regulate both the availability and certain intrinsic properties of CBP which contribute to the degree of the efficacy of transcriptional regulation. The interactions of CREB and N-CoA family members with CBP have been evaluated with regards to their relative abilities to influence histone acetyl transferase (HAT) activity of CBP, an intrinsic enzymatic activity discovered present in GCN5, CBP/P300, and p/CAF coactivators which catalyze acetylation of histones H3 and H4 as well as additional protein targets, resulting in the remodeling of chromatinized DNA templates critical for transcriptional activation (2-9). The investigation of CBP HAT activity following CREB binding to the CBP KIX domain, a consequence of CREB phosphorylation of Serine 133 (10,11), reveals that bacterially purified CREB phosphorylated by protein kinase A does not inhibit CBP acetyltransferase activity as assayed by the target molecules histones H3/H4 (panel A, appendix 2). Additional studies examine the consequences of N-CoA family member interactions with CBP via LXXLL mediated contacts on the intrinsic CBP acetyl transferase activity. This interaction between p/CIP and CBP involves C-terminal domain of CBP 3' to the C/H3 domain at approximately amino acids 2058-2163 and amino acids 947-1084 of p/CIP (1,12). In contrast to results observed with CREB, the interaction of the p/CIP CBP-binding domain with CBP significantly reduces intrinsic HAT activity of CBP on histones H3 and H4 (panel b, appendix 2). Comparison of this domain of p/CIP with a larger domain encompassing the CBP interaction domain, together with adjacent domains including the C terminus, reported to confer weak HAT activity (ref 13, 14), and the nuclear receptor interaction domain demonstrated that this portion of p/CIP failed to inhibit CBP HAT activity (panel C, appendix 2), nor did this protein inhibit intrinsic HAT activity of p/CAF on histones H3/H4 (panel D, appendix 2). Given the inhibitory actions of the p/CIP-CBP binding domain, and the ability of extended p/CIP domains to overcome this inhibition, the observed actions of p/CIP may reflect the opportunity for potential additional cellular cofactors to interact with p/CIP, subsequently resulting in modulation of intrinsic CBP HAT activity under varying types of extrinsic signaling. Over the past year, we have identified such an activity in using cell-types and this binding to CBP is modulating its activity. Utilizing single-cell microinjection assays, we have confirmed *in vivo* that the p/CIP CBP domain interaction with CBP in the presence of forskolin inhibits transcriptional activation from basal reporters regulated by multimerized response elements specific for CREB-dependent transcriptional regulation, but that the extended p/CIP domain abolishes these inhibitory effects (panel E, appendix 2). Under these conditions the cellular response to cAMP is influenced through the modulation of the LXXLL-mediated p/CIP-CBP complex involving interaction motifs within p/CIP accessible to additional transcriptional cofactors. This interaction access domain of CBP identifies regulatory restriction potential for the alternative cellular responses to intracellular changes of cAMP concentration that has been observed in different cell types and suggests a mechanism by which differing and competing transcriptional coregulators may alter the cellular response to cAMP induced CREB activation. We suggest that factors such as NF-1 initiate signal-dependent alterations in these associations.

The identification of cofactors involved in modulation of responses to liganded nuclear receptor, cAMP/CREB, and AP-1 under normal and abnormal physiological conditions, described in Specific Aim II, Tasks 12 and 13, represents a critical element in the definition of molecular events responsible for the ultimate coordination of these signals. As a means to ascertain the essential coregulatory molecules in normal and abnormal cells for which rate-limiting amounts of *in vivo* material exist, such as Schwann cells, we have developed and utilized a method which permits amplification of

differentially expressed messenger RNA (mRNA) from two separate populations of tissues. One consequence of this analysis results in the availability of separate amplified populations of cDNA representative of the original populations of mRNA. Southern blot analyses of these populations (Snorthern analysis) using probes derived from existing coregulatory molecules permits relative assessment of the abundance of these factors in the normal cells compared to those for which signaling pathways have been genetically altered. A further outcome of representational display analysis is the description of groups of genes upregulated in one cellular population relative to the other, thereby offering a direct means of identifying the novel and existing cofactors that, due to over- and under representation relative to normal growth situations, direct the altered transcriptional responses characteristic of cells for which phenotypic development has been altered by the misregulation of second messenger signaling pathways including intracellular levels of cAMP. In this second year of the grant we have progressed from a development of this method based upon abundant starting material to an application directed to a complete analysis of gene expression in a genetic model of mis-regulated Schwann cell development, demonstrating the applicability of this method to genetic models representative of altered second messenger pathway related signaling for which very limited quantities of starting materials exist. This effort is documented in a submitted manuscript; see Appendix 1, Part B. In the past year, this method has been applied to *in vivo* models, the Tst-1 gene-deleted and Brn3.2 gene-deleted mice successfully isolating target genes that, at least in specific cases, can be linked to observed phenotypes. This effort is, in part, documented in Appendix B, Part B and C.

PART 6

KEY RESEARCH ACCOMPLISHMENTS

1. Identification and evaluation of interaction domains required and sufficient for CBP-associated proteins to interact with CBP under various modes of second messenger signaling pathways.

2. Assessment of the role of specific nuclear receptor ligands and the transcriptional coregulators required for alternative transcriptional output from specific nuclear receptors. Documentation that CBP recruits p160 factors including N-CoA, N-CoA2, N-CoA3, and p/CIP, and that they can function as inhibitory modulations of CBP HAT activity.

3. Identification of proteins required for distinct signaling outputs mediated by CBP under varied signaling modes.

4. Assessment of the ability of transcriptional coregulators to confer cAMP-dependent responses.

5. Identification of antibodies capable of the disruption of transcriptional coregulator-directed transcriptional output.

6. Assessment of the role of nuclear receptors in the interaction with transcriptional coregulators of CBP required for the mediation of transcriptional activation, and the role of other cofactors. Development of screens to identify novel partners of CBP that may be required for growth responses to diverse second messenger signaling pathways resulting from extrinsic signals from cellular sources of very limited availability and a method to identify negative regulators of CBP histone acetyltransferase activity.

8. Development of screen to evaluate the availability of transcriptional coregulators to confer cAMP-dependent responses in tissues of *in vivo* genetically altered systems under circumstances of limiting availability of cellular materials.

9. Development of a new method to isolate target genes from mice with defective myelination or specific defects in axonal pathfinding, identifying biologically important targets.

PART 7

REPORTABLE OUTCOMES

1. Published journal article:

Determinants of coactivator LXXLL motif specificity in nuclear receptor transcriptional activation. McInerney E.M., Rose D.W., Flynn S.E., Westin S., Mullen T.M., Krones A., Inostroza J., Torchia J., Nolte R.T., Assa-Munt N., Milburn M.V., Glass C.K., Rosenfeld M.G. ***Genes & Development.*** 12:3357-68 (1998).

2. Manuscript in press:

Bermingham J.R., Shumas S., Whisenhut T.R., O'Connell S.M., Rosenfeld M.G. and Scherer S.S. A modification of representational difference analysis applied to the isolation of forskolin-regulated genes from Schwann cells. ***J. Neurosci Res.*** (in press).

3. Manuscript in press:

Erkman, L., P.A. Yates, T. McLaughlin, R.J. McEvilly, T. Whisenhunt, S.M. O'Connell, A.L. Krones, M.A. Kirby, D.H. Rapaport, J.R. Bermingham, D.D.M. O'Leary, and M.G. Rosenfeld. Cell autonomous regulation of axon pathfinding in the vertebrate visual system by a Brn-3-2-dependent transcriptional program. ***Neuron*** (in press).

PART 8

CONCLUSIONS

Our efforts towards an understanding of the molecular mechanisms underlying the uncontrolled Schwann cell proliferation that characterizes the etiology of the human disease neurofibromatosis type require the ability to evaluate mechanisms underlying alterations in gene expression following the inactivation of important regulators of extrinsically derived signaling pathways including the protein encoded by the *NF1* gene, neurofibromin. While the inheritance of Neurofibromatosis is as an autosomal dominant trait the mechanism appears to be recessive occurring the second allele undergoes somatic mutation. We have hypothesized that competition by transcriptional coregulatory factors for limiting amounts of the nuclear integrator CBP results in differential regulation of the transcription of determined patterns of gene expression through contact with the core transcriptional machinery and that abnormal proliferation of Schwann cells is due to improper integration of intracellular signal transduction pathways including cAMP- and ras-related signals. The ability to evaluate differences in the usage and availability of coregulatory factors dictating these patterns of gene expression is a necessary prelude to the specification of the factors responsible for directing alternative responses specific signaling pathways such as those which increase intracellular cAMP concentration.

We have developed a modification of representational difference analysis methodology for the purpose of the analysis of gene expression in tissues and have now applied this approach to identify alternatively regulated genes expressed in Schwann cells resulting from genetic modifications which preclude normal developmental outcomes. In this approach we have utilized this amplification technique to ascertain the validity of the assessment of the representation of gene expression in tissues of extremely limiting availability. The results we present demonstrate that this method permits the assessment of relative differences in availability of specific molecules under varying genetic backgrounds, thereby allowing an evaluation of specific transcriptional coregulatory factors in differing genetically directed responses to elevated levels of cAMP by means of 'Snorthern' analysis. A further consequence of these procedures is the determination of alternately regulated novel cofactors, the identities of which are established as a consequence of the interpretation of expressed sequences from subtractive hybridization in both directions. We demonstrate the utility of this method by applying it to a selection of genes regulated *in vivo* by deletion of specific POU domain genes encoding Tst-1 and Brn 3.2.

The outcome of these systematic analysis of CBP interaction mechanisms with transcriptional coregulator components now presents a platform by which to assess the relative requirements of existing and novel coregulators expressed in genetic models of altered emphases of second messenger signaling pathways responsible for the observed diametrically opposite cellular transcriptional responses to elevated cAMP observed in systems in which NF-1 or CREB have been mutated. Although we have achieved considerable progress in the identification of the relevant interaction motifs between transcription factors, transcriptional coregulators, and CBP responsible for the integration of extrinsic signals that determine cellular phenotype, and have characterized interaction domains and factors that act to choose between opposing cellular responses to specific second messenger signaling pathways, such as those responsible for the transition from quiescent to uncontrolled proliferation of Schwann cells. The generation of genetic models has progressed less rapidly than ideal, but we are now in a position to

finally complete development of these mice strains in the third review period. We expect that analysis of Schwann cells from these animals according to the procedures outlined defining and characterizing the transcriptional coactivators associated with CBP in these cells. These studies are providing insights into the molecular mechanisms underlying emphasized cellular proliferation of Schwann cells.

PART 9

REFERENCES

1. McInerney E.M., Rose D.W., Flynn S.E., Westin S., Mullen T.M., Krones A., Inostroza J., Torchia J., Nolte R.T., Assa-Munt N., Milburn M.V., Glass C.K., Rosenfeld M.G. Determinants of coactivator LXXLL motif specificity in nuclear receptor transcriptional activation. *Genes Dev* 12:3357-68 (1998).

2. Brownell J.E., Zhou J., Ranalli T., Kobayashi R., Edmondson D.G., Roth S.Y., Allis C.D. Tetrahymena histone acetyltransferase A: a homolog to yeast Gcn5p linking histone acetylation to gene activation. Cell 84:843-51 (1996).

3. Bannister A.J., Kouzarides T. The CBP co-activator is a histone acetyltransferase. *Nature* 384:641-3 (1996)

4. Ogryzko V.V., Schiltz R.L., Russanova V., Howard B.H., Nakatani Y. The transcriptional coactivators p300 and CBP are histone acetyltransferases. *Cell* 87(5):953-9 (1996).

5. Yang X.J., Ogryzko V.V., Nishikawa J., Howard B.H., Nakatani Y. A p300/CBP-associated factor that competes with the adenoviral oncoprotein E1A. *Nature* 382:319-24 (1996).

6. Waltzer L., Bienz M. Drosophila CBP represses the transcription factor TCF to antagonize Wingless signalling. *Nature* 395:521-5 (1998).

7 Munshi, N., Merika, M., Yie, J., Senger, K., Chen, G. & Thanos, D. Acetylation of HMG I(Y) by CBP turns off IFN beta expression by disrupting the enhanceosome. *Mol. Cell* 2, 457-467 (1998).

8. Whyte P, Williamson N.M., Harlow E. Cellular targets for transformation by the adenovirus E1A proteins. *Cell* 56:67-75 (1989).

9. Nevins J.R. E2F: a link between the Rb tumorsuppressor protein and viral oncoproteins. *Science* 258, 424-429 (1992).

10 Kwok RP, Lundblad J.R., Chrivia J.C., Richards J.P., Bachinger H.P., Brennan R.G., Roberts S.G., Green M.R., Goodman R.H. Nuclear protein CBP is a coactivator for the transcription factor CREB. *Nature* 370:223-6 (1994).

11. Arias J., Alberts A.S., Brindle P., Claret F.X., Smeal T., Karin M., Feramisco J., Montminy M. Activation of cAMP and mitogen responsive genes relies on a common nuclear factor. *Nature* 370:226-9 (1994).

12. Torchia J., Rose D.W., Inostroza J., Kamei Y., Westin S., Glass C.K., Rosenfeld M.G. The transcriptional co-activator p/CIP binds CBP and mediates nuclear-receptor function. *Nature* 387:677-84 (1997).

13. Chen H., Lin RJ, Schiltz RL, Chakravarti D, Nash A, Nagy L, Privalsky ML, Nakatani Y, Evans R.M. Nuclear receptor coactivator ACTR is a novel histone acetyltransferase and forms a multimeric activation complex with P/CAF and CBP/p300. *Cell* 90:569-80 (1997).

14. Spencer T.E., Jenster G., Burcin M.M., Allis C.D., Zhou J., Mizzen C.A., McKenna N.J., Onate S.A., Tsai SY, Tsai M.J., O'Malley B.W. Steroid receptor coactivator-1 is a histone acetyltransferase. *Nature* 389:194-8 (1997).

PART 10

APPENDICES

1. Published articles and manuscripts in press:

Part A. Pages 16-27

McInerney E.M., Rose D.W., Flynn S.E., Westin S., Mullen T.M., Krones A., Inostroza J., Torchia J., Nolte R.T., Assa-Munt N.,Milburn M.V., Glass C.K., Rosenfeld M.G. Determinants of coactivator LXXLL motif specificity in nuclear receptor transcriptional activation. . *Genes Dev* 12:3357-68 (1998).

Part B. Pages 28-96

Bermingham J.R., Shumas S., Whisenhut T.R., O'Connell S.M., Rosenfeld M.G. and Scherer S.S. A modification of representational difference analysis applied to the isolation of forskolin-regulated genes from Schwann cells. *J. Neurosci Res.* (in press).

Part C. Pages 28-96

Erkman, L., P.A. Yates, T. McLaughlin, R.J. McEvilly, T. Whisenhunt, S.M. O'Connell, A.L. Krones, M.A. Kirby, D.H. Rapaport, J.R. Bermingham, D.D.M. O'Leary, and M.G. Rosenfeld. Cell autonomous regulation of axon pathfinding in the vertebrate visual system by a Brn-3-2-dependent transcriptional program. *Neuron* (in press).

APPENDICES: PART A

Determinants of coactivator LXXLL motif specificity in nuclear receptor transcriptional activation

Eileen M. McInerney,[1,6] David W. Rose,[3,6] Sarah E. Flynn,[1] Stefan Westin,[2] Tina-Marie Mullen,[1,3] Anna Krones,[1] Juan Inostroza,[1] Joseph Torchia,[1,7] Robert T. Nolte,[5] Nuria Assa-Munt,[4] Michael V. Milburn,[5] Christopher K. Glass,[1,2,3] and Michael G. Rosenfeld[1,8]

[1]Howard Hughes Medical Institute, [2]Division of Cellular and Molecular Medicine, and [3]Whittier Diabetes Program, Department and School of Medicine, University of California at San Diego, La Jolla, California 92093-0648 USA; [4]The Burnham Institute, La Jolla, California 92037 USA; [5]GlaxcoWellcome Inc., Division of Chemistry, Department of Structural Chemistry, and Department of Medicinal Chemistry, Research Triangle Park, North Carolina 27709 USA

Ligand-dependent activation of gene transcription by nuclear receptors is dependent on the recruitment of coactivators, including a family of related NCoA/SRC factors, via a region containing three helical domains sharing an LXXLL core consensus sequence, referred to as LXDs. In this manuscript, we report receptor-specific differential utilization of LXXLL-containing motifs of the NCoA-1/SRC-1 coactivator. Whereas a single LXD is sufficient for activation by the estrogen receptor, different combinations of two, appropriately spaced, LXDs are required for actions of the thyroid hormone, retinoic acid, peroxisome proliferator-activated, or progesterone receptors. The specificity of LXD usage in the cell appears to be dictated, at least in part, by specific amino acids carboxy-terminal to the core LXXLL motif that may make differential contacts with helices 1 and 3 (or 3′) in receptor ligand-binding domains. Intriguingly, distinct carboxy-terminal amino acids are required for PPARγ activation in response to different ligands. Related LXXLL-containing motifs in NCoA-1/SRC-1 are also required for a functional interaction with CBP, potentially interacting with a hydrophobic binding pocket. Together, these data suggest that the LXXLL-containing motifs have evolved to serve overlapping roles that are likely to permit both receptor-specific and ligand-specific assembly of a coactivator complex, and that these recognition motifs underlie the recruitment of coactivator complexes required for nuclear receptor function.

[*Key Words*: Nuclear receptors; NCoA/SRC factors; LXXLL motifs; CBP/p300]

Received August 3, 1998; revised version accepted September 17, 1998.

Nuclear receptors are ligand-activated transcription factors that are critical for development and homeostasis, regulating gene expression, in most cases, via interaction with *cis*-acting DNA elements (Mangelsdorf et al. 1995; Katzenellenbogen 1996; Torchia et al. 1998). Members of the nuclear receptor family share a conserved structural and functional organization with the carboxyl terminus mediating ligand-binding. Upon ligand binding, these transcription factors undergo distinct conformational changes, depending on the type of ligand (Fritsch et al. 1992; Beekman et al. 1993). Crystal structures of the carboxy-terminal ligand-binding domain of several receptors (Bourguet et al. 1995; Renaud et al. 1995; Wagner et al. 1995; Brzozowski et al. 1997; Nolte et al. 1998) reveal that the ligand is almost entirely buried within the conserved core of α helices 3, 7, and 10. A conserved carboxy-terminal helix, referred to as the AF2 domain, required for ligand-dependent gene activation (Danielian et al. 1992; Barettino et al. 1994; Durand et al. 1994; Tone et al. 1994), becomes folded against the ligand-binding domain of agonist-bound retinoic acid receptor (RAR), thyroid hormone receptor (TR), estrogen receptor (ER), and PPARγ receptor structures. This change in conformation is thought to allow a productive interaction with transcriptional coactivators and thus results in an activated transcription factor (Fritsch et al. 1992; Beekman et al. 1993). For many nuclear receptors there is a ligand-dependent exchange of a corepressor complex, containing histone deacetylase activity, for a coactivator complex possessing histone acetylase activity (Horlein et al. 1995; Ogryzko et al. 1996; Alland et al. 1997; Heinzel et al. 1997; Nagy et al. 1997; Spencer et al. 1997; Wong et al. 1997).

The precise repertoire of coactivators and coactivator complexes required for physiological nuclear receptor function remains unresolved. Nuclear receptors can in-

[6]These authors contributed equally to this work.
[7]Present address: London Regional Cancer Centre, London, Ontario N6A 4L6, Canada.
[8]Corresponding author.
E-MAIL mrosenfeld@ucsd.edu; FAX (619) 534-8180.

teract with, and variably require, CBP/p300 for their transcriptional activity, both in vitro and in vivo (Chakravarti et al. 1996; Hanstein et al. 1996; Kamei et al. 1996; Yao et al. 1996, 1998; Kraus and Kadonaga 1998). On the basis of direct biochemical interactions (Halamachi et al. 1994; Cavailles et al. 1994; Kurokawa et al. 1995), a series of p160 factors requiring both ligand and the AF2 domain for association were identified and, at least in some cell types, are required for receptor activation (Halamachi et al. 1994; Oñate et al. 1995; Torchia et al. 1997). These p160 factors include NCoA-1SRC-1 (Oñate et al. 1995; Kamei et al. 1996), the highly related factor TIF2/GRIP-1/NCoA-2 (Hong et al. 1996; Voegel et al. 1996; Torchia et al. 1997), and a third family member p/CIP/AIB1/ACTR (Anzick et al. 1997; Chen et al. 1997; Li et al. 1997; Torchia et al. 1997). These factors, which together constitute the biochemically identified p160 factors (Kamei et al. 1996), are components of a larger complex, apparently assembled upon binding of ligand that is responsible, at least in part, for critical aspects of receptor function (Korzus et al. 1998). There are a large number of additional factors that exert ligand-dependent receptor interactions and serve as potential coactivators (e.g., Lee et al. 1995); a role for CBP/p300 has been clearly established. Further, on the basis of coimmunoprecipitation and chromatography approaches with the thyroid hormone or vitamin D receptors, a large multicomponent complex was identified, the members of which appear distinct from the CBP/p160/p/CAF proteins (Fondell et al. 1996; Ogryzko et al. 1998; Rachez et al. 1998).

Intriguingly, the p160 factors such as NCoA-1/SRC-1, and many of the other factors capable of interacting with liganded nuclear receptors, share a common motif containing a core consensus sequence LXXLL (L, leucine; X, any amino acid; LeDouarin et al. 1996; Heery et al. 1997; Torchia et al. 1997). These motifs are sufficient for ligand-dependent interaction with nuclear receptors, and were predicted to assume helical conformation (Heery et al. 1997; Torchia et al. 1997). NCoA-1/SRC-1, TIF-2/GRIP-1/NCoA-2, and p/CIP/AIB1/ACTR all contain three LXXLL motifs in a conserved central sequence, which has been defined to serve as the nuclear receptor interaction domain. In addition, NCoA-1/SRC-1 has two LXXLL motifs within a more carboxy-terminal domain capable of interacting with CBP/p300, and a single splicing variant has an additional carboxy-terminal LXXLL-containing motif (Oñate et al. 1996; Torchia et al. 1997).

The co-crystal structure of a region of the NCoA-1/SRC-1 nuclear receptor interaction domain (amino acids 623–760) containing two LXXLL motifs with liganded PPARγ revealed a ternary complex in which one LXXLL binds to one PPARγ ligand-binding domain (LBD), while the second LXXLL binds to the other PPARγ LBD of the dimer, with the connecting, unstructured NCoA-1/SRC-1 sequence spanning the receptor homodimer (Nolte et al. 1998). The crystallographic evidence suggests a model in which the conserved glutamic acid of the AF2 helix (E471) hydrogen bonds to the backbone amides of the first leucine of the motifs and the amino-terminal adjacent residue, while a critical lysine in helix 3 of the receptor (K301) hydrogen bonds to the backbone carbonyls of leucines at position 4 and 5 of the LXXLL motif (Nolte et al. 1998), with the hydrophobic face of LXXLL packed into a hydrophobic pocket formed from the helix packed interfaces of receptor helices 3, 4, and 5 and the AF2 helix. Thus, E471 and K301 in the AF2 and H3 helices, respectively, define a charge clamp that allows the orientation and placement of the LXXLL motif into the coactivator-binding site. The nonconserved amino acids of the core motif (LXXLL) are solvent exposed but would not be expected to exhibit specificity. These observations also imply that other LXXLL-containing factors would exhibit similar binding to the ligand-dependent coactivator-binding site, and raise intriguing questions with regard to LXXLL motif specificity and the role of the multiple LXXLL-containing motifs within the p160 factors.

Here, we report that the three LXXLL-containing helical motifs, referred to as LXDs, within the nuclear receptor-interaction domain of NCoA-1/SRC-1 are differentially required, with the second LXD required and sufficient for action of the ER, while TR and RAR require both the second and third LXXLL helical domains and correct spacing between them. In contrast, PPARγ receptor and progesterone receptor (PR) require both LXD1 and LXD2, again with appropriate spacing. The critical amino acid residues required for interactions with ER, RAR, and TR prove in vivo to reside carboxy-terminal to the LXXLL core motif and have been defined to the level of a single amino acid, revealing receptor specificity of required amino acid interactions. Specificity is, surprisingly, further regulated by ligand itself, as different carboxy-terminal residues of LXD2 were required with distinct PPARγ ligands. Finally, LXXLL-containing helices in the CBP/p300 interaction domain of NCoA-1/SRC-1 have proved to also be required for interactions with CBP/p300, and structure/function analysis is consistent with the hypothesis that these interactions involve a hydrophobic pocket defined by multiple helical motifs in the CBP/p300 interaction domain, which is required to mediate the apparent, obligatory requirement for the CBP/p300 cofactor in nuclear receptor function.

Results

Receptor specificity of the LXXLL helical motifs

The three members of the p160 coactivator family contain several regions of high homology, and these include the distinct nuclear receptor- and CBP-interaction domains; the sequences of the 21 amino acids that encompass each component LXD are more related between family members than they are between motifs within a given p160 protein (Fig. 1A). Because the region encompassing LXD1, LXD2, and LXD3 does not interact with CBP/p300, while conversely the region encompassing LXD4 and LXD5 does not effectively interact with liganded nuclear receptors (Torchia et al. 1997), we explored the possibility that there might be a preferential recognition code of LXXLL motifs required for actions of

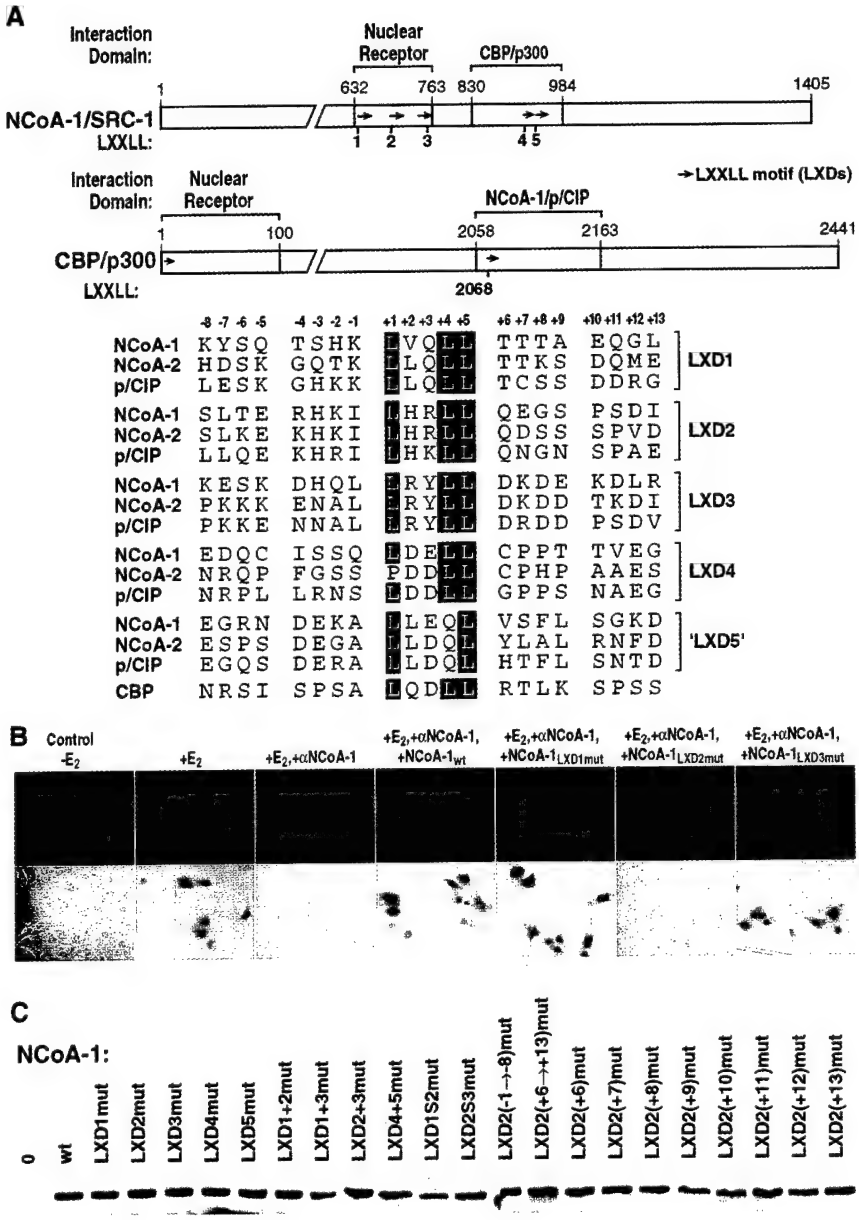

Figure 1. LXXLL helical motif requirements for actions of ER. (*A*) Map of NCoA-1/SRC-1 with LXXLL helical motif (LXDs) indicated, and of CBP, with a portion of a LXXLL motif in the NCoA-1/p/CIP interaction domain. (Arrows) LXXLL motifs; (*bottom*) sequences of these motifs are compared. (*B*) Effects of mutation of LXD1, LXD2, or LXD3 (LXXLL → LAAAA) on ability to rescue 17β estradiol (E_2)-dependent ER activation abolished by nuclear microinjection of anti-NCoA-1/SRC-1 affinity-purified IgG. (*C*) Western blot analysis of expression of NCoA-1/SRC-1, wild type (wt), or the indicated mutations, in extracts of cells transfected with specific IgG. No significant differences in protein levels were observed for the mutations studied.

specific nuclear receptors. This hypothesis was investigated initially at a functional level, determining the ability of NCoA-1/SRC-1 mutated in specific LXDs to rescue receptor function following nuclear microinjection of specific anti-NCoA-1/SRC-1 IgG. In these experiments, we evaluated the function of each LXD; we altered the fourth and fifth (leucine) residue of LXXLL (+1 to +5) to alanines, or altered residues 2, 3, 4, and 5 to alanine, obtaining identical results in all experiments. The mutation of L4 and L5 was chosen on the basis of the critical roles of these leucine residues in binding to the liganded nuclear receptor (Heery et al. 1997; Torchia et al. 1997) and the co-crystal structure of PPARγ with a portion of the NCoA-1/SRC-1 interaction domain, confirming the specificity of the requirement for leucine at the +5 position (Nolte et al. 1998).

We first performed rescue experiments following injection of anti-SRC-1/NCoA1 IgG on 17β-estradiol-stimulated estrogen receptor function, using wild-type NCoA-1/SRC-1 or NCoA-1/SRC-1 derivatives encoding the indicated, specific mutations in LXD1, LXD2, or LXD3. These experiments indicated that only LXD2, but neither LXD1 nor LXD3, were required for function of NCoA-1/SRC-1 on this receptor (Figs. 1B and 2A). Even with mutation of both LXD1 and LXD3, the ER activation function of NCoA-1/SRC-1 remained intact (Figs. 1B and 2A). The mutant forms of NCoA-1/SRC-1 were expressed at apparently equivalent levels as determined by Western blot analysis of transfected cells, as were all other mutated proteins used in these studies (Fig 1C). More definitively, the function of each mutation was established by its ability to rescue other nuclear recep-

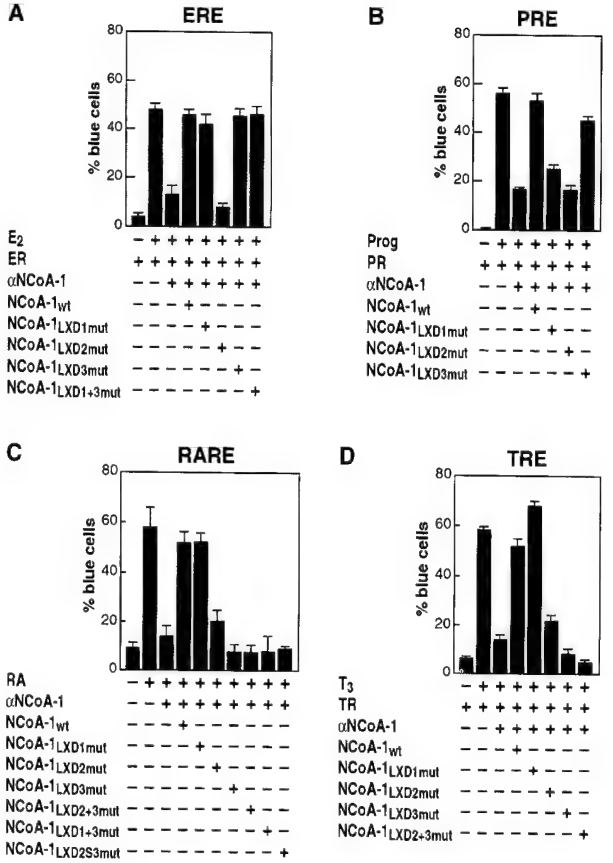

Figure 2. Differential role of LXD motifs in actions of ER (*A*), PR (*B*), RAR (*C*), or TR (*D*) receptors. In each case, ligands were added at 10^{-6} M, and reporters were under control of the appropriate response element (Torchia et al. 1997). (ERE) Estrogen-responds element; (PRE) progesterone-response element; (RARE) retinoic acid-response element; (TRE) thyroid hormone-response element. Rat-1 cells were microinjected with anti-NCoA-1/SRC-1 IgG and the CMV-expression vectors encoding the indicated proteins (Torchia et al. 1997). In addition to the mutations in leucine residues +4 and +5 of each motif, a deletion of 30 amino acids between LXD2 and LXD3 (LXD2S3mut) were created, leaving the 10 amino acids immediately flanking the LXD intact. Ligands were retinoic acid (RA), triiodothyronine (T3), 17β-estradiol (E_2), or progesterone (Prog). Where indicated, receptors were also expressed; similar results were obtained in at least three independent experiments with >300 cells microinjected for each data point.

tors (see below). Similar analysis with the PR revealed a requirement for both LXD1 and LXD2 (Fig. 2B), indicating distinct patterns of LXD usage for different nuclear receptors.

For RAR and TR function, two helical motifs were again required, but now LXD2 and LXD3 proved to be the motifs required, while mutation of LXD1 did not affect NCoA-1/SRC-1 function (Fig. 2C,D). On the basis of the conserved spacing of 50 amino acids between LXD2 and LXD3, we deleted 30 amino acids, leaving 10 amino acids carboxy- and amino-terminal to LXD2 and LXD3, respectively. Rescue experiments with the spacing variant of NCoA-1/SRC-1 (LXD2S3) revealed that, while equivalently expressed and fully functional on PPARγ receptor (see Fig. 3A), this mutant was unable to serve in activation function for either the TR or RAR (Fig. 2C and data not shown). Therefore, we conclude that, in contrast to the requirements for a single LXD by ER, both RAR and TR, as well as PR, require the actions of two, critically spaced LXDs, rather than a single LXD. The critical LXXLL-containing helices, however, are distinct between the PR or PPARγ receptor and the RAR or TR.

A similar microinjection analysis for activity of the PPARγ receptor (Fig. 3A) revealed that mutation of either LXD1 or LXD2, but not of LXD3, resulted in a partial loss of transactivation in response to addition of a thiazolidenedione (troglitazone; TGZ). Mutation of both LXD1 and LXD2 caused complete loss of function (Fig. 3A), while even with simultaneous mutation of LXD1 and LXD3 or LXD2 and LXD3, NCoA-1/SRC-1 remained partially competent to rescue TGZ-stimulated PPARγ function (data not shown). Reduction of the conserved spacing (from 52 to 20 amino acids) between LXD1 and LXD2 abolished the ability of NCoA-1/SRC-1 to serve as a PPARγ coactivator, while altered spacing between LXD2 and LXD3 had no effect, confirming both the effective expression and function of this variant NCoA-1/SRC-1 protein (Fig. 3A).

On the basis of the X-ray crystal structures of liganded receptor carboxy-terminal domains (Bourguet et al. 1995; Renaud et al. 1995; Wagner et al. 1995; Nolte et al. 1998), which document distinct, ligand-dependent placement of the AF2 helix, we considered the possibility that, as a consequence, different ligands might alter the LXD requirements for a particular receptor. This possibility was tested in the case of PPARγ receptor by evaluating several different classes of ligands for PPARγ, each of which would be predicted to bind quite differently in the large ligand-binding pocket and might be expected to alter surface contacts by coactivators (Nolte et al. 1998). Mild distinctions were observed in the quantitative requirements for LXD1 and LXD2; with prostaglandin J2 metabolites (PGJ2) there were equivalent, partial requirements for both LXD1 and LXD2 (PGJ2; Fig. 3B), and with indomethacin, there was a greater quantitative importance of LXD1, but still some effect of LXD2 (Fig. 3C).

Determinants of LXD specificity

While the co-crystal structure of PPARγ with a portion of the SRC-1-interaction domain (amino acids 623–710) provided insight into the critical role of the leucine residues and hydrophobic helix, the molecular basis of specificity of helical choice has remained unclear. The co-crystal of PPARγ LBD with the SRC-1 receptor interaction domain revealed no detectable ordered structure beyond eight amino acids amino- or carboxy-terminal to the conserved LXXLL core (Nolte et al. 1998). Therefore, we investigated the role of these amino- and carboxy-terminal flanking residues as a potential basis for specificity.

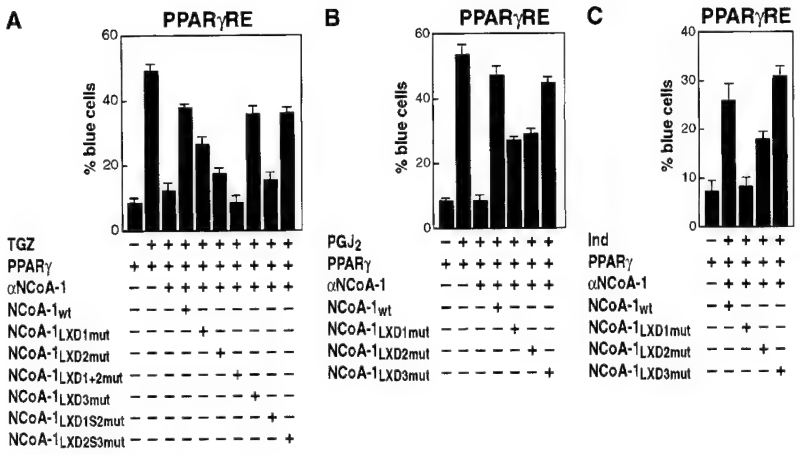

Figure 3. Requirements of LXD domains of NCoA-1/SRC-1 for activation of PPARγ on a response element (PPARγRE)-dependent promoter (AOX/LacZ; Korzus et al. 1998), repeated with different ligands. Nuclear microinjection of at least 300 Rat-1 cells was performed for each data point with αNCoA-1/SRC-1 IgG, and CMV-expression plasmids encoding wild-type NCoA-1/SRC-1 ($NCoA1_{wt}$) or NCoA-1/SRC-1 with point mutations in LXXLL motifs 1, 2 or 3 (LXD1mut, LXD2mut, and LXD3mut). Ligands used were TGZ (10^{-6} M), 15-deoxy$\Delta^{12,14}$- prostaglandin J2 (PGJ2, 10^{-6} M), or indomethacin (Ind, 10^{-3} M). Results were repeated in three separate experiments; mean ± S.E.M.

In initial experiments, the sequences encompassing the entire eight amino-terminal or carboxy-terminal flanking amino acids of LXD2 were mutated to alanine codons, to preserve helical conformation of the NCoA-1/SRC-1 LXD. Subsequently, mutation of residues spanning –1 to –3 (see Fig. 1A) was also introduced, and the efficacy of these mutant NCoA-1/SRC-1 molecules to rescue retinoic acid-, thyroid hormone-, and estrogen-dependent transcription was assessed. Whereas there was no effect of mutation of the flanking amino-terminal residues, mutation of the eight carboxy-terminal residues abolished function on all receptors tested (Fig. 4A–C). A similar result was obtained with biochemical experiments that evaluated the ability of LXD peptides (21-mers flanking LXXLL sequences –7 to +8) to compete for the binding of the nuclear receptor interaction domain (NRID) of NCoA-1/SRC-1 on DNA bound RAR–retinoic X receptor (RXR) heterodimers. Altering residues +8 through +12 to alanines markedly diminished the ability to compete for binding (Fig 4D). As expected, mutation of L+4 and L+5 abolished function entirely (Fig. 4D). However, a cluster of alanine substitutions from –3 to –7 in the context of the 21-mer peptide also led to loss of competition, which may reflect interference with the formation of the amino-terminal cap signal and, hence, decreased LXD2 helical stability. A similar study with GST–ER carboxyl terminus also suggested the importance of the +8 to +12 residues in LXD2 to compete for binding (Fig. 5E).

Therefore, we evaluated the effect of mutation of each individual amino acid from +6 to +13, initially on the ER, which relied entirely on LXD2 for function. This analy-

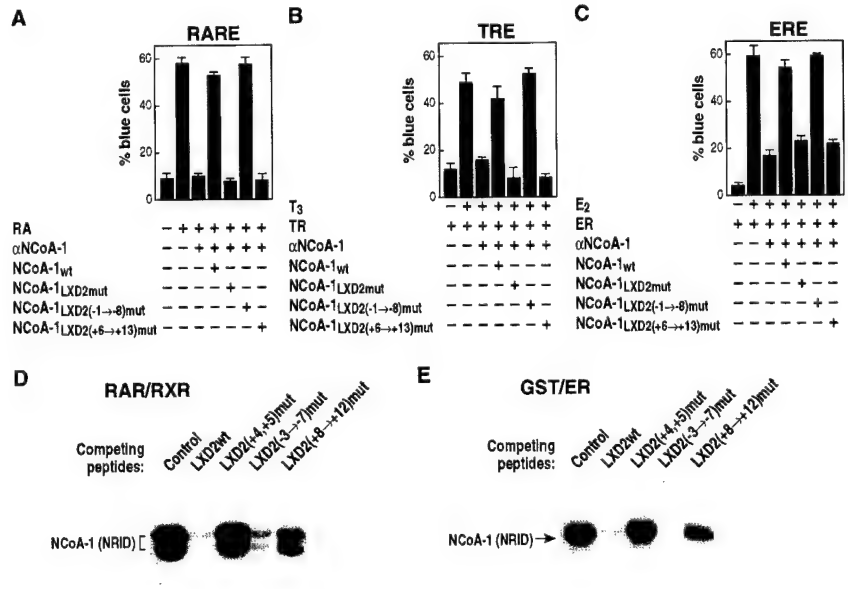

Figure 4. Carboxy-terminal flanking regions dictate specificity of LXXLL domain function. Nuclear microinjection studies in Rat-1 cells were performed with NCoA-1/SRC-1 proteins in which LXD2-flanking residues (–1 → –8) or (+6 → 13) were mutated to alanine and were evaluated RAR, TR, and ER, as shown in *A*, *B*, and *C*, respectively. Results of the average ± S.E.M. of two sets of nuclear microinjected cells; three independent experiments gave similar results. (*D*) Avidin–biotin DNA complex assay with thrombin-cleaved, bacterially expressed RARβ and RXRα proteins were bound to biotinylated direct repeat core sequence spaced by 5 bp (DR+5) oligonucleotide, and the NRID of NCoA-1/SRC-1 (amino acids 700–763) was prepared as a ^{32}P-labeled bacterial protein. Competition was assessed with wild-type LXD2 (21-mer) synthetic peptides (LXD2wt), or peptides containing alanine substitutions in the indicated amino acids used in excess (1 μm) to compete for binding. Binding of the NCoA-1 NRID indicates the efficiency of the peptide competition; with more binding indicating loss of function, as observed with mutation of L4 and L5. (*E*) Similar analysis performed with a bacterially expressed GST–ER carboxy-terminal protein, to evaluate the effects of residue substitution. Mutation of +8 through +12 caused considerable loss of function (i.e., less competition).

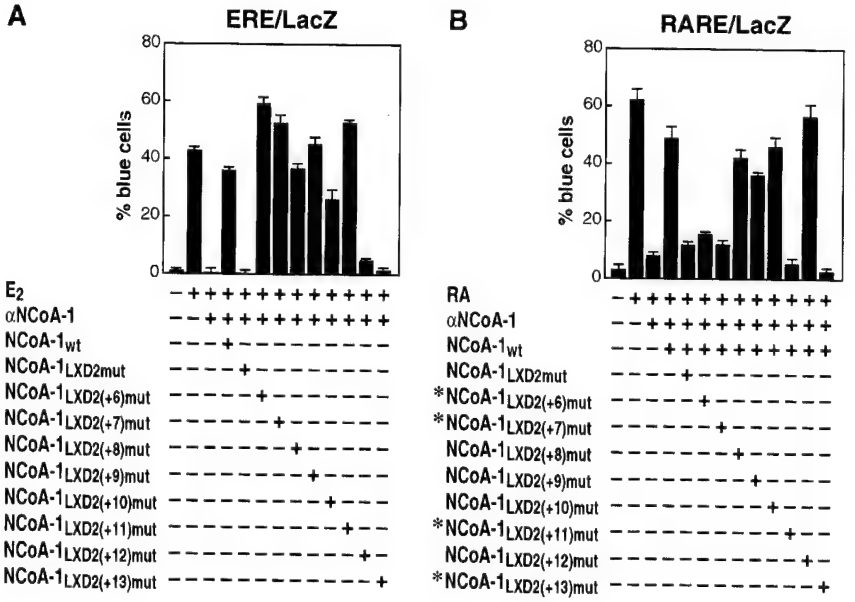

Figure 5. Identification of critical carboxy-terminal residues in the NCoA-1/SRC-1 LXD2 motif for function in transcriptional activation by ER from an expression plasmid (*A*), or endogenous RAR (*B*). In each case, the ability of NCoA-1/SRC-1 wild-type, LXD2 mutant (LAAAA), or NCoA-1 proteins with single amino acid alanine substitutions [LXD2(+6)mut through LXD2(+13)mut] were evaluated by use of the single cell microinjection assay. The critical amino acids differed in the case of ER and RAR; mean ± S.E.M.

sis revealed that, for the ER, there was only a minimal effect of mutation at positions +6 through +11; however, mutation at either +12 or +13 (D, I) abolished the ability of the LXD2 to mediate SRC-1 function on liganded ER entirely (Fig. 5A). Therefore, a similar analysis was performed with RAR to evaluate whether critical residues in LXD2 would prove to be invariant. Surprisingly, when this analysis was performed for RAR–RXR heterodimers on a DR +5 DNA element, distinct residues (+6, +7, and +11), as well as +13, were now required for effective function (Fig. 5B). Thus, the carboxy-terminal amino acids immediately flanking the LXXLL core motif have proved to be responsible for mediating receptor-specific interactions, with preferential interactions required for biological function of the coactivator in the intact cell.

Therefore, we evaluated the residues critical for function of PPARγ, because this receptor can bind multiple structurally distinct ligands, and because of the availability of the co-crystal structure of BRL49653-liganded PPARγ LBD with an 88 amino acid fragment of SRC-1 encompassing LXD1 and LXD2 (amino acids 623–710). With TGZ as ligand, the critical residues were found to be +6, +11, and +13 (Fig. 6A). When a similar analysis was performed with BRL49653 as ligand, to permit direct comparison with co-crystal structure, now residues +9, +10, +12, and +13 proved to be the critical determinant (Fig. 6B). These studies further suggest ligand-specific alterations of receptor structure actually imposes a requirement for different LXD residues to achieve high-affinity interactions.

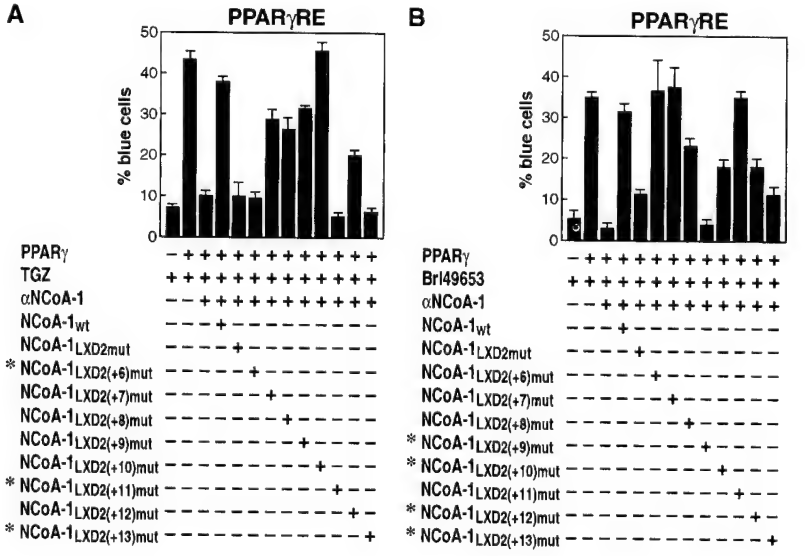

Figure 6. Mapping of critical carboxy-terminal residues in the NCoA-1/SRC-1 LXD2 required for function in transcriptional activation by PPARγ with either TGZ (10^{-6} M) (*A*), or BRL49653 (10^{-6} M) (*B*) as ligand. The entire series of alanine substitutions was evaluated; (*) critical amino acid residues identified.

LXXLL-containing motifs are required for CBP/p300 recruitment to the coactivator complex

Next, it was of particular interest to determine whether LXD motifs in the CBP/p300-interaction domain (Fig. 1A) were important for function and interactions with CBP/p300. As shown in Figure 7A–C, mutation of LXD4 and LXD5 abolished functional activation of the TR, RAR, and PPARγ receptor. Therefore, the effect of these motifs on the strong interactions of NCoA-1/SRC-1 with CBP/p300 was assessed biochemically. As shown in Figure 7D, the interaction with CBP was abolished with mutation of both LXD4 and LXD5.

In concert with these findings, we and others have noted that the major activation domain of NCoA-1/SRC-1 is the sequence encompassing the CBP/300 interaction domain. The role of CBP/p300 in this activation event was further evaluated by use of a GAL4 DNA-binding domain–NCoA-1/SRC-1 fusion protein containing the CBP/p300-interaction domain. The activation properties of this domain were largely abolished by anti-CBP IgG (Fig. 7E). We evaluated whether, conversely, the interaction domain of CBP was required for activation by nuclear receptors; deletion of this interacting region in CBP (CBP ΔNCoA) was sufficient to abolish the ability of CBP/p300 to mediate receptor activation function without affecting expression. In contrast, an amino-terminal region deletion in CBP (CBP ΔN) did not affect its activation function (Fig. 7F). Together, these data suggest that the LXDs of NCoA-1/SRC-1 are themselves required for activation function and that their functional importance is indeed likely to be linked, at least in part, to their requirement for interaction with CBP/p300. Conversely, mutation of the LXXLL-containing motif in the CBP/p300 interaction domain to LAAAA had no ef-

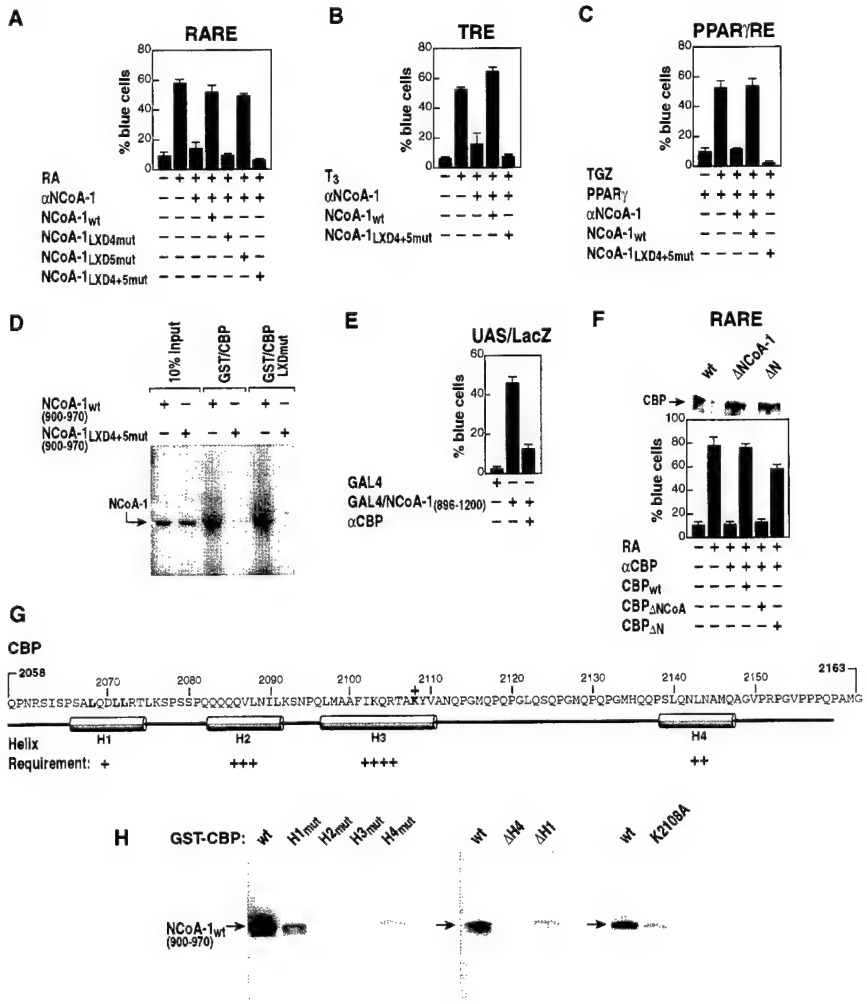

Figure 7. Role of LXDs in the CBP/p300-interaction domain of NCoA-1/SRC-1 in interaction and receptor activation function. (*A*) The LXD motifs (4, 5; Fig. 1A) were mutated to place alanines in positions 2, 3, 4, 5 alone, or together, and evaluated for function on RAR-dependent gene activation. Mutations of LXD4 or LXD4 and LXD5 abolished the ability of SRC-1/NCoA-1 to function in retinoic acid-dependent activation events in Rat-1 single cell nuclear microinjection studies. (*B,C*) The requirement for the LXD4 and LXD5 in the CBP/p300-interaction domain of NCoA-1/SRC-1 is demonstrated for coactivation of the TR and PPARγ. (*D*) Role of LXDs in the interactions between ^{35}S-labeled NCoA-1/SRC-1 CBP-interaction domain and CBP (wild type) or CBP in which the CBP LXD is mutated (LXXLL → LAAAA; CBP LXDmut). The mutation of LXD4 and LXD5 virtually abolished interactions by GST pull-downs, but mutation of the CBP LXXLL motif in the interaction domain did not affect interactions. (*E*) Gal4–NCoA-1 (896–1200) fusion protein activates transcription from the UAS p36 promoter (Torchia et al. 1997) and was blocked by addition of anti-CBP IgG (Kamei et al. 1996). (*F*) Effect of deletion of the NCoA-1 interaction domain of CBP on function of CBP in RAR activation. Anti-CBP IgG (Kamei et al. 1996) was used to block RAR activation, and CMV-expression vectors encoding wild-type CBP, CBPΔN (Δ 2–468), or CBP ΔNCoA-1 (Δ 2098–2163) were evaluated for their ability to rescue. The three CBP protein variants were expressed at comparable levels in transcripted cells as detected by anti-Flag IgG (*top*). (*G*) Predicted structure of the CBP region interacting with SRC-1/NCoA-1, with helix 3 as a predicted hydrophobic helix. (*H*) Requirements of each helix were tested by mutation to break the helix (helix 1, QDLL → PDPG; helix 2, QQQV → PQPG; helix 3, FIKQ → PIPG; helix 4, NLNA → PLPG), or by helix removal (ΔH4, amino acids 2058–2133; ΔH1, amino acids 2078–2163). Regions were tested in vitro for their ability to interact with amino acids 900–970 of NCoA-1/SRC-1, ^{35}S-labeled by in vitro transcription and translation.

fect on interactions (Fig. 7D). The predicted structure of CBP suggests that hydrophobic helices could form a binding pocket, analogous to that of the nuclear receptor-binding pocket, by which the LXXLL motifs of NCoA-1/SRC-1 bind to CBP/p300 (Fig. 7G). To begin to explore this possibility, we mutated each of the four predicted helices by various algorithms introducing a PXPG motif into each helix, as well as creating a deletion of helix 1 (ΔH1) or helix 4 (ΔH4). As shown in Figure 7H, helix 3 proved to be absolutely required for interaction; helix 2 was less quantitatively important, but still significant; and lesser roles were exerted by helices 4 and 1. Even a single point mutation of helix 3 (K2109A) significantly impaired the interaction of CBP with NCoA-1/SRC-1, consistent with the critical importance of this hydrophobic helix.

Discussion

LXDs as a code for receptor, coactivator assembly

The finding that nuclear receptors require coactivators to mediate their regulation of gene transcription and that many potential coactivators share a conserved LXXLL motif in the nuclear receptor-interaction domain has suggested intriguing potential regulatory strategies with respect to control of nuclear receptor function. Members of the p160/NCoA/SRC family of coactivators, which can associate in the cell and in vitro with liganded nuclear receptors appear, at least for some promoters, to be required for ligand-dependent transcription (Halachmi et al. 1994; Oñate et al. 1995; Kamei 1996; Torchia et al. 1997). The p160 proteins interact with nuclear receptors via an internal region containing three LXDs with core LXXLL motifs that are modestly conserved amongst family members, with respect to the amino- and carboxy-terminal residues that immediately flank the core LXXLL residues (Heery et al. 1997; Torchia et al. 1997) and which are found in other nuclear receptor-associated factors (LeDouarin et al. 1996). Structural algorithms predicting these motifs would be helical were confirmed by co-crystallization of a sequence encompassing two motifs of NCoA-1/SRC-1 with liganded PPARγ (Nolte et al. 1998). This structure revealed that the LXXLL helix was oriented by a conserved lysine residue in helix 3 and a conserved glutamic acid residue in the AF2 helix of the PPARγ ligand-binding domain, permitting the leucine residues of the LXXLL to pack into a hydrophobic pocket formed by helices 3, 4, and 5, and AF2. This mechanism of interaction, however, fails to explain differences in the specific LXDs required for transcriptional actions by different nuclear receptors. In this report, we have provided several independent types of evidence that there is a receptor-specific code of interaction that reflects usage with distinct NCoA-1/SRC-1 LXXLL-containing motifs (LXDs). These observations are in concert with the finding that the distinct LXXLL-containing motifs in the carboxyl terminus of NCoA-1/SRC-1 account for recruitment of CBP/p300 and are also required components of the coactivator machinery (Chakravarti et al. 1996; Hanstein et al. 1996; Kamei et al. 1996; Yao et al. 1998). The finding that LXDs serve as protein–protein interaction interfaces that assemble the coactivator receptor complex is consistent with reports over the past several years of the critical importance of a series of small regulatory motifs, such as SH2, SH3, PTB, and PBZ domains that have been identified in a series of platform and adaptor proteins that serve to assemble and coordinate complexes regulating signaling events at the plasma membrane, in protein trafficking, and in nuclear transport (Koch et al. 1991; van der Geer and Pawson 1995; Pawson and Scott 1997).

Furthermore, we have documented that amino acids flanking the LXXLL-containing helices subserve specific functions, and this specificity provides several insights into the serial events by which nuclear receptor–coactivator interactions operate to activate gene expression. The presence of multiple LXXLL motifs in the p160 factors, and in several other potential coactivators, has suggested the possibility that there may be an underlying code of differential utilization and an advantage to the presence of more than one motif. There has proved to be at least two layers of specificity to the LXD preference code. The first involves a differential requirement for the number of LXXLL-containing helices utilized by the different nuclear receptors. Thus, in the case of the ER, the second LXD is required and sufficient. The requirement by ER for only a single LXD, and the inability of other, otherwise effective motifs to functionally substitute, implies that a single motif is capable of high-affinity interactions with the estrogen receptor in the intact cell, and suggests that each liganded estrogen receptor of the DNA-bound homodimer is likely to associate with one NCoA-1/SRC-1/p/CIP family member. In contrast, receptors binding as heterodimers with RXR and PR homodimers, require two LXDs. This requirement is consistent with the co-crystal structure of the PPARγ LBD with a region of the NCoA-1/SRC-1-interaction domain containing two LXXLL motifs, in which the two LBDs of the dimer were contacted by LXXLL helices from a single NCoA-1/SRC-1 molecule (Nolte et al. 1998) and the observation that two LXDs are required for cooperative binding to RAR–RXR and PPARγ–RXR heterodimers bound to DNA (Westin et al. 1998). In addition, the requirement for activation of two LXDs for RAR or TR heterodimers with RXR, might reflect the observation that the RXR AF2 domain can interact directly with the LXXLL-binding pocket and competes with NCoA-1/SRC-1 (Westin et al. 1998). It is tempting to speculate that, although a single LXD can displace the RXR AF2 from RAR, the presence of a second LXXLL motif, looping over the receptor heterodimer on DNA and binding to the activation surface of unliganded RXR, might hold the AF2 of RXR in an active configuration.

The second layer of the specificity code concerns the requirements of specific residues adjacent to the LXXLL core motif for function of a particular nuclear receptor. The present findings indicate that receptor-specific differences are dictated by flanking carboxy-terminal residues (+6 to +13), with different residues modulating specific interactions with the ligand-binding domains of dif-

ferent receptors. Thus, the presence of multiple LXXLL-containing motifs has provided a mechanism for receptor-specific interactions. For example, in the case of ER, residues +12 and +13 of LXD2 provide specificity; in contrast, residue +6 proved critical for RAR function. However, the most striking specificity is the difference in residues in LXD2 required by PPARγ when TGZ (amino acids +6, +11, and +13) or BRL49653 (amino acids +9, +10, +12, and +13) are used as ligands. The carboxy-terminal amino acids of LXD2 interact primarily with four separate helices in the PPARγ LBD. As shown in Fig. 8, the +12 and +13 side chains are solvent exposed and the +4 and +6 side chains primarily form interactions with amino acids at the carboxyl terminus of helix H3 in PPARγ. The +7 and +8 side chains point out toward solvent, and the +9 and +10 amino acids form interactions with the small helix, H3', between H3 and H4. The +11 side chain is again solvent exposed and the +12 and +13 amino acids form weak interactions at the amino-terminus of H1 in PPARγ. Taken together, the amino acids carboxy-terminal to the LXXLL motif could provide specificity at positions +4, +5, +6, +9, +10, +12, and +13, although a small conformational change in this region of SRC-1 could result in different amino acid specificity for other nuclear receptors or for PPARγ with different ligands. Our data (Fig. 6B) indicate a functional importance of positions +9, +10, +12, +13 of LXD2 in vivo for BRL49653-liganded PPARγ, in accordance with these structural predictions. Conformational alterations in this region of SRC-1 are likely to occur when it contacts other nuclear receptors, and these variations are suggested to underlie the differential usage of specific LXD2 residues for different nuclear receptors. We suggest that there may be sufficient flexibility in LXD2 residue placement between NCoA-1/SRC-1 family members that despite the switch in conserved residues between +12 D, +13 I (NCoA-1/SRC-1) to +12 A, +13 E (p/CIP), they may subserve similar specificity functions. Finally, the regions of H1 and H3 in PPARγ with which specific contacts are made with LXD2 are poorly conserved between different nuclear receptors, consistent with the observation that there are receptor-specific contacts; these data imply further that there will be receptor specificity of recognition of LXXLL motifs in other putative coactivators.

LXXLL motifs recruit CBP/p300 as well as nuclear receptors

In parallel, distinct LXXLL motifs in NCoA-1/SRC-1 are themselves required for the interactions with CBP/p300, and in this report, we have provided several independent types of evidence that it is CBP/p300 itself that is specifically required for at least a portion of the activation functions imparted by NCoA-1/SRC-1. It is predicted that the region carboxy-terminal to the LXXLL core sequence will also exert important roles in determining whether it will interact with nuclear receptors or with CBP/p300. The precise structure of the interacting region of CBP is unknown, but our data suggest that the interaction is likely to involve a hydrophobic pocket formed by several helices that might, in a fashion analogous to the coactivator-binding domain pocket of the nuclear receptor carboxyl terminus that selectively binds LXXLL motifs (Fig. 7G). Interactions between CREB and another specific region of CBP (KIX domain) are dependent on phosphorylation and induced conformational structuring of this CBP interaction domain (Radhakrishnan et al. 1997); analogous induced-fit

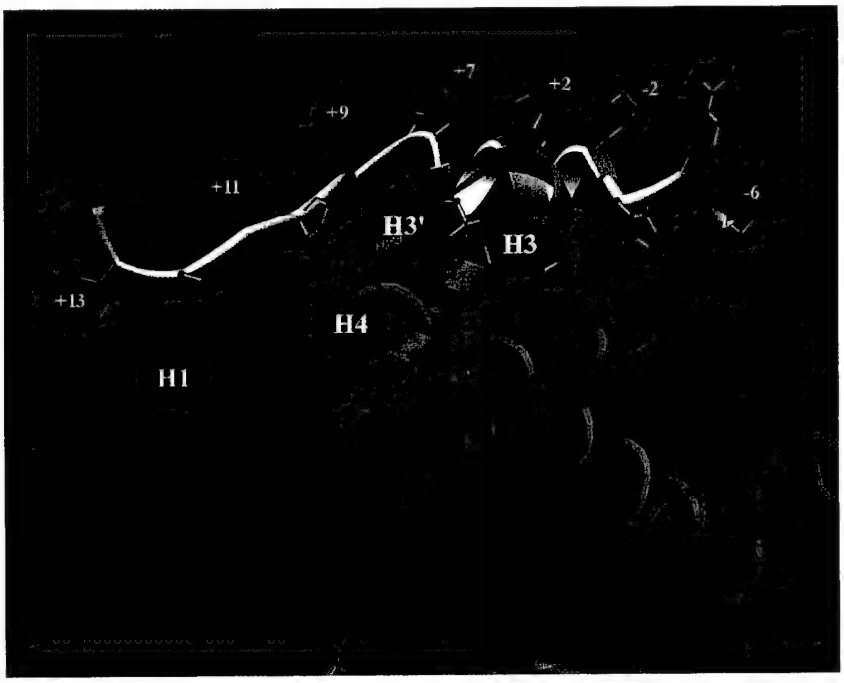

Figure 8. Model of SRC-1 LXD2 (–6) through (+14) bound to BRL49653-liganded PPARγ LBD based on the co-crystal structure with SRC-1 amino acids 623–710 (Nolte et al. 1998). A ribbon drawing of the LXD2 motif of human SRC-1 is shown in yellow with the human PPARγ LBD shown in green. When the electron density maps of the co-crystal structure of the SRC-1 heterodimer with liganded PPARγ (Nolte et al. 1998) are examined and modeled, the +12, +13 amino acids form weak interactions at the amino terminus of helix 1; the +6 side chains contact the carboxyl terminus of helix 3; amino acids +9 and +10 form interactions with the small helix (H3') between helices 3 and 4.

events may apply to NCoA-1/SRC-1-CBP/p300 interactions.

Thus, it is suggested that the duplication/mutation of primordial LXXLL motifs over evolutionary time has permitted the appearance of coactivator proteins with enhanced repertoires of both nuclear receptors with which they can interact, as well as the proper interfaces to recruit additional cofactors to a DNA-bound transcription factor. On the basis of altered specificity in response to ligands, it is tempting to speculate that other cofactors containing LXXLL motifs will be differentially recruited on the basis of cell type, levels of coactivators, and ligand. Thus, structural features, duplication, and spacing between LXXLL motifs have evolved to provide specificity in the assembly of critical components of a coactivator complex required for function of a large family of regulated transcription factors.

Materials and methods

DNA-dependent protein–protein interaction and GST pull-down assays

GST–ERα(302–595), GST–RXRα(45–462), and GST–RARα(20–462) proteins were prepared as crude bacterial lysates, immobilized on a glutathione affinity matrix, and washed twice in buffer H [20 mM HEPES (pH 8.0) 50 mM KCl, 20% glycerol, 0.1% NP-40] and once in CHAPS buffer [8 mM Tris-phosphate (pH 7.4), 0.12 M KCl, 8% glycerol, 4 mM DTT, 0.5% CHAPS]. Where indicated, thrombin-cleaved products were prepared. Then, the receptors were incubated in CHAPS buffer with the appropriate ligand for 30 min of competition experiments, incubated in NET-N buffer [50 mM Tris (pH 8.0), 5 mM EDTA, 150 mM NaCl, 0.1% NP-40] in the absence or presence of a NCoA-1/SRC-1 fragment. Peptides were synthesized to contain a tyrosine residue at the carboxyl terminus and, where indicated, labeled with ^{125}I by use of Iodo-gen (Westin et al. 1998). Of each peptide, 3×10^5 cpm was incubated with the liganded receptors. The sequences of the wild-type LXD2 peptide was LTERHKI**LHRL**LQEGSPSDIY; variants involved substitutions with alanine (A) residues and were as follows: LXD2(+4,+5)mut, LTERHKI**LHR-AA**QEGSPSDIY; LXD2(−3 → −7), AAAAAKI**LHRLL**QEGSPSDIY; LXD2(+8 → +12), LTERHKI**LHRLL**QEAAAAAIY. For DNA-dependent ABCD assays, oligonucleotides were synthesized to contain biotin residues at the 5′ end. The sequence of the sense strand of the retinoic acid response element was: 5′biotin-AAGGGGATCCGGGTAGGGTTCACCGAAGTTCACGAGATCT-3′. Purified, double-stranded oligonucleotides (1 μg) were incubated with 100 ng each of purified RARα or PPARγ and RXR produced as GST-fusion proteins in *Escherichia coli* and cleaved from the GST portion with thrombin. DNA binding was performed in CHAPS buffer. Receptor–DNA complexes were captured by use of 25 μl of a slurry of streptavidin–agarose and washed two times in buffer H and once in CHAPS buffer. Receptors were then incubated in the binding buffer with the indicated ligands or solvent alone for 30 min at room temperature. Following ligand binding, the receptor–DNA complexes were incubated with either 1×10^5 cpm ^{35}S-labeled NCoA-1/SRC-1 proteins generated by in vitro transcription and translation, or with 1×10^5 cpm ^{32}P-labeled NCoA-1/SRC-1 protein labeled by protein kinase A, for 1 hr at 4°C in NET buffer. Competing peptides were present at 1 μm. Complexes were washed five times in buffer H, resolved by SDS-polyacrylamide gels and either dried and autoradiographed, or transferred to nitrocellulose membranes for Western blotting. The generated NCoA-1/SRC-1 fragments were amino acids 626–783 containing LXD1, LXD2, and LXD3, or amino acids 626–716 containing LXD1 and LXD2.

GST–CBP fusion proteins were prepared as crude bacterial lysates and immobilized on glutathione–agarose affinity beads. The GST-fusion protein bound to glutathione–agarose was washed and incubated with in vitro-transcribed and translated NCoa-1/SRC-1 as indicated for 2 hr at 4°C. Following washing, proteins were eluted from beads and analyzed by SDS–PAGE.

Single-cell microinjection assay and immunoblots

Microinjection assays of coactivator function were performed essentially as described previously (Torchia et al. 1997). Briefly, insulin-responsive Rat-1 fibroblasts were seeded on acid-washed cover slips and rendered quiescent by incubation in serum-free medium for 24–36 hr. Plasmids were injected into the nuclei of cells at 100 μg/ml. Preimmune IgG or anti-NCoA-1/SRC-1 IgG was coinjected and the injected cells unambiguously identified by immunofluorescence microscopy. Cells were stimulated with ligand 6 hr after injection to allow expression of NCoA-1/SRC-1 from coinjected plasmids. After overnight incubation, cells were fixed and stained to detect injected IgG and β-galactosidase expression. At least 200 injected cells were quantitated for each condition; experiments were repeated at least three times. A large series of mutant NCoA–1/SRC-1 expression plasmids were generated, including mutations of L4 and L5 of LXD1, LXD2, LXD3, LXD4, and LXD5, deletions of 32 and 30 amino acids, respectively, from LXD1S2 and LXD2S3 leaving 10 flanking residues adjacent to each LXXLL motif. All mutants were constructed by a standard protocol from the Quick Change Mutagenesis Kit (Stratagene), and were confirmed by complete DNA sequencing. Western blots were performed as described previously (Xu et al. 1998); anti-HA antibodies (Babco) were utilized for SRC-1 detection, as all NCoA-1/SRC-1 proteins used contain an HA epitope tag.

Structural model

The electron density of the PPARγ ligand-binding domain–SRC–TGZ ternary complex (Nolte et al. 1998) was used to identify and build the structure of helical domain 2 of SRC-1 around the PPARγ ligand-binding domain. The SRC-1 model was built with the O software package (Jones et al. 1989), and refined with X-PLOR (Brunger 1992).

Acknowledgments

We thank Mathias Treier, Degeng Wang, and Riki Kurokawa for discussions and reagents, Peggy Meyer for her expertise in the preparation of illustrations, and Marie Fisher for assistance with the manuscript preparation. E.M.M. is supported by a National Research Service Award (National Institute of Diabetes and Digestive and Kidney Diseases); D.W.R by an American Diabetes Association Career Development Award; S.W. by the Swedish Cancer Society. C.K.G. is an Established Investigator of the American Heart Association and M.G.R. is an Investigator in the Howard Hughes Medical Institute. These studies were supported by grants from CAP CURE and the National Institutes of Health to C.K.G. and a U.S. Army Medical Research Program Award to M.G.R.

The publication costs of this article were defrayed in part by payment of page charges. This article must therefore be hereby marked 'advertisement' in accordance with 18 USC section 1734 solely to indicate this fact.

References

Alland, L., R. Muhle, H. Hou, J. Potes, L. Chin, N. Schreiber-Agus, and R.A. DePinho. 1997. Role for NCoR and histone deacetylase in Sin3-mediated transcriptional repression. *Nature* **387:** 49–55.

Anzick, S.L., J. Kononen, R.L. Walker, D.O. Azorsa, M.M. Tanner, X.Y. Guan, G. Sauter, O.P Kallioniemi, J.M. Trent, and P.S. Meltzer. 1997. AIB1, a steroid receptor coactivator amplified in breast and ovarian cancer. *Science* **277:** 965–968.

Barettino, D., M.M. Vivanco Ruiz, and H.G. Stunnenberg. 1994. Characterization of the ligand-dependent transactivation by steroid hormone receptors. *EMBO J.* **13:** 3039–3049.

Beekman, J.M., G.F. Allan, S.Y. Tsai, and B.W. O'Malley. 1993. Transcriptional activation by the estrogen receptor requires a conformational change in the ligand binding domain. *Mol. Endocrinol.* **7:** 1266–1274.

Bourguet, W., M. Ruff, P. Chambon, H. Gronemeyer, and D. Moras. 1995. Crystal structure of the ligand-binding domain of the human nuclear receptor RXR-α. *Nature* **375:** 377–382.

Brzozowski, A.M., A.C.W. Pike, Z. Dauter, R.E. Hubbard, T. Bonn, O. Engstrom, L. Ohman, G.L. Greene, J.-A. Gustafsson, and M. Carlquist. 1997. Molecular basis of agonism and antagonism of oestrogen receptor. *Nature* **389:** 753–758.

Brunger, A. 1992. *X-PLOR Version 3.0: A system for crystallography and NMR*. Yale University Press, New Haven, CT.

Cavailles, V., S. Dauvois, P.S. Danielain, and M.G. Parker. 1994. Interaction of proteins with transcriptionally active estrogen receptors. *Proc. Natl. Acad. Sci.* **91:** 10009–10013.

Chakravarti, D., V.J. LaMorte, M.C. Nelson, T. Nakajima, I.G. Schulman, H. Juguilon, M. Montminy, and R.M. Evans. 1996. Role of CBP/p300 in nuclear receptor signalling. *Nature* **383:** 99–103.

Chen, H., R.J. Lin, R.L. Schiltz, D. Chkravarti, A. Nash, L. Nagy, M.L. Privalsky, Y. Nakatani, and R.M. Evans. 1997. Nuclear receptor coactivator ACTR is a novel histone acetyltransferase and forms a multimeric activation complex with p/CAF and CBP/p300. *Cell* **90:** 569–580.

Collaborative Computational Project Number 4. 1994. The CCP4 suite: Programs for protein crystallography. *Acta Crystallogr. Sect. D Biol. Crystallogr.* **50:** 760–776.

Danielian, P.S., R. White, J.A. Lees, and M.G. Parker. 1992. Identification of a conserved region required for hormone-dependent transcriptional activation by steroid hormone receptors. *EMBO J.* **11:** 1025–1033.

Durand, B., M. Saunders, C. Gaudon, B. Roy, R. Losson, and P. Chambon. 1994. Activation function-2 (AF-2) of retinoic acid receptor and 9-cis retinoic acid receptor: Presence of a conserved autonomous constitutive activating domain and influence of the nature of the response element on AF-2 activity. *EMBO J.* **13:** 5370–5382.

Fondell, J.D., H. Ge, and R.G. Roeder. 1996. Ligand induction of a transcriptionally active thyroid hormone receptor coactivator complex. *Proc. Natl. Acad. Sci.* **93:** 8329–8333.

Fritsch, M., C.M. Leary, J.D. Furlow, H. Ahrens, T.J. Schuh, G.C. Mueller, and J.Gorski. 1992. A ligand-induced conformational change in the estrogen receptor is localized in the steroid binding domain. *Biochemistry* **31:** 5303–5311.

Halachmi, S., E. Marden, G. Martin, H. MacKay, C. Abbondanza, and M. Brown. 1994. Estrogen receptor-associated proteins: Possible mediators of hormone-induced transcription. *Science* **264:** 1455–1458.

Hanstein, B., R. Eckner, J. DiRenzo, S. Halachmi, H. Liu, B. Searcy, R. Kurokawa, and M. Brown. 1996. p300 is a component of an estrogen receptor coactivator complex. *Proc. Natl. Acad. Sci.* **93:** 11540–11545.

Heery, D.M., E. Kalkhoven, S. Hoare, and M.G. Parker. 1997. A signature motif in transcriptional coactivators mediates binding to nuclear receptors. *Nature* **387:** 733–736.

Heinzel, T., R.M. Lavinsky, T.M. Mullen, M. Soderstrom, C.D. Laherty, J. Torchia, W. M. Yang, G. Brard, S.D. Ngo, J.R. Davie, E. Seto, R.N. Eisenman, D.W. Rose, C.K. Glass, and M.G. Rosenfeld. 1997. A complex containing NCoR, mSin3 and histone deacetylase mediates transcriptional repression. *Nature* **387:** 43–48.

Hong, H., K. Kohli, A. Trivedi, D.L. Johnson, and M.R. Stallcup. 1996. GRIP1, a novel mouse protein that serves as a transcriptional coactivator in yeast for the hormone binding domains of steroid receptors. *Proc. Natl. Acad. Sci.* **93:** 4948–4952.

Horlein, A.J., A.M. Naar, T. Heinzel, J. Torchia, B. Gloss, R. Kurokawa, A. Ryan, Y. Kamei, M. Soderstrom, C.K. Glass, and M.G. Rosenfeld. 1995. Ligand-independent repression by the thyroid hormone receptor mediated by a nuclear receptor co-repressor. *Nature* **377:** 397–404.

Jones, T.A., M. Bergdoll, M. Kjeldgaard, and S. Ealick. 1989. In *Crystallographic computing and modeling methods in molecular design* (ed. C. Bugg). Springer, New York, NY.

Kamei, Y., L. Xu, T. Heinzel, J. Torchia, R. Kurokawa, B. Gloss, S.C. Lin, R.A. Heyman, D.W. Rose, C.K. Glass, and M.G. Rosenfeld. 1996. A CBP integrator complex mediates transcriptional activation and AP-1 inhibition by nuclear receptors. *Cell* **7:** 1266–1274.

Katzenellenbogen, B.S. 1996. Estrogen receptors: Bioactivities and interactions with cell signaling pathways. *Biol. Reprod.* **54:** 287–293.

Koch, A., D. Anderson, M.F. Moran, C. Ellis, and T. Pawson. 1991. SH2 and SH3 domains: Elements that control interactions of cytoplasmic signaling proteins. *Science* **252:** 668–674.

Korzus, E, J. Torchia, D.W. Rose, L. Xu, R. Kurokawa, E.M. McInerney, T.M. Mullen, C.K. Glass, and M.G. Rosenfeld. 1998. Transcription factor-specific requirements for coactivators and their acetyltransferase functions. *Science* **279:** 703–707.

Kraus, W.L. and J.T. Kadonaga. 1998. p300 and estrogen receptors cooperatively activate transcription via differential enhancement of initiation and reinitiation. *Genes & Dev.* **12:** 331–342.

Kurokawa, R., M. Soderstrom, A. Horlein, S. Halamachi, M. Brown, M.G. Rosenfeld, and C.K. Glass. 1995. Polarity-specific activities of retinoic acid receptors determined by a corepressor. *Nature* **377:** 451–454.

LeDouarin, B., A.L. Nielsen, J.M. Garnier, H. Ichinose, F. Jeanmougin, R. Losson, and P. Chambon. 1996. A possible involvement of TIF1α and TIF1β in the epigenetic control of transcription by nuclear receptors. *EMBO J.* **15:** 6701–6715.

Lee, J.W., H.S. Choi, J. Gyuris, R. Brent, and D.D. Moore. 1995. Two classes of proteins dependent on either the presence or absence of thyroid hormone for interaction with thyroid hormone receptor. *Mol. Endocrinol.* **9:** 243–254.

Li, H., P.J. Gomes, and J.D. Chen. 1997. RAC3, a steroid/nuclear receptor-associated coactivator that is related to SRC-1 and TIF2. *Proc. Natl. Acad. Sci.* **94:** 8479–8484.

Mangelsdorf, D.J., C. Thummel, M. Beato, P, Herrlich, G. Schutz, K. Umesono, B. Blumberg, P. Kastner, M. Mark, P.

Chambon, and R.M. Evans. 1995. The nuclear receptor superfamily: The second decade. *Cell* **83:** 835–839.

Nagy, L., H.Y. Kao, D. Chakravarti, R.J. Lin, C.A. Hassig, D.E. Ayer, S.L. Schreiber, and R.M. Evans. 1997 Nuclear receptor repression mediated by a complex containing SMRT, mSin3A, and histone deacetylase. *Cell* **89:** 373–380.

Nolte, R.T., B. Wisely, S. Westin, J.E. Cobb, M.H. Lambert, R. Kurokawa, M.G. Rosenfeld, T.M. Willson, C.K. Glass, and M.V. Milburn. 1998 Ligand binding and coactivator assembly of the peroxisome proliferator-activated receptor γ. *Nature* **395:** 137–144.

Ogryzko, V.V., R.L. Schiltz, V. Russanova, B.H. Howard, and Y. Nakatani. 1996. The transcriptional coactivators p300 and CBP are histone acetyltransferases. *Cell* **87:** 953–959.

Ogryzko, V.V., T. Kotani, X. Zhang, R.L. Schiltz, T. Howard, X.J. Yang, B.H. Howard, J. Qin, and Y. Nakatani. 1998. Histone-like TAFs within the pCAF histone deacetylase complex. *Cell* **94:** 35–44.

Oñate, S.A., S.Y. Tsai, M.J. Tsai, and B.W. O'Malley. 1995. Sequence and characterization of a coactivator for the steroid hormone receptor superfamily. *Science* **270:** 1354–1357.

Pawson, T. and J.D. Scott. 1997. Signaling through scaffold, anchoring, and adaptor proteins. *Science* **278:** 2075–2081.

Rachez, C., Z. Suldan, J. Ward, C.P.B. Chang, D. Burakov, H. Erdjument-Bromage, P, Tempst, and L.P. Freedman. 1998. A novel protein complex that interacts with the vitamin D3 receptor in a ligand-dependent manner and enhances VDR transactivation in a cell-free system. *Genes & Dev.* **12:** 1787–1800.

Radhakrishnan, I., G.C. Perez-Alvarado, D. Parker, H. J. Dyson, M.R. Montminy, and P.E. Wright. 1997. Solution structure of the KIX domain of CBP bound to the transactivation domain of CREB: A model for activator:coactivator interactions. *Cell* **91:** 741–753.

Renaud, J.P., N. Rochel, M. Ruff, V. Vivat, P. Chambon, H. Gronemeyer, and D. Moras. 1995. Crystal structure of the RAR-γ ligand binding domain bound to all-trans retinoic acid. *Nature* **378:** 681–689.

Spencer, T.E., G. Jenster, M.M. Burcin, C.D Allis, J. Zhou, C.A. Mizzen, N.J. McKenna, S.A. Onate, S.Y. Tsai, M.J. Tsai, and B.W. O'Malley. 1997 Steroid receptor coactivator-1 is a histone acetyltransferase. *Nature* **389:** 194–198.

Tone, Y., T.N. Collinwood, M. Adams, and V.K. Chattergee. 1994. Functional analysis of a transactivation domain in the thyroid hormone receptor. *J. Biol. Chem.* **269:** 31157–31161.

Torchia, J., D.W. Rose, J. Inostroza, Y. Kamei, S. Westin, C.K. Glass, and M.G. Rosenfeld. 1997. The transcriptional coactivator p/CIP binds CBP and mediates nuclear receptor function. *Nature* **387:** 677–684.

Torchia, J., C.K. Glass, and M.G. Rosenfeld. 1998. Co-activators and co-repressors in the integration of transcriptional responses. *Curr. Opin. Cell. Biol.* **10:** 373–383.

Tzukerman, M.T., A. Esty, D. Santiso-Mere, P. Danielian, M.G. Parker, R.B. Stein, J.W. Pike, and D.P. McDonnell. 1994. Human estrogen receptor transactivation capacity is determined by both cellular and promoter context and mediated by two functionally distinct intramolecular regions. *Mol. Endocrinol.* **8:** 21–30.

van der Geer, P. and T. Pawson. 1995. The PTB domain: A new protein module implicated in signal transduction (phosphotyrosine-binding). *Trends Biochem. Sci.* **20**.

Voegel, J.J., M.J.S. Heine, C. Zechel, P. Chambon, and H. Gronemeyer. 1996. TIF2, a 160kDa transcriptional mediator for the ligand-dependent activation function AF-2 of nuclear receptors. *EMBO J.* **15:** 3667–3675.

Wagner, R.L., J. W. Apriletti, M.E. McGrath, B.L. West, J.D. Baxter, and R.J. Fletterick. 1995. A structural role for hormone in the thyroid hormone receptor. *Nature* **378:** 690–697.

Westin, S., R. Kurokawa, R.T. Nolte, B. Wisely, E.M. McInerney, D.W. Rose, M.V. Milburn, M.G. Rosenfeld, and C.K. Glass. 1998. Allosteric interactions governing the assembly, structure and function of nuclear receptor heterodimer-coactivator complexes. *Nature* **395:** 199–203.

Wong, J., Y.B. Shi, and A.P. Wolffe. 1997. Determinants of chromatin disruption and transcriptional regulation instigated by thyroid hormone receptor: Hormone-regulated chromatin disruption is not sufficient for transcriptional activation. *EMBO J.* **11:** 3158–3171.

Xu, L., R.M. Lavinsky, J.S. Dasen, S.E. Flynn, E.M. McInerney, T.-M. Mullen, T. Heinzel, D. Szeto, E. Korzus, R. Kurokawa, A.K. Aggarwal, D.W. Rose, C.K. Glass, and M.G. Rosenfeld. 1998. Distinct histone acetyltransferases and CBP domains are required for activation of Pit-1 by different signalling pathways. *Nature* **395:** 301–306.

Yao, T.-P., G. Ku, N. Zhou, R. Scully, and D.M. Livingston. 1996. The nuclear hormone receptor coactivator SRC-1 is a specific target of p300. *Proc. Natl. Acad. Sci.* **93:** 10626–10631.

Yao, T.P., S.P. Oh, M. Fuchs, N.-D. Zhou, L.-E. Ch'ng, D. Newsome, R.T. Bronson, E. Li, D.M. Livingston, and R. Eckner. 1998. Gene dosage-dependent embryonic development and proliferation defects in mice lacking the transcriptional integrator p300. *Cell* **93:** 361–472.

APPENDICES: PART B

A modification of representational difference analysis applied to the isolation of forskolin-regulated genes from Schwann cells

John R. Bermingham, Jr.[1], Sue Shumas[2], Tom Whisenhunt[3], Michael G. Rosenfeld[3], and Steven S. Scherer[2]

[1]McLaughlin Research Institute
1520 23rd Street South
Great Falls, MT
(406) 454-6003
Fax: (406) 454-6019
Email: jrbjr@po.mri.montana.edu

[2]Dept. of Neurology, Room 460
Stemmler Hall
36th Street and Hamilton Walk
University of Pennsylvania
Philadelphia PA 19104-6077
(215) 573-3198

[3]Howard Hughes Medical Institute
Department of Medicine
University of California, San Diego
9500 Gilman Drive 0648
La Jolla CA 92093-0648
(619) 534-5858

Running Title: Forskolin regulated Schwann cell genes.

ABSTRACT

Many aspects of Schwann cell differentiation can be induced *in vitro* by the adenylyl cyclase activator forskolin. However, the role of cAMP signalling in regulating the response of Schwann cells to axonal cues *in vivo* remains unclear. To better understand the role of cAMP signalling in Schwann cell differentiation, we used cDNA representational difference analysis (RDA) to isolate differentially expressed genes from Schwann cells cultured with or without forskolin. We isolated additional forskolin-regulated genes, including MKP-3, a regulator of ERK signalling, and the sphingosine-1-phosphate receptor edg-3/lp_{B3}. These genes could play important roles in mediating the differentiation of Schwann cells. Furthermore, we demonstrate a modification of cDNA RDA that will be useful in assaying differential gene expression using small amounts or RNA.

INTRODUCTION

Schwann cells are the main glial cells of the PNS. Myelinating Schwann cells form a single myelin sheath around a single axon, whereas non-myelinating Schwann cells typically ensheathe several unmyelinated axons. Axons are thought to regulate the differentiation of Schwann cells: presumptive myelinated axons signal Schwann cells into the myelinating lineage, whereas the axons lacking this signal remain associated with non-myelinating Schwann cells (reviewed in [Taylor, 1997 #11; Mirsky, 1999 #279]. Although the nature of the axonal signal(s) that promote myelination remain unknown, cAMP signalling appears to be a critical mediator of axon-induced Schwann cell development.

Many aspects of axon-induced Schwann cell proliferation and differentiation can be mimicked by the adenylate cyclase activator forskolin or the membrane permeable analogue of cAMP, dibutryl cAMP. Forskolin synergistically potentiates the effects of Schwann cell mitogens, including neuregulins, fibroblast growth factors, platelet-derived growth factors, insulin-like growth factors, and TGF-betas [Eccleston, 1992 #220; Dong, 1997 #221]. cAMP signalling also regulates Schwann cell differentiation [Morgan, 1991 #35; Morgan, 1994 #36; Cheng, 1996 #234; Dong, 1997 #221]. Forskolin induces the expression of the mRNAs for many myelin-related genes, including P0, MBP, myelin P2, PMP-22, and connexin 32 [Lemke, 1988 #192; Monuki, 1989 #4; Suter, 1994 #202; Scherer, 1995 #227]. Conversely, forskolin inhibits the expression of genes that are expressed by non-myelinating and denervated Schwann cells, such as p75, brain-derived neurotrophic factor, and growth-associated protein 43 kDa [Lemke, 1988 #192; Curtis, 1992 #236; Meyer, 1992 #237; Scherer, 1994 #238]. Forskolin also reduces expression of the transcription factors Pax-3 and c-jun, which are expressed by non-myelinating and denervated Schwann cells, and increases the expression of Tst-1/Oct-6/SCIP and Krox-20, which are expressed by promyelinating and myelinating

Schwann cells, respectively [Kioussi, 1995 #239; Monuki, 1989 #4; Zorick, 1996 #9; Arroyo, 1998 #66]. Tst-1/Oct-6/SCIP and Krox-20 are required for normal myelination by Schwann cells [Bermingham, 1996 #1; Jaegle, 1996 #2; Topilko, 1994 #12]. These data indicate that cAMP may be a second messenger of axonal signal(s) that promote myelination. However, the role of cAMP signalling in regulating the phenotype of Schwann cells is unclear. In cultured Schwann cells, forskolin can promote both proliferation and differentiation. In injured nerves, an *in vivo* model of Schwann cell differentiation, intracellular cAMP levels rise after re-expression of P0, and increasing the concentration of intracellular cAMP does not induce myelin gene expression [Poduslo, 1995 #13]. The identification of additional genes that are regulated by forskolin in Schwann cells would enhance our understanding of the functions of cAMP signalling in Schwann cell differentiation. These genes could represent upstream regulators or targets of the forskolin-induced transcription factors Tst-1/Oct-6/SCIP and Krox-20, or they could be components of additional, independent regulatory pathways.

Representational difference analysis (RDA) is one of several techniques for isolating differentially expressed genes (reviewed in [Sagerstrom, 1997 #182]. Here we demonstrate a modification of RDA that can be performed on one microgram or less of total RNA. We piloted this modification using RNA isolated from Schwann cells grown with or without forskolin, an activator of adenylate cyclase [Seamon, 1986 #198], as this was a relevant cellular model of myelination. We report the isolation of additional forskolin-induced or –repressed genes, several of which may regulate Schwann cell differentiation perhaps by linking cAMP signalling to other signal transduction pathways.

RESULTS

RDA of Schwann cells following forskolin stimulation

RDA is a PCR-based technique that permits the isolation of DNA fragments that are present in one DNA sample but absent in another [Lisitsyn, 1993 #199; Lisitsyn, 1995 #200]. The procedure (as applied to cDNA) is summarized as follows. cDNAs from two sources are digested with a restriction enzyme (typically DpnII) that cleaves at a four base recognition site to generate fragments with an average size of approximately 250 bp. Linkers are ligated to the resulting overhangs to provide primer binding sites for the PCR amplification, after which the linkers are removed. For a small portion of the material, new linkers are added; this material will serve as "tester" cDNA. Tester cDNA from one source is denatured and reannealed in the presence of excess PCR-amplified cDNA from a second source, which serves as "driver". If a single-stranded DNA consists of sequences that are present in both driver and tester, it will reanneal predominantly with cognate driver DNA. However, single-stranded DNAs with sequences that are present in the tester, but are absent in the driver, will reanneal with other tester-derived DNAs. Only reannealed DNAs that consist of two strands of tester DNA will possess the new linkers at both ends that allow subsequent re-amplification by PCR.

We used total RNA derived from rat Schwann cells that had been cultured for three days in the presence (+F) or absence (–F) of 20 μM forskolin. Four RDA experiments were performed; one pair of experiments screened for genes that are upregulated by forskolin (using –F cDNA as the driver); the other pair screened for genes that are downregulated by forskolin (using +F cDNA as the driver). These experiments also served as controls for each other, as no genes should be both up-and downregulated by forskolin. One pair of experiments used 10μg of total RNA (for both the +F and –F RNA samples) while the other pair used 1μg total RNA (for both the +F and –F RNA

samples) plus 1μg of a "carrier" mRNA. This carrier was derived from *in vitro* transcription of a DNA fragment from the P1 promoter of the *Drosophila Antennapedia* gene, to which a poly A:T sequence had been added (see Materials and Methods). After cDNA synthesis and DpnII digestion, those fragments with two appropriately spaced adaptors (50-600 bp under the conditions used here), were amplified by two rounds of PCR. Figure 1 shows the PCR-amplified cDNA for all four samples. This material was used as "driver" for two rounds of denaturation, reannealing with tester DNA, and PCR amplification. The DNAs that result from the first round of selection, the first difference products (DP1), and the second round, the second difference products, (DP2), are also shown in Figure 1. The DP1 and DP2 DNAs can be distinguished from driver in the enhancement of specific bands. For those samples to which carrier had been added, a band whose size is consistent with aberrant amplification of carrier cDNA can be seen in the driver DNAs. Given the substantial amount of carrier added in these experiments, this observation is not surprising. The putative carrier-derived DNA is removed by the first round of RDA, and the band is absent in the DP1 samples.

DP2 DNAs were shotgun cloned into BamHI-digested pBKSII$^+$ plasmid DNA, and 96 clones were sequenced. Some clones contained multiple inserts; 135 total inserts were analyzed. 66 inserts were derived from experiments that selected for forskolin-upregulated cDNAs, of which 40 were isolated without carrier mRNA, and 26 with carrier. Similarly, 69 inserts were derived from experiments that selected for cDNAs that were downregulated by forskolin, of which 43 were isolated without carrier, and 26 with carrier. 15 inserts (11%) were likely to be artifactual, because they appeared to be both up-regulated and downregulated by forskolin. The genes that are putatively activated or repressed by forskolin in Schwann cells are tabulated in Table 1. Several genes that have been shown previously to be expressed in Schwann cells were isolated, and two of these genes, P0, and PMP22, have been shown previously to be upregulated by forskolin in Schwann cells [Lemke, 1988 #192; Suter, 1994

#202]. Although Tst-1/Oct-6/SCIP also is induced by forskolin in Schwann cells [Monuki, 1989 #4], we found that rat Tst-1/Oct-6/SCIP is not easily amplified under the conditions used (data not shown). Many genes are represented by single inserts, indicating many more genes may be differentially expressed that were not identified in this limited sample.

We selected 11 putative upregulated clones, and 12 putative downregulated clones for further analysis based on either their sequences, or the results of dot blots probed with +F or –F drivers (data not shown). The inserts were radiolabelled, and used to probe equal amounts of +F and –F driver DNA that had been electrophoresed, and transferred to a nylon membrane. These "snorthern" blots are technically Southern blots, but like a northern blot, they indicate whether a given sequence is expressed in a given tissue. Of 23 inserts that were tested, 19 appeared to be differentially expressed by snorthern blot (Table 1), representative examples of which are shown in Figure 2. Several genes that are known to be expressed in Schwann cells were tested. Myelin and lymphocyte protein (MAL), CD9, and NF-L, are expressed in differentiating Schwann cells [Schaeren-Wiemers, 1995 #163; Frank, 1998 #203; Kaprielian, 1995 #204; Kelly, 1992 #206; Fabrizi, 1997 #207], and our observation that they may be upregulated by forskolin is expected. In contrast, the Schwann cell expression of vimentin, dystroglycan, and prosaposin [Autilio-Gambetti, 1982 #208; Neuberger, 1989 #209; Yamada, 1994 #212; Yamada, 1996 #214; Hiraiwa, 1997 #218], appears not to be regulated by forskolin (Figure 2 and data not shown). Six of eight genes that were isolated from RDA experiments that used carrier mRNA were tested by snorthern hybridization and appear to be differentially expressed, including three genes isolated both by experiments with and without carrier, NF-L, unknown gene 40-8, and γ-filamin. Of the genes that we selected for further analysis, the efficiency with which differentially expressed genes were recovered from experiments using carrier was 75%, not significantly different from the overall efficiency of 83%. These results indicate that RDA effectively selects for

differentially expressed cDNAs, and that the use of carrier mRNA does not interfere with the procedure.

To determine whether the snorthern blots were accurate, several clones were chosen for RNase protection. Since RDA cDNA clones contained inserts that were typically between 200 – 400 bp, they could be used directly to produce antisense RNA of an appropriate length for RNase protection. Total RNA isolated from forskolin-treated and –untreated Schwann cells, was hybridized with antisense RNA from 10 clones that correspond to genes putatively upregulated (edg-3/LP_{B3}, MAL, NF-L, MGP-3, ecto-ATPase, RDA65), downregulated (K13, Ulip, GPR41) or unaffected (prosaposin) by forskolin (Figure 3). For 10 of the 11 clones tested, the RNase protection results confirmed the snorthern blot results. The exception is the G-protein coupled receptor edg-3/lp_{B3}, in which the snorthern blots showed no significant regulation by forskolin, perhaps due to cross-hybridization to the closely related receptors edg-1/LP_{B1} and edg-2/LP_{A1} which also are expressed by Schwann cells [Allard, 1998 #144; Weiner, 1999 #402], while the RNase protections demonstrated that edg-3/lp_{B3} mRNA is upregulated by forskolin. These results demonstrate that differential expression on snorthern blots is an excellent indicator of whether a cDNA is differentially regulated.

Tst-1/Oct-6/SCIP is a POU domain transcription factor that is required for timely peripheral myelination [Bermingham, 1996 #1; Jaegle, 1996 #2] and is induced in cultured Schwann cells by forskolin [Monuki, 1989 #4]. We wished to determine if any of the forskolin-regulated genes that we isolated are differentially expressed in the absence of Tst-1/Oct-6/SCIP; if so, they could mediate Tst-1/Oct-6/SCIP function during Schwann cell differentiation. The expression of several clones was examined by hybridization to snorthern blots of PCR-amplified sciatic nerve cDNA from P0 (= the day of birth) wild-type or *Tst-1/Oct-6/SCIP* (-/-) pups, or by in situ hybridization. The snorthern blot analysis demonstrates that MKP-3 and ecto-ATPase, which are upregulated by

forskolin, and Ulip, which is downregulated by forskolin, are expressed in sciatic nerve, but are not regulated by Tst-1/Oct-6/SCIP (Figure 4A). Similarly, we determined that mRNAs for MAL, CD9, NF-L, and the unknown gene RDA40-8 are not regulated by Tst-1/Oct-6/SCIP (data not shown). We examined the expression of edg-3/lp_{B3} in P0 *Tst-1/Oct-6/Scip* +/+ and −/− mouse sciatic nerve by in situ hybridization (Figure 4B). At P0, edg-3/lp_{B3} mRNA was abundantly expressed in sciatic nerve, in both *Tst-1/Oct-6/Scip* +/+ and -/- mice, demonstrating that its expression does not directly depend on Tst-1/Oct-6/SCIP.

The response of Schwann cells to nerve injury has been studied extensively as a model of their differentiation. The steady state levels of many myelin-related mRNAs fall dramatically within a few days of axotomy, which is thought to reflect a profound decrease in their rates of transcription. We wished to determine whether the expression of several of the forskolin-regulated genes that we have identified is modulated by nerve injury; if so, their patterns of expression would determine if the genes are expressed in differentiated or immature Schwann cells. Total RNA was isolated from the distal stumps of rat sciatic nerve at various times following transection or crushing, and used to generate a northern blot that was probed sequentially with cDNA clones corresponding to MKP-3, edg-3/lp_{B3}, and ecto-ATPase, P0, 75NGFR, and a "housekeeping" gene, GAPDH. MKP-3, edg-3/lp_{B3}, and ecto-ATPase were expressed both before and after injury (Figure 5, and data not shown), in contrast to the marked changes in P0 and P75 NGFR mRNAs. However, the mRNA levels of MKP-3 and edg-3/lp_{B3} did increase transiently at one day following transection when their expression was compared to that of GAPDH, or to ecto-ATPase.

These results, taken together, demonstrate that our modification of RDA can be used to isolate genes that are both up-regulated and downregulated. Because many of the genes that are differentially expressed in

forskolin-stimulated Schwann cells are expressed by Schwann cells *in vivo*, the analysis of these genes is a promising approach toward understanding the mechanisms by which increases in intracellular cAMP affect Schwann cell differentiation. Not all genes whose mRNA levels are up-regulated by forskolin *in vitro* are down-regulated by axotomy *in vivo*, demonstrating a shortcoming in the model that forskolin promotes differentiation into a myelinating phenotype.

DISCUSSION

Technical considerations

RDA using cDNA offers concrete advantages over other, currently available techniques for differential gene expression. Differential display is another PCR-based method for detecting differentially expressed genes. The cDNA fragments that are obtained by differential display are strongly biased toward the 3' ends of genes, many of which are not present in the current databases. Therefore additional cDNA sequences often must be isolated before the candidate gene can be identified. A comparison between differential display and subtractive hybridization revealed that these techniques generate overlapping but distinct sets of differentially expressed genes [Wan, 1996 #191]. Serial analysis of gene ends (SAGE) [Velculescu, 1995 #398] involves the sequencing of concatamers of small fragments of cDNA 3' ends. Extensive sequencing is required to reliably determine if a gene is differentially expressed, and again, additional work often will be required to identify the gene in question. Arrays of cDNAs are the newest and potentially the most powerful way to identify differentially expressed genes, but are limited to the cDNAs that are on the array. Thus, until arrays become available that contain all of the genes expressed by the tissue or cell type of interest, RDA using cDNA will remain a useful approach for differential gene analysis. An additional advantage of RDA, as shown in this paper, is that the lengths of the isolated sequences are appropriate for RNase protections, so that candidates can be rapidly confirmed by an independent and more definitive technique. Here we demonstrate that addition of a carrier RNA to a microgram or less of total RNA permits RDA to be performed using small amounts of starting material.

We applied our modification of RDA to cDNA from forskolin-stimulated Schwann cells, and we isolated both forskolin-induced and

–repressed genes. The genes that we identified with this approach include genes known to be expressed by Schwann cells (and to be affected by forskolin stimulation) but also potentially novel genes whose roles in Schwann cell biology have not yet been established. It is unlikely that we have identified all of the Schwann cell genes that are regulated by forskolin. For the sequences that we have analyzed, the proportion that are represented by single isolates suggests that our sampling of RDA-enriched sequences is incomplete. Furthermore, RDA does not amplify equally all sequences or cDNAs. Sequences at the extreme 5′ and 3′ end of cDNAs are not amplified because they cannot be linkered. The PCR conditions that we have used bias against G-C rich sequences (data not shown), and cDNAs that lack appropriately spaced restriction sites (less than approximately 600nt apart). The drivers and testers were reannealed to a Cot of approximately 300-400; sequences from transcripts that are present in only a few copies per cell may not have had sufficient time to reassociate. Nevertheless, we isolated genes that are not abundantly expressed, indicating that the technique can identify such genes.

cAMP signalling in Schwann cells

To better understand the role played by cAMP signalling in Schwann cell differentiation, we characterized 11 putative forskolin-induced and 9 putative forskolin-repressed genes from cultured Schwann cells. The identities of several of the induced genes suggest that cAMP signalling regulates Schwann cell differentiation at least in part through the modulation of other signal transduction pathways. Although cAMP signalling induces myelin-related genes [Lemke, 1988 #192], it is not sufficient to promote a myelinating phenotype. Following nerve crush, recovery of intracellular cAMP levels follows a delayed time course relative to P0 mRNA levels, and increases in intracellular cAMP in injured nerves, mediated by forskolin and phosphodiesterase inhibitors, fail to induce myelin genes [Poduslo, 1995 #13]. Many effects of cAMP signalling are mediated through phosphorylation of CREB by PKA (reviewed in [Andrisani, 1999 #399]. Stimulation of Schwann

cells by forskolin and other growth factors produces transient CREB phosphorylation, while CREB phosphorylation following neuregulin treatment is sustained [Tabernero, 1998 #55; Rahmatullah, 1998 #401]. Axon-induced CREB phosphorylation in Schwann cells appears to be dependent on both PKA and PKC activity [Lee, 1999 #280]. These observations suggest that additional signalling pathways function in the induction or maintenance of a myelinating phenotype. Several of the forskolin-regulated genes that we found may modulate other signal transduction pathways; two of these are diagrammed in figure 6.

We found that edg-3/LP_{B3} (figure 6A), a G protein-coupled receptor for sphingosine-1-phosphate (S1P) [Yamaguchi, 1996 #154; An, 1997 #251; Zhang, 1999 #250; Van Brocklyn, 1999 #247], is induced by forskolin in cultured Schwann cells, and is downregulated in sciatic nerve as Schwann cells myelinate. S1P has profound effects on intracellular signalling pathways: it can mobilize intracellular Ca^{2+}, activate MAP/ERK kinase signalling pathways, and alter cAMP levels [Spiegel, 1996 #249; Merrill, 1997 #248; Spiegel, 1998 #246]. S1P activation of phospholipase C and Ca^{2+} is enhanced by edg-3/LP_{B3} [An, 1997 #251; Sato, 1999 #347]. edg-3/LP_{B3} can mediate changes in cell morphology in response to S1P [Van Brocklyn, 1999 #247], suggesting that signalling through the edg-3/LP_{B3} receptor may trigger some of the cytoskeletal changes that accompany myelination. Alternatively, S1P can suppress ceramide-mediated apoptosis (reviewed in [Spiegel, 1998 #246]. Premyelinating rat Schwann cells undergo extensive apoptosis soon after birth that can be prevented by contact with axons, or by neuregulins [Nakao, 1997 #252; Grinspan, 1996 #253; Syroid, 1996 #54]. The expression of edg-3/LP_{B3} at this time could modulate apoptotic signalling. These observations suggest that expression of edg-3/LP_{B3} may be an important step in Schwann cell differentiation.

MKP-3 (Pyst1, rVH6; figure 6B) is a cytosolic dual specificity protein phosphatase that specifically deactivates the ERK class of mitogen-activated

protein kinases [Muda, 1996 #185; Groom, 1996 #283]. ERKs and MKP-3 form a regulatory feedback loop that may limit ERK signalling, because activated ERK2 stimulates MKP-3 phosphatase activity through direct binding to MKP-3 [Camps, 1998 #188]; ERK activation also appears to induce transcription of the *mkp-3* gene [Mourey, 1996 #189; Muda, 1996 #187]. We have found that MKP-3 mRNA expression is induced by forskolin in cultured Schwann cells. MKP-3 induction by forskolin may be mediated by ERKs, or it may represent an independent mode of activation. In Schwann cells, adipocytes and CHO cells, mitogen activation of ERKs is attenuated by forskolin [Kim, 1997 #29; Sevetson, 1993 #391]; in Schwann cells, this effect does not involve inactivation of Raf-1 by PKA that has been observed elsewhere [Cook, 1993 #400; Kim, 1997 #29]. Based on our findings, we suggest these observations result from MKP-3 induction. We have shown also that MKP-3 is expressed in sciatic nerve *in vivo*, independently of Tst-1/Oct-6/SCIP, and is transiently upregulated following sciatic nerve transection. Thus MKP-3 induction is regulated by transcription factor(s) other than Tst-1/Oct-6/SCIP, such as CREB or Krox-20, and its expression correlates with changes in the differentiation state of Schwann cells. Mitogenic signalling requires ERK activation (reviewed in [Robinson, 1997 #184]. Our observations suggest that MKP-3 induction represents a potentially important mechanism of cross-regulation between ERK and cAMP signalling pathways, and that MKP-3 could play an important role in the transition of Schwann cells between proliferating and non-proliferating stages.

Ecto-ATPases terminate extracellular ATP signalling by ATP hydrolysis (reviewed in [Zimmermann, 1998 #260]. Schwann cells respond to extracellular ATP by increasing intracellular calcium concentrations, stimulating phospholipase C, decreasing adenylyl cyclase activity, and by releasing the excitatory amino acids glutamate and aspartate [Lyons, 1994 #32; Lyons, 1995 #257; Amedee, 1995 #258; Berti-Mattera, 1996 #21; Mayer, 1997 #262; Ansselin, 1997 #259; Jeftinija, 1998 #263]. The response to extracellular

ATP is stimulated by agents that increase intracellular cAMP, and by axonal contact [Lyons, 1994 #32; Lyons, 1995 #257]. We isolated multiple independent RDA clones for a transmembrane ecto-ATPase [Kegel, 1997 #261] and found that it is induced by forskolin treatment of Schwann cells, and is expressed in sciatic nerve. These results suggest that the response of Schwann cells to extracellular ATP results from a balance of the opposed activities of ATP receptors, ecto-ATPases, and levels of intracellular cAMP. The absence of nerve injury modulation of ecto-ATPase expression suggests that it functions in the homeostasis of Schwann cells, rather than in their differentiation.

We also found several forskolin-repressed genes, including K13, CD11c and Ulip1. K13 defines a new subfamily of K^+ channel [Drewe, 1992 #392; Verma-Kurvari, 1997 #393]; its human homolog is called kH2 [Su, 1997 #394]. Its repression by forskolin suggests that it is present in undifferentiated Schwann cells. One of two types of K^+ conductance also is downregulated by forskolin in Schwann cells [Despeyroux, 1997 #395], and there is a correlation between K^+ channel function and proliferation during Wallerian degeneration [Chiu, 1989 #396]. Perhaps K13 channel function is responsible for these observations, at least in part. CD11c (integrin αX) mediates leucocyte adhesion and signal transduction (reviewed in [Mazzone, 1995 #255]; it could function in the adhesion of immature Schwann cells to axons, and/or their basal laminae. It has been shown to be upregulated by c-jun, [Noti, 1996 #256]; we find that it, like c-jun [Monuki, 1989 #4], is downregulated in forskolin-treated Schwann cells. Ulip1 is homologous to Unc-33, a phosphoprotein in *C. elegans* that is involved in axonal outgrowth and guidance [Byk, 1996 #173], and is transiently expressed during neuronal differentiation in the brain [Byk, 1998 #172]. In Schwann cells, Ulip1 could play a similar role, perhaps in the initial wrapping of axons. By analogy to other forskolin-repressed genes, these genes may be expressed by "denervated" Schwann cells, which play essential roles in promoting axonal regeneration and reinnervation of denervated muscle cells [Scherer, 1996 #254].

Gene expression in Schwann cells in response to nerve injury.

Injury of peripheral nerve causes dedifferentiation of Schwann cells distal to the injury (reviewed in Poduslo, 1993, Stoll and Muller, 1999; [Scherer, 1996 #254]. Dedifferentiation down-regulates the expression of many genes that function in myelinating Schwann cells. In contrast, expression of mRNAs that are diagnostic for undifferentiated Schwann cells, such as P75NGFR, display an opposite expression pattern, increasing following injury. The RDA screen for forskolin-regulated genes has produced several genes in common with differential hybridization screens for genes that are activated or repressed following nerve injury [De Leon, 1991 #405; Gillen, 1995 #403], including PMP-22 and MAL. These genes, and P0, represent bona fide injury- and forskolin-regulated genes that have been isolated because their expression was both reduced in injured nerve and induced by forskolin. In contrast, NF-L was upregulated by forskolin, but is also upregulated after axotomy [Fabrizi, 1997 #207]. The modulation of expression of edg-3/lp_{B3} and MKP-3 by nerve injury was modest compared to other markers of Schwann cell differentiation. However, we have observed transient increases in edg-3/lp_{B3} and MKP-3 expression one day following nerve transection. In both cases, the mRNA levels for both genes had declined by four days after the injury. The induction of edg-3/lp_{B3} and MKP-3 may result from a transient increase in intracellular cAMP following nerve injury [Poduslo, 1995 #13], and suggests that signalling by sphingosine-1-phosphate, or inhibition of ERK signalling, could mediate early responses to nerve injury. Thus, a discrete stage in Schwann cell differentiation may be marked by elevated expression of these genes. Together, these results indicate a complicated relationship between forskolin gene induction in cultured Schwann cells and Schwann cell differentiation and de-differentiation *in vivo*.

In addition to demonstrating that our modification of RDA works, the characterization of forskolin-induced and -repressed genes indicates that

altering the levels of intracellular cAMP in Schwann cells induces extensive changes in the signal transduction machinery in these cells. The majority of forskolin-regulated genes described here and elsewhere are expressed independently of Tst-1/Oct-6/SCIP, indicating that other transcription factors regulate their expression. Indeed, some of the signalling molecules that are regulated by forskolin in Schwann cells may be involved in the activation of Tst-1/Oct-6/SCIP, or Krox-20.

MATERIALS AND METHODS

Schwann cell culture: Schwann cells were isolated from 3 day old rat pups [Brockes, 1979 #241], and expanded on 10 cm plates coated with poly-L-lysine in DME supplemented with 10% FCS, 2 μM forskolin [Porter, 1987 #268], and 10 ng/ml recombinant human secreted β isoform of neuregulin (rhGGF2). The cells were passaged 6 times, grown to confluence, then maintained for 3 days in DMEM and 10% FCS. The cells were maintained for an additional 3 days in DMEM and 10% FCS alone, or supplemented with 20 μM forskolin. All of the cultures used in these experiments were essentially free of fibroblasts. RNA was isolated by $CsCl_2$ gradient centrifugation [Chirgwin, 1979 #242].

Carrier: The template that encodes the carrier was generated as follows: a 584 bp BstX1-XbaI fragment of *Drosophila* genomic DNA, located 1310 bp 5′ to the transcription initiation site of the *Antennapedia* P1 promotor [Laughon, 1986 #128], chosen because it lacks sites for DpnII and Nla III, was cloned into the XbaI and SmaI sites of pBKS. Oligonucleotides that encode an artificial poly A tract were introduced by adjacent to the *Antp* sequences. The carrier itself was synthesized in vitro using T7 polymerase (Promega).

cDNA synthesis: For the cultured Schwann cell experiments that tested the carrier RNA, 1μg of carrier RNA was added to 1μg of total RNA. For subsequent experiments that used mouse sciatic nerve tissue, 150ng of carrier RNA was added to 1μg of total RNA. In this case, the amount of carrier added was designed to bring the total amount of poly A+ RNA to 200 ng. Poly A+ RNA was selected using oligotex beads (Qiagen) and cDNA was synthesized using the Superscript system (Gibco-BRL); both oligo dT and random oligonucleotides were used to prime the first strand synthesis.

Representational Difference Analysis: The RDA procedure was performed essentially as described [Lisitsyn, 1995 #201]; [Hubank, 1994 #124]; [Edman, 1997 #126], with the following modifications: Carrier mRNA was added to total RNA for most experiments, prior to the isolation of poly A+ RNA and subsequent cDNA synthesis. cDNAs that were derived from cultured Schwann cells were digested with DpnII, while cDNAs that were derived from mouse tissue were digested, separately, with DpnII and NlaIII. DpnII cleaves at the recognition site GATC, and because the four base 5′ overhang that results from its cleavage is identical to that generated by BglII, the previously designed RDA primers for RDA experiments that utilize BglII could be used to amplify DpnII-generated fragments. "N" adaptors [Lisitsyn, 1995 #201] were ligated to the Dpn II ends, and "O" primers were ligated to NlaIII ends. Those fragments with two appropriately spaced adaptors were amplified by two rounds of PCR. PCR syntheses were performed with Gibco-BRL Taq polymerase and 1x Taq polymerase buffer, 2mM $MgCl_2$ and 0.2mM dNTPs. The first round of PCR consisted of four 50 µl reactions run in parallel for 5 cycles (95°C, 1 min., 72°C, 3 min), then pooled. The second round of PCR consisted of 16 100µl reactions run in parallel for 12 cycles, and subequently pooled. It was determined empirically that amplification remained exponential under these conditions. Typically these reactions yielded 50-600bp fragments. Excess primers were removed from the PCR products using Qiaquick columns (Qiagen). A small proportion of each of the drivers was digested with Dpn II to remove the "N" adaptors, or with NlaIII to remove the "O" adaptors, after which they were replaced with "R" or "S" adaptors, respectively. Each "tester" DNA was mixed with an excess of driver that was derived from the other source, denatured, and permitted to anneal in a 5µl volume at 67°C, under oil, for 24-36 hours, which corresponds to a Cot of approximately 300-400. Because single-copy genomic DNA reassociates between Cot 100 and 10^4, and approximately 3% of the non-repetitive genome is transcribed [Lewin, 1994 #277], a Cot of 3-300 should be sufficient for cDNA. The reannealed DNA was amplified in four

parallel 100µl reactions for 10 cycles of PCR using R or S primers. This material was phenol extracted, ethanol precipitated, resuspended in 2mM Tris, 0.2mM EDTA, and digested with mung bean nuclease (New England Biolabs) to remove the single strands that result from priming at only one end of a template. The resulting material was subjected to a second round of amplification in four parallel 100µl PCR reactions for 16 cycles with R or S primers. DP1 DNA was digested with DpnII or NlaIII to remove the R or S adaptors, after which they were replaced with "J" or "K" adaptors. This material was used as the tester for a second round of subtraction, after mixing with an excess of driver. The products of the second round of subtraction were subjected to two rounds of PCR amplification to produce the second difference products, DP2. The linkers were removed from the DP2 DNA, after which it was cloned. DpnII fragments were ligated into the BamH1 site of pBKSII$^+$ (Stratagene), while the NlaIII fragments were ligated into the Sph site of pGEM7Zf+ (Promega). Ligations were transfected into DH5α (Gibco-BRL).

Adaptors/primers: The J, N, and R oligonucleotides were designed by [Lisitsyn, 1995 #201], for use on genomic RDA with BglII, and are used here with DpnII. The K, O, and S primers are the corresponding adaptors/primers designed to be used with Nla III.

K Sph 24 (RDA with NlaIII):	5' GAC AAC CGA CGT CGA CTA TGC ATG 3'
K Sph 12 (RDA with NlaIII):	5' CAT AGT CGA CGT 3'
O Sph 24 (RDA with NlaIII):	5' AGG CAA CTG TGC TAT CCG AGC ATG 3'
O Sph 12 (RDA with NlaIII):	5' CTC GGA TAG CAC 3'
S Sph 24 (RDA with NlaIII):	5' GGC ACT CTC CAG CCT CTC AGC ATG 3'
S Sph 12 (RDA with NlaIII):	5' CTG AGA GGC TGG 3'

"snorthern" blots: cDNA that was amplified by PCR for use as driver in the RDA experiments was used also for snorthern blots. As described above, the PCR conditions were optimized to ensure that amplification was exponential, and parallel PCR reactions were pooled, to minimize variation from

individual samples, and to obtain sufficient material. 0.5μg or 1μg of driver DNA was electrophoresed through 3% NuSieve 3:1 agarose (FMC) or 4% acrylamide gels, then transferred by conventional Southern blotting or electroblotting onto Hybond N+ membranes (Amersham).

RNase protection assays: Single-stranded anti-sense transcripts were generated with the appropriate RNA polymerase. Equal amounts (10 μg) of total RNA rat Schwann cells were incubated with 100,000 cpm of riboprobes. The RNA was denatured at 85°C for 10 min., hybridized overnight at 48°C, then digested with RNase T1 and RNase A (final concentrations 1 μg/μl and 40 μg/ml, respectively) for 1 hour at 30°C. The reaction was stopped by adding proteinase K and SDS (final concentrations 0.28 μg/μl and 0.56%, respectively) for 30 min. at 37°C. The RNA was purified by phenol-chloroform extraction and precipitation with LiCl, yeast tRNA, and 100% ethanol. The RNA pellet was resuspended in loading dye, counted, and the protected fragments were separated on a sequencing gel.

***In situ* hybridization:** Mice were anesthetized and perfused with formalin. Hindquarters were dissected to expose the sciatic nerve, then stored in at 4°C in formalin. Tissues were frozen in a 1:1 mixture of OCT and Aquamount, and sectioned at 20 microns. In situ hybridization was performed as described in [Simmons, 1989 #175]. The probes used were as follows: edg-3/lp_{B3}: a 291 bp RDA clone that contains sequence between the DpnII sites at positions 423 and 713 of AF108021; P0: rat cDNA as described in [Bermingham, 1996 #1].

Northern blot analysis of normal and lesioned adult rat sciatic nerves: Adult Sprague Dawley rats were anesthetized with 50 mg/kg pentobarbitol i.p., and the sciatic nerves were exposed at the obturator tendon. To prevent axonal regeneration, nerves were doubly ligated and transected between the ligatures. Nerves were crushed by compression with flattened forceps twice, each time for 10 seconds. Animals were allowed to survive for various periods of time

prior to sacrifice by $C0_2$ inhalation. For RNA extraction, several millimeters of nerve adjacent to the lesion site were trimmed off, and the distal nerve-stumps were frozen in liquid nitrogen. Where indicated, the distal stumps of crushed nerves were subdivided into proximal and distal segments of equal lengths. Unlesioned nerves were taken from animals of various ages. Total RNA was isolated from the sciatic nerves by $CsCl_2$ gradient centrifugation [Chirgwin, 1979 #242]. Equal samples (10 μg) of RNA were electrophoresed in 1% agarose, 2.2 M formaldehyde gels, transferred to nylon membranes in 6X SSC, and UV cross-linked (0.12 joules). Blots were prehybridized, hybridized, and washed using standard techniques [Sambrook, 1989 #397]. cDNA probes were ^{32}P-labeled with specific activities of 2-5 x 10^9 cpm/mg, prepared by primer extension with random hexamers using the Prim-a-gene kit (Promega) according to the manufacturer's instructions. Probes were obtained as follows: For MKP-3, edg-3/lp_{B3}, and ecto-ATPase, cDNAs that comprise the entire coding region, 1.1kb, 1.1kb, and 1.5kb, respectively, were amplified by PCR from rat P0-P2 sciatic nerve cDNA using the following primers: MKP-3 sense: 5′ TCC TGC AGC TCG ACC CCC ATG ATA GAT ACG CT 3′; MKP-3 antisense: 5′ CAA GAG AAA CTG AAG GAA TGA GAC ACT CCC GGC TAG G 3′. Edg-3/lp_{B3} sense: 5′ CCA TGG CAA CCA CGC ATG CGC AGG 3′; edg-3/lp_{B3} antisense: 5′ CAC TTG CAG AGG ACC CCG TTC TGA AAC GAC C 3′. Ecto-ATPase sense: 5′ ACC ATG GCT GGA AAG TTG GTG TCA CTG GTG CC 3′; ecto-ATPase antisense: 5′ CTC ATG AGG GCG CCT GGA GAC TTG GCA GA 3′. After confirmation of their identity by sequencing, these cDNAs were used as probes. Other probes used were a full length cDNA (2.0 kb) of rat P0 [Lemke, 1985 #407], a 0.7 kb BamHI fragment of rat NGFR [Radeke, 1987 #409], and a full-length (1.3 kb) cDNA of glyceraldehyde 3-phosphate dehydrogenase (GAPDH) [Fort, 1985 #406].

FIGURE AND TABLE LEGENDS:

Figure 1: Ethidium bromide stained acrylamide gel of drivers, difference product 1 (DP1), difference product 2 (DP2) DNAs from cultured Schwann cells. +F: cDNA derived from Schwann cells cultured with forskolin; –F: cDNA derived from Schwann cells cultured without forskolin; +FC: +F cDNA generated with carrier; –FC: –F cDNA generated with carrier; M: ϕX174 HaeIII digest. Driver DNAs: In these experiments, amplification of carrier mRNA generated a band of approximately 700bp. Faint bands, presumably due to ribosomal RNA or other highly repetitive RNAs, can be seen. DP1 DNAs: After one round of RDA, specific bands begin to appear, and the carrier band is absent. DP2 DNAs: After two rounds of RDA, distinct banding patterns seen in +F, –F lanes. The patterns are less distinct in the samples with carrier, suggesting that in these experiments, a third round of RDA would increase their efficacy. DP2 DNAs were cloned into pBKSII+ for analysis.

Figure 2: Snorthern blots of select differentially expressed Schwann cell genes. Evaluation of RDA clones demonstrates that some are activated, some are repressed, and some are unregulated by forskolin. +F and –F refer to PCR-amplified cDNA from Schwann cells treated or untreated with forskolin. The sizes of known hybridizing bands are indicated on the right of each autoradiograph, and include 48bp that is derived from 24bp linkers on each end of the amplified DNA. Because cDNAs vary in PCR efficiency, and the probe sizes and exposure times varied between clones, the intensities of hybridization signals on different autoradiographs are not reliable indicators of relative mRNA abundance. **RDA8:** MAL appears to be activated; **RDA20:** double insert clone. RRP22 (503bp) and KIAA0013 (351bp) both appear to be repressed; **RDA21:** K13 appears to be repressed; **RDA40-8:** unknown gene 40,70, a sequence that was isolated both with and without carrier mRNA, appears to be activated; **RDA62-17:** MKP-3 appears to be activated; **RDA63:** NF-L, also

isolated both with and without carrier, appears to be activated; **RDA65:** This clone corresponds to expressed sequence tag (EST) cDNAs from kidney (AI232310), ganglia (AW530272), and embryos (AW141798). RDA clones with and without a putative intron were isolated; RDA65 contains the intron. The 384bp band corresponds to the expected size of the fragment with the intron, while the 212bp band corresponds to the expected size of the fragment without the intron. **RDA67:** Prosaposin appears to be unregulated by forskolin, and the probe hybridizes to multiple bands in addition to the expected fragment at 420bp. **RDA76:** Ulip1 appears to be repressed by forskolin. The 316bp band is expected, while the larger band may correspond to a splice variant, or a related gene. **RDA79:** double insert clone CD11c (315bp) and GPR41 (418bp). GPR41 alone hybridizes only to the 418bp fragment (data not shown).

Figure 3: RNAse protections confirm that differentially expressed genes have been isolated.

For each gene, lanes consist of undigested probe (P), probe protected by RNA from forskolin-treated Schwann cells (+F), and probe protected by RNA from untreated Schwann cells (–F), and unprotected probe (U). The relevant protected fragments are marked with arrows, and their sizes are highlighted in black. Sizes of fragments were verified by comparison with radiolabelled marker DNA that was elecrophoresed in parallel for each experiment (not shown). In some experiments, a 180bp GAPDH probe was added as an internal standard; it produces a protected fragment of 160bp. **A.** Myelin and lymphocyte protein (MAL) expression is induced by forskolin. Probe: 343bp; protected fragment: 253bp. **B.** RDA65 (EST) is induced by forskolin. Probe: 426bp; protected fragment: 336bp. **C.** Prosaposin is not regulated by forskolin. Probe: 467bp; protected fragment: 377bp. **D.** ecto-ATPase expression is induced by forskolin. Probe: 167bp; protected fragment: 122bp. **E.** Phosphatase MKP-3 is induced by forskolin. MKP-3 probe: 316bp; MKP-3 protected fragment: 230bp. **F.** NF-L expression is upregulated by forskolin. NF-L probe: 347bp; NF-L protected fragment: 261bp. **G.** Potassium channel K13 expression is

downregulated by forskolin. K13 probe: 454bp; K13 protected fragment: 363bp; **H.** Forskolin treatment increases expression of edg-3/lp_{B3} . edg-3/lp_{B3} probe: 358bp; edg-3/lp_{B3} protected fragment: 291bp. **I.** ULIP1 expression is moderately downregulated by forskolin. ULIP1 probe: 354bp; ULIP1 protected fragment: 268bp. **J.** GPR41 is downregulated by forskolin. GPR41 probe: 431bp; protected fragment: 368bp.

Figure 4: Cultured Schwann cell cDNAs isolated by RDA do not appear to be regulated by Tst-1/Oct-6/SCIP.

A. Snorthern blots of cDNA from sciatic nerve: Pairs of lanes consist of Tst-1/Oct-6/SCIP (+/+) and (–/–) PCR-amplified sciatic nerve cDNA. Ecto-ATPase and MKP-3 are upregulated by forskolin, while Ulip is downregulated by forskolin; all are expressed in sciatic nerve, and their expression levels appear not to be altered by the absence of Tst-1/Oct-6/SCIP. G in the Ulip panel refers to genomic DNA; its distinct hybridization pattern shows that the hybridization pattern from PCR-amplified cDNA does not result from contamination of genomic DNA.

B. Detection of edg-3/lp_{B3} in sciatic nerve by *in situ* hybridization: Strong edg-3/lp_{B3} expression is seen at P0, in both Tst-1/Oct-6/SCIP (+/+) and (–/–) sciatic nerves, indicating that edg-3/lp_{B3} is expressed in Schwann cells *in vivo*, and is not regulated by Tst-1/Oct-6/SCIP. In contrast, little edg-3/lp_{B3} expression is seen at P13, indicating that its expression is modulated during Schwann cell differentiation (data not shown).

Figure 5: MKP-3 and edg-3/lp_{B3} appear to be transiently upregulated following nerve transection.

At various times following a transection injury, or crush injury (not shown), total RNAs were isolated from rat sciatic nerve distal to the injury, and used to generate northern blots. The number of days after transection is indicated at the bottom of the panel; the '0' time point is from unlesioned nerves. Panels depict the results of hybridization, from top to bottom, with ectoATPase, MKP-

3, edg-3/lpB3, P0, P75 nerve growth factor receptor, and GAPDH; sizes of the major mRNAs for these genes are listed on the right. Both MKP-3 and edg-3/lpB3 appear to be upregulated one day following transection, as can be ascertained by comparison of their hybridization signals in the day 1 and adjacent lanes to the corresponding ecto-ATPase and P0 hybridization signals. Exposure times were as follows: MKP-3: 10 days; EctoATPase: 7 days; edg-3/lpB3: 8 days; P0: 4hrs; P75NGFR: 7 days; GAPDH: 1 day.

Figure 6: Control of Schwann Cell Differentiation by cAMP.

Modulation of cAMP levels in Schwann cells mimics critical aspects of Schwann cell differentiation, such as induction of the transcription factors Tst-1/Oct-6/SCIP and Krox-20, and the myelin structural protein P0. Two proteins, the G-coupled receptor edg-3/lp_{B3} (A), and the ERK-specific phosphatase MKP-3 (B), are induced by forskolin in cultured Schwann cells, and may mediate some aspects of cAMP signalling in Schwann cell differentiation. $\rightarrow$ denotes induction; $\dashv$ denotes repression; in most cases, these effects will be indirect. AC: adenylyl cyclase. Dashed lines represent hypothetical regulatory pathways. Effectors of cAMP signalling, such as PKA and CREB, are not shown explicitly; neither are other signal transduction pathways that also are important in Schwann cell differentiation. **(A).** Sphingosine-1-phosphate (S1P) signalling through the edg-3/lp_{B3} receptor could promote Schwann cell survival and/or differentiation. Note that adenylyl cyclase and edg-3/lp_{B3} could form a regulatory loop that may be positive or negative, depending on whether the isoform(s) of adenylyl cyclase that are present in Schwann cells are activated or inhibited by calcium. **(B).** MKP-3 may promote Schwann cell differentiation by inhibiting mitogenic signalling.

Table 1: Genes isolated by RDA using cDNAs from Schwann cells cultured with or without forskolin.

The genes that have been identified by each of the four Schwann cell RDA experiments are listed. Activated by forskolin refers to experiments in which the tester cDNAs were derived from Schwann cells treated with forskolin; these genes are putatively upregulated by forskolin. Down-regulated by forskolin refers to experiments in which the tester cDNAs were derived from untreated Schwann cells; forskoin treatment putatively represses the expression of these genes. The panels on the left list genes that were isolated without the addition of carrier mRNA, while those genes that are listed on the right were isolated using carrier mRNA. Sequences corresponding to some genes were isolated multiple times; the number of independent isolates for a cDNA (either the same or different sequences corresponding to that cDNA) are also indicated. For known sequences, the GenBank accession number is given for the most homologous sequence; in the case of equivalent homology to multiple sequences, only one is listed. For unknown sequences, the clone numbers are given, i.e. RDA40-8. The abundance of clones that correspond to these genes could be due to an abundance of amplifiable fragments within their cDNAs, or to the abundance of the cDNAs derived from forskolin-treated or -untreated cells. Genes such as ribosomal RNA genes that appear in both +Forskolin and –Forskolin experiments are (by definition) artifactual. Many of the genes have been tested by Southern hybridization of PCR-amplified driver cDNA ("Snorthern" blots, Figure 2) or by RNAse protection (Figure 3). Those genes that have been shown to be activated or repressed by forskolin are marked by an asterisk; those that have been shown not to be differentially expressed in the presence or absence of forskolin are shown in ~~strikethrough type~~.

ACKNOWLEDGEMENTS

We wish to thank Mark Sornson and Linda Erkman for providing insightful discussions during all phases of this work; Peggy Myer for assistance with the figures, and Jamie Pennington and Jill O'Moore for technical assistance. We also wish to thank Linda Erkman and George Carlson for their comments on the manuscript. This work was supported by NARSAD Young Investigator Award to JRB, Jr., and an NIH grant to SSS.

Table 1

Activated by Forskolin Isolated without Carrier mRNA	Activated by Forskolin Isolated with Carrier mRNA
*MAL X82557 (9 copies, 3 different) *Ecto ATPase Y11835 (6 copies, 3 different) *EST AI232310 (3 copies without intron, 2 copies with intron) *EST AW529340 (2 copies) *68kd neurofilament protein (NF-L) M13016 *EST AA817876 *Traf4 AF233449 *EST AA346230 *MKP-3 X94185 Sequence on BAC AC024339 (2 copies) EST AA207500 (2 copies) Unknown sequence 4-2 EST AF077757 Unknown sequence 6 EST W84171 KIAA0005 D13630 Furin X55660 N10/nurr77 U17254 Unknown sequence 59 neurotrypsin Y13192	*edg-3/lp_{B3} AF108021 *CD9 X76489 *68kd neurofilament protein (NF-L) M13016 Extracellular SOD X68041 (2 copies) EST T07169 (perlecan) (2 copies) Semaphorin A X85990 EST AA762924 EST AA068111 Collagen I Z78279 HSP90 heat shock protein/chaperone S45392 18S, 5.8S, 28S rRNAs V01270 Mitochondrial adenine nucleotide translocator D12770 EST AI230456 Myelin P0 M62860 EST AA240567 SR13/PMP-22 S55427 18S rRNA M29839 (4 copies) gas7 AJ131902 ~~Vimentin X62952 (3 copies, 2 different)~~
Down-regulated by forskolin Isolated without Carrier mRNA	**Down-regulated by forskolin Isolated with Carrier mRNA**
*CD11c/integrinαX M81695 (4 copies, 2 different) *γ filamin NM001458 (3 different copies) *KIAA0013 D87717 (3 copies, 2 different) *K13 K+ channel M81784 (2 different copies) *RRP22 Y07847 *Unknown sequence 40-8 *Ulip1 X87817 *GPR41 U92802 Transferrin D38380 (2 copies) EST AI102436 Annexin VI X86086 EST AI272270 EST W53158 EST AA420321 EST AF077757 G protein β2 subunit U34959 EST W77252 EST W57231 EST AA349394 Human c-some 16 cosmid AC005222 Unknown sequence 82 Vesicular monoamine transporter L00603 EST AI603937 18S rRNA M29839 (4 copies) 18S, 5.8S, 28S rRNAs V01270 (3 copies) ~~Prosapocin S81373 (2 copies; alt splice??)~~ ~~Dystroglycan U13512 (2 different copies)~~	*Unknown sequence 40-8 *H36-α7 integrin X65036 *γ-filamin NM001458 Brain hexokinase J04526 Agrin precursor U84407 Unknown sequence 38 Unknown sequence 39 Insulin-1 J00747 EST AI137218 multidrug resistance associated protein AF022908 Unknown sequence 46 βig-h3 L19932 PP2A protein phosphatase (65kd) Z34955 EST AA272137 β-actin J00691 Est W66776 MAP1B X15396 Ezrin X60671 Immunosuperfamily member B12 AF061260 Unknown sequence 94 Unknown sequence 95 TACC1 AF049910 18S rRNA M29839 (2 copies) gas7 AJ131902 ~~OR-1 orphan nuclear receptor U20382~~

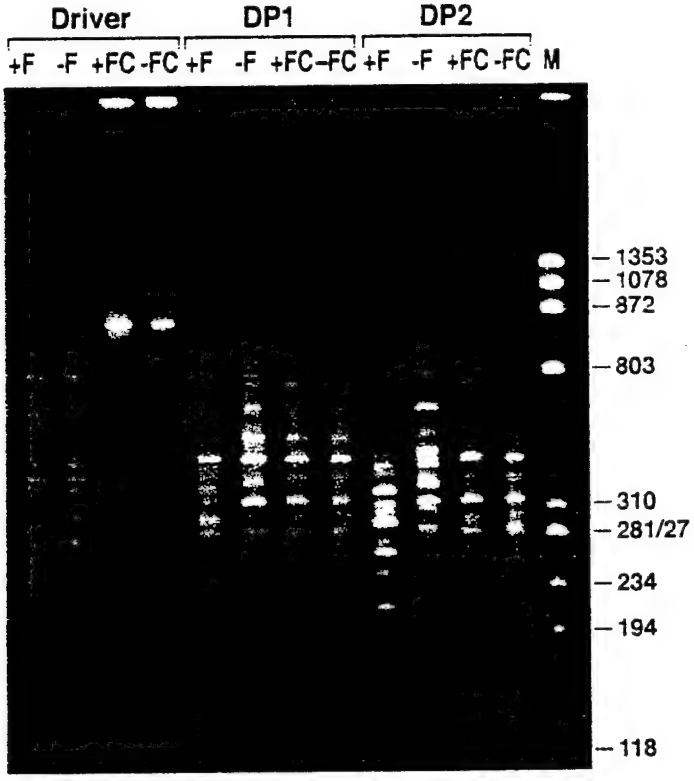

SCRDA figure 1

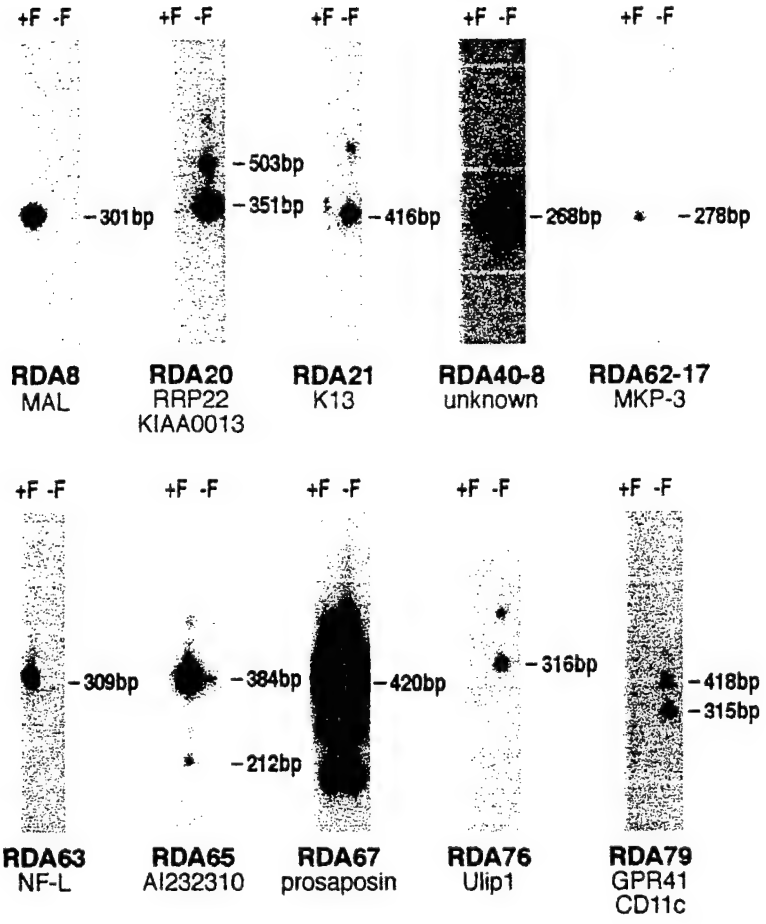
+F -F
+F -F
+F -F
+F -F
+F -F
-503bp
-351bp
-301bp
-416bp
-268bp
-278bp
RDA8
MAL
RDA20
RRP22
KIAA0013
RDA21
K13
RDA40-8
unknown
RDA62-17
MKP-3
+F -F
+F -F
+F -F
+F -F
+F -F
-309bp
-384bp
-212bp
-420bp
-316bp
-418bp
-315bp
RDA63
NF-L
RDA65
AI232310
RDA67
prosaposin
RDA76
Ulip1
RDA79
GPR41
CD11c

SCRDA figure 3

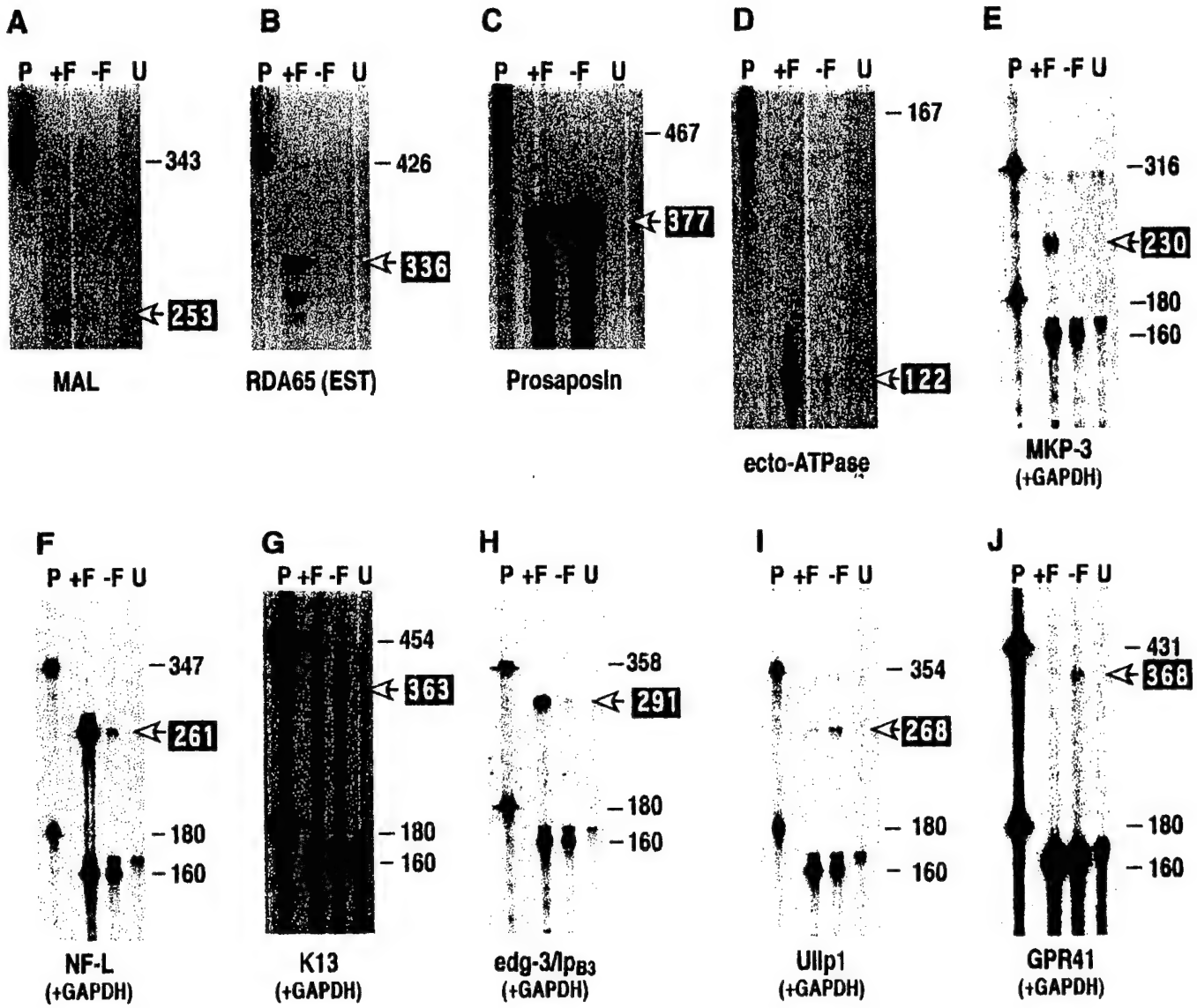

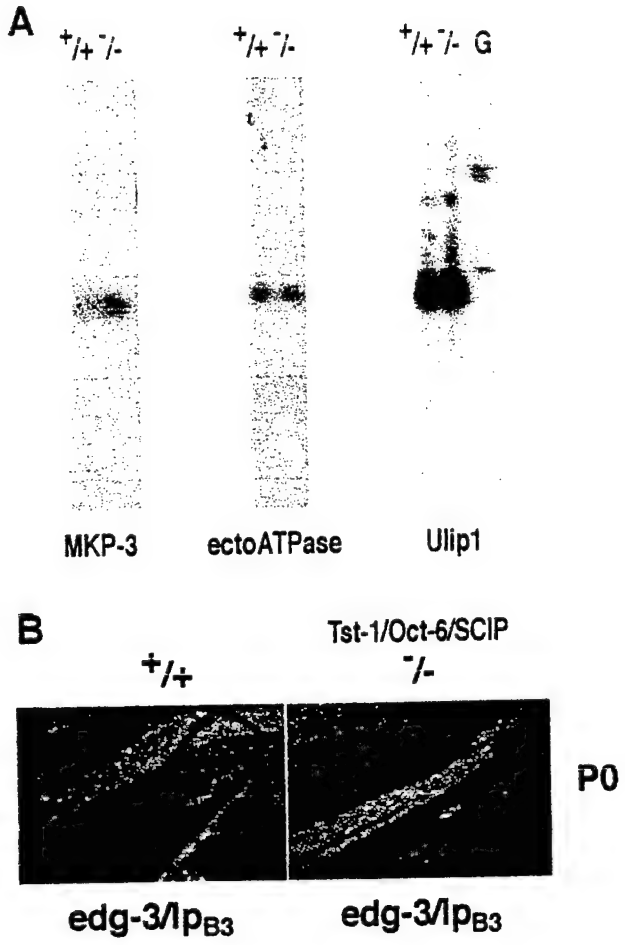
A
+/+ -/-
+/+ -/-
+/+ -/- G
MKP-3
ectoATPase
Ulip1
B
Tst-1/Oct-6/SCIP
+/+
-/-
P0
edg-3/Ip$_{B3}$
edg-3/Ip$_{B3}$

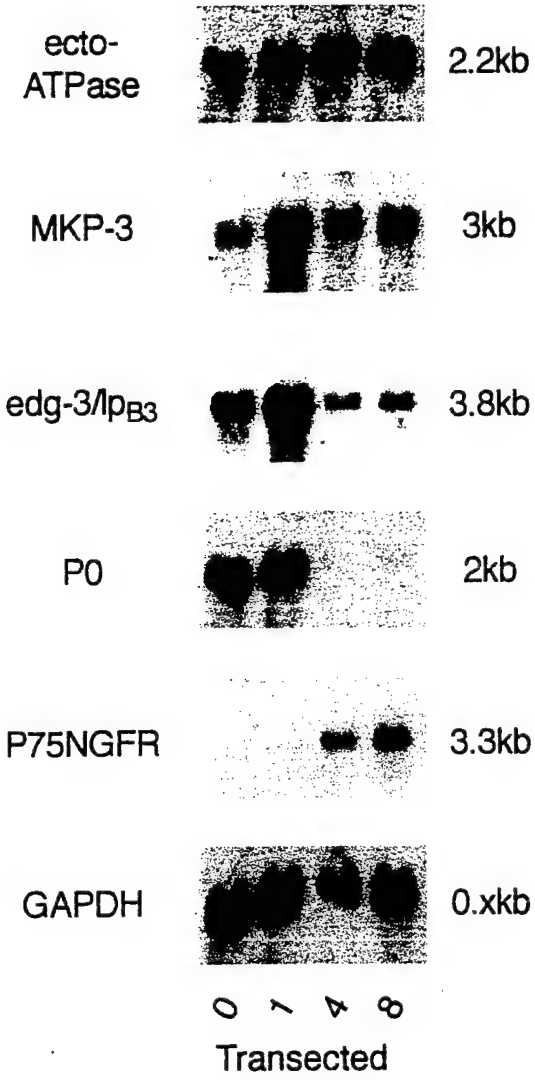
ecto-
ATPase
2.2kb
MKP-3
3kb
edg-3/lp$_{B3}$
3.8kb
P0
2kb
P75NGFR
3.3kb
GAPDH
0.xkb
0 1 4 8
Transected

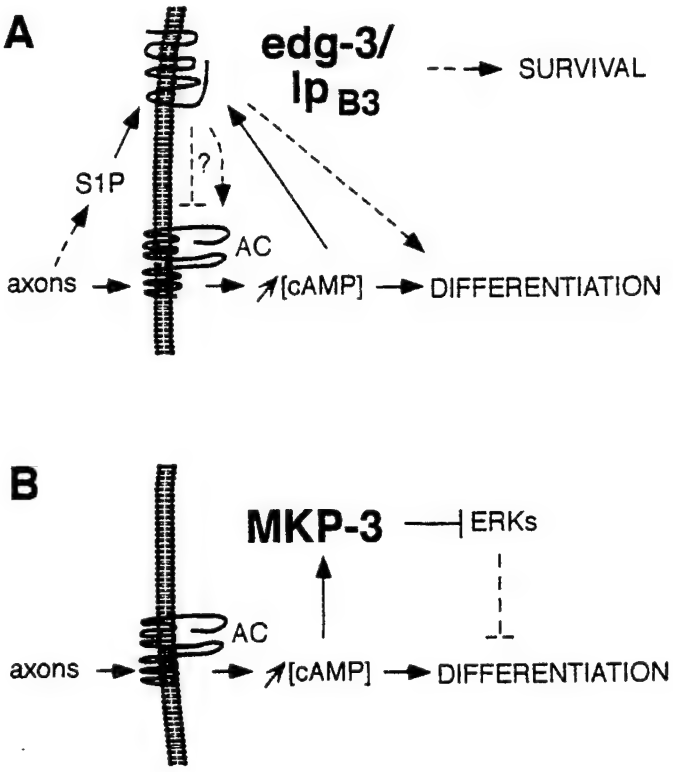

SCRDA figure 6

APPENDICES: PART C

A POU Domain Transcription Factor-Dependent Program Regulates Axon Pathfinding in the Vertebrate Visual System

Linda Erkman[1,6], Paul A. Yates[2], Todd McLaughlin[2] Robert J. McEvilly[1], Thomas Whisenhunt[1], Shawn M. O'Connell[1], Anna I. Krones[1], Michael A. Kirby[3], David H. Rapaport[4], John R. Bermingham Jr.[1,5], Dennis D.M. O'Leary[2,6] & Michael G. Rosenfeld[1,6]

1. Howard Hughes Medical Institute, Department of Medicine, University of California, San Diego, La Jolla, CA 92093
2. Molecular Neurobiology Laboratory, The Salk Institute, La Jolla, CA 92037
3. Department of Pediatrics and Anatomy, Loma Linda University, Loma Linda, CA 92350
4. Department of Surgery, University of California, San Diego, La Jolla, CA 92093
5. Present address: McLaughlin Research Institute, Great Falls, Montana, MT 59405
6. Corresponding authors:
   mrosenfeld@ucsd.edu
   doleary@salk.edu
   lerkman@ucsd.edu

Running Title: Brn-3.2-dependent regulation of axon pathfinding

Summary

Navigational decisions required for axon pathfinding and the establishment of topographic maps rely on the ability of the growth cone to detect and interpret guidance cues, and the modulation of cytoskeletal changes in response to these signals. We report that the murine POU domain factor Brn-3.2 mediates a transcriptional program that regulates retinal ganglion cell (RGC) axon pathfinding within the retina and at multiple points along central pathways, as well as the establishment of topographic order in the superior colliculus. Using representational difference analysis, we identified target genes of Brn-3.2 that are likely to act on axon guidance at the levels of transcription, cell-cell interaction, and signal transduction, including the actin-binding LIM domain protein abLIM. We present evidence that abLIM plays a crucial role in RGC axon pathfinding, sharing functional similiarity with Unc-115, its homologue in *C. Elegans*. Our findings provide insights into a Brn-3.2-directed hierarchical program linking signaling events to cytoskeletal changes required for axon pathfinding.

Introduction

The development of highly organized neuronal connections relies on the coordinated movements of axons along precise pathways leading to their targets, and the establishment of synaptic connections at topographically appropriate sites. As growth cones progress in a dynamic environment, they make navigational choices by recognizing and interpreting molecular cues presented along their pathway. The vertebrate visual system has long served as a model for the study of axon guidance. Retinal ganglion cells (RGCs) extend their axons along defined paths, and ultimately establish topographically ordered connections in the central nervous system. Navigational decisions become more complex as the growth cone encounters boundaries between structures that differ in their cellular and molecular composition (Holt, 1989; Tuttle et al., 1998). First, RGC axons extend toward the optic disc, making a transition from neural retina to the non-neuronal environment of the optic disc, and grow into the optic nerve (Halfter et al., 1985). Further along the pathway, at the optic chiasm, the majority of RGC axons cross the ventral midline of the forebrain, and project dorsally along the surface of the contralateral diencephalon (Marcus and Mason, 1995). Finally, they reach their most distal target in the midbrain, the superior colliculus (SC), and establish a highly ordered topographic map of the visual field. Axons from the nasal retina terminate in

the caudal (posterior) SC, and temporal RGCs terminate in the rostral (anterior) SC (Simon and O'Leary, 1992). The behavior of the growth cone along these pathways and at boundaries is governed by a delicate balance of attractive and repulsive events leading to axon fasciculation, pathfinding, and establishment of topographic maps. Genetic and molecular approaches have uncovered three major ligand/receptor classes involved in these processes (see reviews by Bashaw and Goodman, 1999; Frisén et al., 1999; O'Leary et al., 1999; Seeger and Beattie, 1999; Tear, 1999, and references therein).

Recent investigation has established a key role for these ligand/receptor complexes in RGC axon pathfinding during the development of the mouse visual system. Disruption of the genomic loci encoding the midline signaling molecule Netrin-1 and its receptor, DCC, results in pathfinding defects by RGC axons, whereby axons from the peripheral retina are not correctly guided into the optic nerve (Deiner et al., 1997). Receptor tyrosine kinases of the Eph family and their ligands, ephrins, are also key regulators of axon pathfinding and establishment of topographic order in the mouse visual system (O'Leary and Wilkinson, 1999). Kinase independent functions of EphB receptors are required for pathfinding by dorsal RGC axons to the optic disc (Birgbauer et al., 2000), and alteration of the EphA gradient in mouse retina causes axon pathfinding and topographic errors in retinocollicular projections (Brown et al., 2000). Targeted mutagenesis of *ephrin-A2* and *ephrin-A5* genomic loci, alone or in combination, results in topographically aberrant projections in the SC of mice (Frisén et al., 1998; Feldheim et al., 2000). Finally, recent evidence has implicated members of the slit family of axon repellents and their robo receptors in mediating RGC axon pathfinding (Erskine et al., 2000; Niclou et al., 2000; Ringstedt et al., 2000).

Spatial and temporal coordination of the molecular machinery governing the presentation of guidance cues along the pathway and their detection by the growth cone are essential for correct axon pathfinding and must be regulated at the transcriptional level. Transcription factors expressed along the retinocollicular pathways control non-cell-autonomous components of axon guidance in the mouse visual system. Targeted deletion of the paired domain transcription factor *Pax2* and the homeodomain transcription factor *Vax-1* results in RGC axon pathfinding defects consistent with their expression pattern in the glial cells of the optic stalk and the midline structures of the ventral forebrain (Torres et al., 1996; Bertuzzi et al., 1999; Hallonet et al., 1999).

Relatively little information is available regarding transcription factors involved in cell-autonomous regulation of axon guidance. The identification of such transcription factors and their targets would provide new insights into molecular pathways governing the ability of the growth cone to sense and process navigational cues, and to undergo morphogenetic movements. We have initiated such a study, to investigate the role of the POU domain

transcription factor Brn-3.2 in the development of the mouse visual system. *Brn-3.2/Brn-3b/Pou4f2*, and its closest family members *Brn-3.0/Brn-3a/Pou4f1 and Brn-3.1/Brn-3c/Pou4f3*, which together constitute the mammalian class IV POU domain transcription factors, are important regulators of neural development (reviewed in Ryan and Rosenfeld, 1997, and McEvilly and Rosenfeld, 1999). Targeted deletion of individual genomic loci results in phenotypes reflecting their spatially and temporally unique sites of expression. Mice with *Brn-3.0* gene-deletion have defects in the peripheral sensory ganglia as well as motor and sensory components of the hindbrain (McEvilly et al., 1996; Xiang et al., 1996; Huang et al., 1999). *Brn-3.1* mutation results in deafness and balance problems owing to a failure in the differentiation of cochlear and vestibular hair cells (Erkman et al., 1996; Xiang et al., 1997). In *Brn-3.2* gene-deleted mice, the majority of RGCs in the retina are lost, without any other defects observed in the central or peripheral nervous systems (Erkman et al., 1996; Gan et al., 1996). Previous observations suggest that excessive neuronal loss in the RGC layer of *Brn-3.2*$^{-/-}$ mice is not due to problems in the initial generation and cell fate determination (Erkman et al., 1996; Xiang et al., 1998; Gan et al., 1999).

Here we demonstrate a critical role for Brn-3.2 in the guidance of RGC axons intraretinally, as well as at major choice points along the central visual pathways, and report the identification of a series of candidate target genes with potential roles in RGC axon guidance, that we isolated using a modification of the representational difference analysis (RDA). Using the developing chick retina as a model, we provide evidence that one of these genes, a putative component of the signal transduction pathway, is part of the molecular cascade controlled by Brn-3.2 that regulates specific aspects of axon guidance events.

Results

Hypoplastic optic nerve and aberrant intraretinal axon trajectories in *Brn-3.2* mutants

Brn-3.2 is expressed in the developing mouse retina from embryonic day (E) 11.5, and targeted deletion of its genomic locus results in the loss of the majority of RGCs, without noticeable defects in the other components of the nervous system, where the lack of Brn-3.2 function is probably compensated by the closely related family member, Brn-3.0 (Erkman et al., 1996; Gan et al., 1996). The observation that at postnatal day 0 (P0), cell numbers in the RGC layer of *Brn-3.2*$^{-/-}$ mice are still comparable to those in wild type mice, suggested that excessive RGC loss is not due to problems in cell fate determination or a premature onset of naturally-occurring RGC death, and therefore may result from defects in axon growth and pathfinding. We first performed a qualitative comparison of the magnitude of the

retinocollicular projection by examining the numbers of RGCs retrogradely labeled with the fluorescent tracer DiI, injected at multiple sites covering the medial-lateral axis of rostral SC at P0 (n = 5 wild type, 8 mutant). Retinal wholemounts from *Brn-3.2*$^{-/-}$ mice contained substantially fewer labeled cells as compared to their wild-type littermates (Figures 1A and B), suggesting that RGCs exhibit defective pathfinding in the *Brn-3.2* mutants.

To gain insight into the time course of axonal and neuronal loss in the retina of *Brn-3.2*$^{-/-}$ mice, we determined the number of RGC axons in mutant and wild type littermates from E12.5 through adulthood, using electron micrographs of optic nerve cross-sections. RGCs are generated between E11 and E18, the latter age coinciding with the onset of naturally-occurring RGC death (Dräger, 1985). The axon numbers peaked coincidentally in the wild type and mutant between E16.5 and P0 (Figure 1C), indicating that the time course of axon addition and loss is similar in normal and mutant retina. However, in *Brn3.2*$^{-/-}$ mice, axon counts were substantially lower at every time point, suggesting that the reduction in the number of RGC axons begins prior to the normal onset of naturally-occurring RGC death. Therefore, we sought to determine whether diminished numbers of RGC axons at early developmental stages in *Brn-3.2*$^{-/-}$ mice were due, at least in part, to pathfinding defects within the retina. The intraretinal trajectories of RGC axons were traced in wild type and mutant mice by a focal injection of DiI in the retina of fixed E14.5 littermates (n = 3 wild type, 3 mutant). In the wild type retina, RGC axon fascicles grew directly toward the optic disc (Figure 1D). In contrast, in the mutant retina, many RGC axons did not fasciculate and followed abnormal trajectories, a substantial proportion failing to reach the optic disc (Figure 1E). These findings indicate that the reduced number of optic nerve axons in *Brn-3.2*$^{-/-}$ mice is due in part to defects in the pathfinding of RGC axons within the retina and their failure to enter the optic nerve.

Axon guidance defects along the retinocollicular pathway in *Brn-3.2* mutants

To investigate potential pathfinding defects of RGC axons along central pathways in *Brn-3.2* mutants, we used anterograde and retrograde DiI labeling of RGCs. In mice, RGC axons first reach the optic chiasm at E12, and their most distal target, the SC, at E14; additional RGC axons continue to grow through the optic tract and into the SC at least until birth (Simon and O'Leary, 1992; Marcus and Mason, 1995). We first used anterograde DiI tracing to analyze the projection of RGC axons at P0 (n = 5 wild type, 10 mutant). Examination of the ventral diencephalon revealed that in the mutant, a large proportion of RGC axons pass through the optic chiasm and extend into the contralateral optic tract, as in the wild type (Figure 2A). However, in contrast to the wild type, a sizeable proportion of RGC

axons in the mutant exhibited several different pathfinding defects at the optic chiasm. In some cases, an abnormally large number of RGC axons passed through the chiasm and into the opposite optic nerve (Figure 2B). In other cases, an abnormally large contingent of RGC axons failed to decussate at the chiasm and instead projected through the ipsilateral optic tract (Figure 2B), aberrantly deviated at the midline dorsally into the hypothalamus, (Figure 2C), or appeared to stop their extension at the midline (Figure 2D). Subsets of these phenotypes were observed in different mutant animals. In addition, in the *Brn-3.2* mutant, a substantial proportion of RGC axons extending through the contralateral optic tract appeared to stall within the optic tract in dorsal diencephalon as they approached the midbrain, and failed to extend caudally to the SC (Figure 2E and F). This stalling of RGC axons within the dorsal optic tract is perhaps better appreciated by labeling smaller numbers of RGC axons using focal injections (Figure 2G). The accumulated attrition of RGC axons due to these pathfinding defects within the brain, as well as the intraretinal ones described above, results in a substantial reduction in the number of RGC axons that reach the SC in *Brn-3.2*$^{-/-}$ mice (Figures 2E and F; also see Figure 1). Together, these data indicate that RGC axons in *Brn-3.2*$^{-/-}$ mice exhibit pathfinding defects at multiple points along their pathway.

To determine whether the RGC axons that reach the SC in *Brn-3.2*$^{-/-}$ mice establish correct topographic projections, we made small focal injections of DiI either into the retina (n = 4 wild type, 5 mutant) or the SC (n = 4 wild type, 6 mutant) at P14, after the mature retinocollicular topographic map is normally established (Simon and O'Leary, 1992). In wild type mice, anterograde labeling from an injection in temporal-dorsal retina labeled a dense termination zone formed by the overlapping arbors of RGC axons confined to the topographically appropriate rostral-lateral SC (Figure 3A). In contrast, in *Brn-3.2*$^{-/-}$ mice, a similar injection did not result in the labeling of a discrete, dense termination zone, but instead labeled widely branched axons that diffusely covered much of the SC, with little indication of appropriate topography (Figure 3B). In addition, the medial-lateral topography of the entry point of RGC axons into the SC is aberrant in *Brn-3.2*$^{-/-}$ mice. In wild type mice, axons labeled by an injection into temporal-dorsal retina normally enter the SC from its lateral aspect (Figure 3A), whereas in the mutant, the SC entry point of temporal-dorsal axons is deviated medially (Figure 3B). A similar aberrant medial deviation was also observed at earlier time points (see for example Figure 2F). Retrograde labeling of RGCs by a focal injection of DiI in the SC confirmed the lack of topography observed with anterograde labeling. For example, in wild type mice, a focal DiI injection in mid-SC labeled a dense cluster of RGCs at the topographically correct location in mid-retina (Figure 3C), whereas a similar injection in the mutant resulted in the labeling of RGCs scattered across the retina with little or no bias for the correct topographic location (Figure 3D). These results indicate that

RGCs fail to form an appropriate topographic map within the SC of *Brn-3.2* mutants, and that individual RGC axons broadly arborize across the mutant SC.

Pathfinding defects in *Brn-3.2* mutants are likely to be RGC autonomous

Next, we determined whether Brn-3.2 acts in a manner autonomous to RGCs, and whether it is involved in the regulation of molecules shown to control RGC axon pathfinding in the vertebrate visual system. We first examined the expression of *Netrin-1* and its receptor, *DCC*, since mice deficient for either one exhibit defects in RGC axon pathfinding within the retina resulting in a hypoplastic optic nerve (Deiner et al., 1997), similar to the *Brn-3.2* mutant. *Netrin-1* expression in the optic stalk was similar in wild type (Figure 4A) and mutant (Figure 4B) mice, as was the expression of *DCC* within the retina (Figures 4C and D). Thus, the intraretinal and optic nerve defects observed in the *Brn-3.2* mutant are not due to changes in the expression of *Netrin-1* or *DCC*.

Although *Brn-3.2* expression in the ventral diencephalon has not been detected, one cannot rule out transient expression during a brief period of development which might have consequences on the later patterning of the optic pathway. We addressed this issue by analyzing the expression of *Shh*, *Nkx2.1* and *Nkx2.2*, each of which have distinct expression domains in ventral diencephalon and are thought to be important for the determination of axon pathways in this region (Marcus et al., 1999). Wholemount in situ hybridization analysis performed at E11.5, just before the first RGC axons reach the ventral diencephalon, did not reveal any abnormalities in the patterned expression of these markers in *Brn3.2*$^{-/-}$ mice (Figure 4E and F, and data not shown). These findings, together with the lack of *Brn-3.2* expression in the mouse ventral diencephalon, suggest that in the *Brn-3.2* mutant, RGC axon pathfinding defects are likely to be RGC autonomous.

Brn-3.2 is expressed in the developing SC, along with the closely related family member, *Brn-3.0*. Histological examination of the mutant SC did not reveal major abnormalities in its size, shape, or architecture (data not shown). In addition, both the level and pattern of expression of *ephrin-A2* and *-A5* in the SC appeared normal in *Brn-3.2*$^{-/-}$ mice at E15.5 (data not shown) and at P0 (Figures 4G and H), suggesting that the developing SC is normal in the *Brn-3.2* mutants, with the lack of Brn-3.2 function possibly compensated by Brn-3.0. The expression of the ephrin receptors, *EphA6* and *EphB2* in the retina, and of *ephrin-B2* in the SC, also appeared normal at E15.5 in *Brn-3.2*$^{-/-}$ mice (data not shown). These findings suggest that the aberrant topographic mapping of RGC axons in the SC of *Brn-3.2* mutants may be due to cell-autonomous defects in RGCs, but it may also be due to a diminished competitive interaction between RGC axons resulting from the substantial reduction in the number that reach the SC.

Representational difference analysis and isolation of candidate target genes

To understand the molecular mechanisms by which Brn-3.2 exerts its effects on RGC axon guidance, we began to identify candidate target genes using a modification of RDA. Our approach is based on the protocol originally designed for the identification of polymorphisms in genomic DNA (Lisitsyn et al., 1994) and later applied to positional cloning (Sornson et al., 1996) and subtraction of cDNA populations (Hubank and Schatz, 1994). To address the technical constraints imposed by the relatively small size of embryonic mouse retina, we introduced modifications to permit subtractive hybridization of cDNA populations synthesized from minute amounts of mRNA. Briefly, ~50 ng of cDNA were prepared from twenty E14.5 retinas, in the presence of a "carrier" mRNA (see Experimental Procedures). We used (-/-) amplicons as the driver, and (+/+) amplicons as the tester, to identify genes that may be upregulated by Brn-3.2. Following three rounds of hybridization and amplification with increasing ratios of driver to tester (100, 800, 1000), the RDA products were cloned directly into plasmid vectors and sequenced. For an initial test of differential expression, a sample of RDA inserts were picked randomly, radiolabeled, and hybridized to Southern blots consisting of drivers from wild type and *Brn-3.2*$^{-/-}$ retinas. About 80% of the genes tested by Southern blot analysis appeared to be differentially expressed in mutant retina (Figure 5A, and data not shown). After correction for multiple occurrences of identical inserts, and sequences representing different fragments of the same gene, we obtained 28 potential targets for Brn-3.2.

Thus far, our screening has yielded 3 potentially novel genes, and 7 with matching sequences in mouse EST and human genomic and cDNA databases (Figure 5B), the structure and function of which are not reported. We also obtained a number of genes that share a very low degree of homology with known genes, and cannot be classified at this time. In addition, we identified five candidate target genes that represent previously characterized molecules, including the transcription factors Irx6 (Cohen et al., 2000), EBF/Olf-1, EBF/Olf-2 (Garel et al., 1997; Wang et al., 1997), a mouse homologue of rat Neuritin (Naeve et al., 1997). *Irx6*, a homeodomain transcription factor with homology to the *Drosophila* genes of the iroquois complex, *Olf-1* and *Olf-2*, belonging to the Early B Cell Factor (EBF) family of HLH transcription factors, and Neuritin, a GPI-anchored neuronal cell-surface protein, are well characterized (see references above). The sequence homology of corresponding RDA products are indicated in Experimental Procedures. One RDA product which did not present homology to published sequences was ultimately identified by analysis of cDNA clones as part of the 3'UTR of the mouse homologue of the human actin-binding zinc finger protein abLIM (Roof et al., 1997). The sequence of the LIM domain containing all 4 LIM motifs specific for the retinal isoform was highly conserved and showed 97% identity to the human

sequence (Figure 5C). In situ hybridization analysis of *m-abLIM* in E15.5 mice showed, in addition to its expression in the inner layer of the retina, expression in other neuronal structures including peripheral sensory ganglia, spinal cord, SC and non-neural tissues such as the thymus (Figures 5E-H).

If these genes are regulated by Brn-3.2, their mRNA levels should decrease in *Brn-3.2*$^{-/-}$ retina, and their spatial and temporal patterns of expression should support such an assumption. Indeed, comparison of mRNA levels in E15.5 wild type and *Brn-3.2*$^{-/-}$ retinas revealed a dramatic decrease in the levels of *Irx6*, *Olf-1*, *m-abLIM* and *Neuritin*, and a modest effect on *Olf-2* mRNA levels (Figure 6), indicating that even relatively small differences can be detected by our modified RDA protocol. Temporal expression patterns of *Brn-3.2*, *Irx6*, *Olf-2*, and *m-abLIM* were determined using adjacent sections of retina at different developmental stages. Expression of *Brn-3.2* mRNA, first detectable in the retina at E11.5 (data not shown), precedes initial detectable expression of *Irx6* and *Olf-2* around E12.5, and *m-abLIM* around E13.5 (Figure 7 and data not shown). Thus, these genes may represent components of a molecular cascade regulated by Brn-3.2.

Functional analysis of abLIM in the developing chick visual system

To address the functional significance of our RDA findings, we used the RCAS(B) recombinant retroviral vector system (Homburger and Fekete, 1996). Among the candidates identified thus far, abLIM appeared to be particularly well-suited to have a direct role in mediating RGC pathfinding, based on its functional and structural characteristics and its expression in the chick retina, confirmed by in situ hybridization and Northern blot analysis (data not shown). Human abLIM, originally cloned as a homologue of dematin (Roof et al., 1997) and the C. Elegans unc-115, which is involved in axon pathfinding (Lundquist et al., 1998), contain an N-terminal LIM domain, and a C-terminal domain sharing homology with the villin headpiece (see diagram in Figure 5D). The LIM domains have a well-established role in assembling protein complexes through their protein-protein interaction interfaces (reviewed in Dawid et al., 1998), and the C-terminal domain of abLIM has been shown to effectively bind actin (Roof et al., 1997), strongly suggesting a role for this protein in bridging cytoplasmic proteins with cytoskeletal elements. Therefore, we designed a truncated form of abLIM consisting only of the LIM domain to perturb the function of the native protein, and act as dominant-negative, as has been demonstrated for other LIM domain proteins (Kikuchi et al., 1997; O'Keefe et al., 1998). To permit direct visualization of transfected RGC axons, a bicistronic construct consiting of the LIM domain upstream of an IRES-EGFP (diagramed in Figure 5E) was designed and inserted into the RCAS(B) vector. Due to size constraints precluding overexpression of the full-length abLIM in the replication

competent retrovirus, and the difficulty of interpreting potential phenotypes resulting from expressing a different LIM domain, we limited our controls to transfection with RCAS(B)-EGFP. In ovo electroporation of the RCAS-abLIM$_{DN}$-IRES-EGFP vector permitted unilateral transfection, limiting the spread of viral particles to the transfected eye. Electroporation was performed at Hamburger-Hamilton stages 10-12, and the transfected retinas were analyzed nine days later. The transfection domains were confined to the right retina and covered approximately 5% to 100% of its area, including all retinal layers.

RGC axons in retinas transfected with the control vector (RCAS-EGFP) appeared unaffected (Figure 8A), and extended directly from the cell body to the centrally-located optic fissure, with neighboring axons taking trajectories that parallel one another as in the normal retina (Halfter et al., 1985; Nakamura and O'Leary, 1989). However, the axons of RCAS-abLIM$_{DN}$-IRES-EGFP transfected RGCs often appeared to be more highly fasciculated than normal, and had aberrant trajectories characterized by an exaggerated wave-like appearance (Figure 8B). This phenotype was observed in 10 of 26 E10 retinas transfected with RCAS-abLIM$_{DN}$-IRES-EGFP, compared to only 1 of 16 E10 retinas transfected with the control RCAS-EGFP. In the more extreme cases, the abLIM$_{DN}$ transfected RGC axons made sharp turns, and even reversed their direction of growth and extended toward the periphery of the retina instead of the optic fissure (Figure 8C); these behaviors were not observed in the control transfected retinas.

RGCs transfected with RCAS-abLIM$_{DN}$-IRES-EGFP also displayed axon guidance defects at the optic chiasm. In chick, the vast majority of RGC axons project to the contralateral tectum, with sparse, transient projections to the ipsilateral optic tract and the contralateral optic nerve (McLoon and Lund, 1982; O'Leary et al., 1983; Thanos and Bonhoeffer, 1984), that may persist until E10. In our study, only 1 of 11 E10 chicks transfected with the control RCAS-EGFP vector had a projection to the ipsilateral optic tract or the contralateral optic nerve, although all had a large contingent of heavily labeled RGC axons which crossed the optic chiasm and entered the contralateral optic tract (Figure 8D). In contrast, in 10 of 23 E10 chicks transfected with the RCAS-abLIM$_{DN}$-IRES-EGFP vector, we observed significant RGC pathfinding defects, including a substantial projection from the transfected retina into the ipsilateral optic tract or contralateral optic nerve, or both (Figure 8E), much larger than those previously identified in normal chicks with whole eye fills of axon tracers. Further, in one case, a large fascicle of labeled RGC axons invaded the retina contralateral to the transfected eye (Figure 8F). Thus, overexpression of abLIM$_{DN}$-IRES-EGFP causes RGC axon guidance defects that are qualitatively similar to those observed *in Brn-3.2*$^{-/-}$ mice, and further support the finding of abLIM as a functional target of Brn-3.2.

Discussion

In this manuscript, we provided evidence that the class IV POU domain transcription factor Brn-3.2 has a critical role in regulating RGC axon pathfinding and the establishment of topographic maps in the developing mouse visual system. To begin to unravel the Brn-3.2-dependent regulatory program that underlies these events, we initiated the identification of candidate target genes using a modification of RDA, which resulted in the cloning of a series of genes connected to axon pathfinding, and likely to function at the levels of gene tanscription, signal transduction, and cell-cell interactions. The spatio-temporal patterns of expression of these genes in the developing retina, combined with the alteration of their mRNA levels in *Brn-3.2*$^{-/-}$ mice, suggest that Brn-3.2 may be responsible for the hierarchical control of molecules mediating the response of the growth cone to environmental cues required for proper axon pathfinding. Using the chick visual system as a model, we have provided data strongly supporting the view that that one of these targets, the mouse homologue of the actin-binding zinc-finger protein abLIM (m-abLIM) is part of the Brn-3.2-dependent program regulating RGC axon pathfinding. Our data indicate that at least one aspect of Brn-3.2-dependent program may involve a signal transduction cascade that links cell surface events to cytoskeletal changes.

Role of Brn-3.2 in axon guidance at major decision points

Brn-3.2 is essential for the survival of RGCs in mice, and previous studies suggested that excessive RGC loss in the mutant does not result from problems in cell fate determination or premature onset of naturally-occurring RGC death, but may be due to defects in axon growth and pathfinding (Erkman et al., 1996; Gan et al., 1996, 1999; Xiang et al., 1998). Our present study examining the developmental time course of changes in axon number in the optic nerve of wild type and *Brn-3.2*$^{-/-}$ mice has revealed that axons are added and removed from the optic nerve at similar rates, but the absolute numbers of axons are lower in the mutant at all developmental stages including those that precede detectable apoptotic cell death (Xiang et al., 1998; Gan et al., 1999). This suggested that defects in RGC axon pathfinding within the retina contributes to the hypoplastic optic nerve phenotype in *Brn-3.2*$^{-/-}$ mice. DiI labeling in *Brn-3.2*$^{-/-}$ mice revealed that RGC axons have abnormal trajectories and many fail to reach the optic disc. Our data, taken together with the abnormal fasciculation pattern of RGC axons within the retina (Gan et al., 1999), suggest, at least in part, that the reduction in axon numbers in *Brn-3.2*$^{-/-}$ mice is due to an inability of a certain percentage of axons to reach the optic nerve.

Brn-3.2 is also essential for RGC axon pathfinding along the central visual pathways, including the midline of the ventral diencephalon at the optic chiasm, and within the optic tract near the border between dorsal diencephalon and midbrain. In *Brn-3.2*$^{-/-}$ mice, pathfinding at the optic chiasm is severely compromised, with an abnormally large proportion of RGC axons failing to properly decussate, and instead growing into the ipsilateral optic tract or the contralateral optic nerve. Within the dorsal optic tract, a sizeable contingent of RGC axons stall and a substantially reduced number extend into the SC. Thus, the severe attrition of RGC axons is a consequence of their pathfinding defects within the retina, the optic chiasm and the dorsal optic tract. The RGC axons that do reach the SC fail to establish dense termination zones at the topographically correct sites, and instead form diffuse, widely branched arbors that sparsely cover much of the SC. Although the rodent retinocollicular projection initially lacks appropriate topographic order, the diffuse arbors observed in the *Brn-3.2* mutant do not resemble those normally observed at any developmental stage (Simon and O'Leary, 1992).

Brn-3.2 is likely to control RGC autonomous components of axon guidance, since the morphology of neural structures and expression domains of many regulatory molecules are normal along the pathway. The morphology of the optic stalk, as well as the expression of *Netrin-1*, which is known to direct axons to the optic nerve, appeared normal. In the ventral diencephalon of E11.5 embryos, expression domains of *Shh*, *Nk2.1* and *Nkx2.2*, did not reveal any abnormalities in *Brn-3.2*$^{-/-}$ mice. Even in the SC, where *Brn-3.2* is expressed, we did not observe major morphological defects in *Brn-3.2* gene-deleted mice, and in situ hybridization analysis revealed normal expression patterns for *ephrin-A2*, *-A5* and *-B2*. These data further support the view that axon pathfinding and topographic aberrancies observed in *Brn-3.2* gene-deleted mice are unlikely to result from defects in the SC where the coincident expression of *Brn-3.0* appears to compensate for the lack of Brn-3.2 function. Although the formation of abnormally diffuse, poorly ordered arbors in the SC of *Brn-3.2* mutants may be due to RGC's inability to respond appropriately to topographic guidance molecules, it is also likely that a contributing factor is a diminished competitive interaction between RGC axons due to their substantially reduced number (Simon et al., 1992, 1994).

We also considered the possibility that genes expressed in RGCs that have well-established roles in axon guidance could represent targets for Brn-3.2. However, we found that in the mutant retina, expression of two members of the Eph family of receptor tyrosine kinases, *EphA6* and *B2*, as well as the Netrin-1 receptor *DCC*, were normal. Axon pathfinding defects at the optic chiasm of *Brn3.2*$^{-/-}$ mice are intriguingly similar to the phenotype observed in *GAP-43*$^{-/-}$ mice (Sretavan and Kruger, 1998; Zhu and Julien, 1999). We found a modest decrease in the levels of *GAP-43* mRNA in *Brn-3.2*$^{-/-}$ retina (data not shown), which

is unlikely to account for all components of *Brn-3.2*$^{-/-}$ phenotype, since neither the guidance of RGC axons within the retina nor their topographic mapping in the SC are affected in *GAP-43* gene deleted mice. Taken together, these observations suggest that Brn-3.2 regulates the expression of critical gene targets not yet linked to pathfinding by RGC axons in the vertebrate visual system.

The role of class IV POU domain transcription factors appears to be well conserved during evolution. The *C. elegans* orthologue *unc-86* is also likely to regulate genes controlling axon pathfinding in motor neurons (Sze et al., 1997), and the single member of class IV POU domain factors in *Drosophila*, Acj6, has recently been reported to have a role in axon pathfinding of central neurons (Certel et al., 2000).

Brn-3.2 regulates the expression of components of a molecular cascade governing axon guidance

Of the transcription factors currently proposed to function in axon pathfinding in the mouse visual system, Brn-3.2 appears to be unique, in that it may directly affect the ability of growth cones to respond to environmental cues. In addition, many molecules known to play important roles in RGC axon pathfinding and establishment of topographic maps appear to be expressed normally in *Brn-3.2*$^{-/-}$ mice. Identification of Brn-3.2 target genes, therefore, appeared to be a promising approach for the characterization of additional molecules involved in RGC axon pathfinding by the growth cone, and for dissection of the molecular pathways controlled by Brn-3.2. Using a modification of RDA we cloned several potential Brn-3.2 target genes. This method was previously applied to the detection of differential gene expression, but only from abundant sources of mRNA, and with large differences between transcript levels to be compared (see, for example, Hubank and Schatz, 1994; Niwa et al., 1997; Morris et al., 1998). To overcome the limitations due to the relatively small size of the embryonic mouse retina and its cellular heterogeneity, with developing RGCs representing only a fraction of the total population, we introduced modifications to the RDA approach. These included the addition of a synthetic mRNA to the cDNA synthesis reaction, and the adjustment of the ratios of driver to tester used in each round of annealing prior to PCR amplification. Thus, the method was amenable to studies of subtle differences between small and heterogeneous cell populations in the nervous system, and, importantly, permitted the cloning of several novel sequences, which, at the present time, is not fully achievable using the microarray technology.

The candidate target genes presenting identity or significant homology to previously characterized genes include *Irx6*, *Olf-1*, *Olf-2*, *abLIM*, which have been shown to function in

axon pathfinding in other species, and therefore, are excellent candidates for mediating specific aspects of the axon guidance program regulated by Brn-3.2. *Irx6* is a member of the homeodomain transcription factor family, with substantial homology to the *Drosophila iroquois* complex, shown to determine somatotopy in sensory neurons (Grillenzoni et al., 1998). In *C. elegans*, *unc-3* (Prasad et al., 1998), the homologue of *Olf-1* and *Olf-2* HLH transcription factors of the *EBF/Olf* family, as well as *unc-115*, the homologue of the actin-binding LIM domain protein (*m-abLIM*) (Lundquist et al., 1998), are required for axon guidance. Finally the small GPI-anchored cell surface protein, Neuritin, may also be involved in this pathway, based on its expression in neural structures associated with plasticity, and its ability to promote neurite outgrowth in culture (Naeve et al., 1997). The ontogeny of expression of these genes, as well as alteration of their mRNA levels in *Brn-3.2*$^{-/-}$ mice is consistent with either direct or indirect regulation of their expression by Brn-3.2.

Role of m-abLIM RGC in axon pathfinding

We provided evidence for the role of m-abLIM in RGC axon pathfinding using in ovo transfection of chick retina with a recombinant retroviral vector expressing the LIM domain and EGFP. The bicistronic construct in which IRES-EGFP was cloned downstream of the LIM domain of m-abLIM (RCAS-LIM$_{DN}$-IRES-EGFP) permitted unequivocal identification of the axons of transfected RGCs. Interference with the endogenous ab-LIM in chick retina by overexpression of the LIM domain of m-abLIM caused a variety of pathfinding errors. In the infected retinas, RGC axons did not follow their normal trajectory to the optic disc, and had abnormal fasciculation and growth patterns. At the optic chiasm, abnormal projections to the ipsilateral optic tract and the contralateral optic nerve were observed. These pathfinding abnormalities bear striking qualitative similarities to those observed in the retina and at the optic chiasm of *Brn3.2*$^{-/-}$ mice. Thus, despite limitations of a "dominant-negative" strategy, the recapitulation of the *Brn-3.2*$^{-/-}$ phenotype at two crucial sites of RGC axon guidance provides strong support for abLIM being involved in a Brn-3.2-dependent program. The function of this putative component of the signal transduction cascade appears to be conserved during evolution because its homologue in *C. elegans*, *unc-115*, operates in a remarkably similar manner in sensory neurons (Lundquist et al., 1998), since in both cases, axon pathfinding is affected at boundaries where the growth cone changes environments. Taken together, these observations suggest that m-abLIM is a crucial component of the Brn-3.2-dependent program, and has the potential to link the signaling events on the cell surface to cytoskeletal changes in the growth cone of RGC axons.

The transcription factors identified in our screen (*Irx6*, *Olf-1* and *Olf-2*) are also likely to have functions conserved during evolution with respect to axon pathfinding events, and to

modulate specific molecular pathways controlled by Brn-3.2, serving, in some instances, as intermediates in the regulation of genes encoding cytoplasmic and cell surface molecules. The temporal pattern of *Brn-3.2* expression followed by *Irx6*, and *Olf-2*, and finally *m-abLIM* in RGCs is very suggestive of such a role for these transcription factors. We have obtained preliminary indication for a role for *Irx6* in NGF- and cAMP-induced neurite extension, as transient transfection in the 26W sensory cell line of an expression vector containing the homeodomain of *Irx6* fused in frame to the repressor domain of *Drosophila engrailed* gene resulted in fewer neurite-bearing cells after induction. This effect was comparable to that elicited by a fusion protein between the *engrailed* repressor domain and the C-terminal portion of *Brn-3.2* starting at the POU domain (A.K. and L.E, unpublished observations). Sequential activation of transcription factors that may act either individually or in synergy on specific promoters is well documented. For example, in *C. elegans* touch receptors, the LIM homeoprotein *mec-3* is regulated by *unc-86*, and these two transcription factors act synergistically on the *mec-3* promoter (Xue et al., 1992), as well as on the *mec-4* and *mec-7* promoters (Duggan et al., 1998).

In conclusion, our studies establish a unique role for Brn-3.2 in RGC axon pathfinding in the mouse visual system. Brn-3.2 appears to activate a complex developmental program crucial for RGC axon guidance within the retina and at major choice points along central visual pathways, as well as topographic order within the retinocollicular projection. Based on the roles of the targets thus far established, the novel targets of Brn-3.2 that have been isolated should permit further dissection of the molecular cascade controlling axon pathfinding in the mouse visual system.

Experimental Procedures

Mice

Brn-3.2$^{-/-}$ mice were generated by homologous recombination (Erkman et al., 1996). All analyses were carried out using a mouse line on a pure 129/Sv genetic background in order to avoid variations in RGC numbers that can occur even between littermates on mixed genetic background (due to strain related differences in the numbers of RGCs in the mouse; see Williams et al., 1996), and artifactual gene cloning in RDA experiments, by amplifying genetic polymorphisms.

Anterograde and Retrograde Axon Labeling

Anterograde and retrograde DiI labeling was done as previously described by Simon and O'Leary (1992). After a 24-hour labeling period the mice were perfused, and wholemounts of the optic chiasm, contralateral SC (anterograde labeling) and retina (retrograde labeling) were examined on a BioRad 1000 confocal microscope.

Electron Microscopy

Electron microscopic counts of RGC axons in the optic nerve were performed essentially as described by Kirby et al. (1988). Optic nerves were fixed in 4% paraformaldehyde-2% glutaraldehyde in 0.1M PBS, post-fixed in 1% osmium tetraoxide in phosphate buffer, and dehydrated in an ascending methanol series followed by absolute propylene oxide. The tissue was embedded in Epon, and the cross sectional area of the nerve face was measured on semi-thin sections stained with tolulidine blue. Thin sections were mounted onto copper grids (#200 or #300, Pelco), stained with uranyl acetate followed by lead citrate, and viewed with a Zeiss HC-10 electron microscope. A photo was taken of optic nerve visible in each grid square, providing a systematic sampling (Williams et al., 1986; Kirby et al., 1988). The total axon population in each nerve was estimated by extrapolating the axon density determined for the sample area to the area of the nerve cross-section.

Representational difference analysis (RDA)

The RDA of cDNA described by Hubank and Schatz (1994) was used in this study, with modifications. mRNA was prepared using a direct method from a pool of twenty wild

type and *Brn-3.2*$^{-/-}$ retinas. The synthesis of cDNA was carried out in the presence of 150 ng of "carrier" mRNA, using Superscript cDNA synthesis kit (Gibco BRL). The carrier mRNA was transcribed in vitro from a 500bp fragment in the promoter region of Drosophila Antennapedia gene, with an artificial poly(A) sequence fused to the 3'end (J.R.B.Jr., unpublished). This sequence lacks the recognition sites for the restriction enzymes used in the generation of amplicons, and cannot be amplified in subsequent PCRs. Therefore, it does not contribute significantly to the drivers/testers. Amplicons used in this study were prepared from DpnII digested cDNA corresponding to an estimated amount of 50 ng of carrier, and 15 ng of retina-specific messages. The amount of "N-24" and "N-12" primers used in the ligation prior to the amplification of drivers was reduced to 125 and 62.5 ng, respectively, to adapt the proportion of cDNA/primer to the very low amounts of cDNA used in this study; otherwise, hybridizations were analogous to that described by Hubank and Schatz (1994). Three rounds of subtraction were performed, using an increasing excess of driver versus tester (100X, 800X, and 1000X), determined, in trial experiments, to give the best stringency conditions without leading to the loss of low copy messages.

In situ Hybridization

In situ hybridization on sections was performed as described in (Simmons et al., 1990). Non- radioactive in situ hybridization was carried out according to Wilkinson et al., (1993) with slight modifications. Riboprobes used in this study are as follows: *Brn-3.2* probe corresponds to 450 bp in the 3'UTR region, immediately following the stop codon. *Irx6*, *Olf-1*, *Olf-2*, *Neuritin*, and *ab-LIM* cRNA probes were transcribed from the plasmids containing the RDA inserts. The sequence of m-abLIM RDA product is indicated in Figure 4C. The segments of sequence in the databases corresponding to the other inserts are as follows: Irx6: Accession # AF165986 nt 432-651; Olf-1: Accession # L12147 nt 885-1179; Olf-2: Accession # U92704 nt 889-1246; Neuritin: Accession #U88958 nt 1248-2427. Ephrin A2 probe was generated by RT-PCR from P0 mouse retina, and corresponds to nucleotides 546-1095 of the published sequence (Accession # U14941). Shh probe corresponds to the full-length mouse cDNA (a gift from A. McMahon).

Retroviral Expression

Eggs of the white leghorn strain and incubated at 38^{o}C for 40 hours prior to in ovo electroporation. RCAS-EGFP or RCAS-abLIM$_{DN}$-IRES-EGFP viral DNA was injected into the developing right eye cup at Hamburger-Hamilton stage 10. A pair of parallel platinum coated electrodes spaced at 4mm were placed along the anterior-posterior axis of the embryo. A small drop of L15 was placed on the embryo and five square pulses of 50 milliseconds at

25V were applied by a T820 Electrosquare porator (BTX). At E10, the embryos were fixed with 4% paraformaldehyde, dissected, and examined with a confocal microscope (Zeiss). These injections typically resulted in the labeling of the right retina, and occasional embryos with EGFP labeling in the left (contralateral) eye or along the optic pathway, as well as those with fewer than 20 visible RGC axons were discarded.

Acknowledgements

We gratefully acknowledge Rebecca Tuttle, Aimee Ryan and Bogi Andersen for many helpful discussions and critical reading of the manuscript; Jeremy Dasen, Yasushi Nakagawa, Alex Langston and Tod Sugihara for sharing reagents; Mary Frazer for expert and dedicated help with animal care, Thomas Herman for technical assistance with sequencing, and Peggy Myer for help with illustrations. Our special thanks go to Dr. Geneviève Rougon (CNRS, France) for the generous gift of 26W sensory cell line. M.G.R. is an investigator with HHMI; R.J.M. is a recipient of NARSAD young investigator award. This work was supported by grant # 17-97-2-7016 NMTB to M.A.K., and NIH grants to D.H.R. (EY11875), D.D.M.O'L (EY07025), and M.G.R. (NS34934).

References

Bashaw, G. J., and Goodman, C. S. (1999). Chimeric axon guidance receptors: the cytoplasmic domains of slit and netrin receptors specify attraction versus repulsion. Cell *97*, 917-26.

Bertuzzi, S., Hindges, R., Mui, S. H., O'Leary, D. D. M., and Lemke, G. (1999). The homeodomain protein vax1 is required for axon guidance and major tract formation in the developing forebrain. Genes and Development *13*, 3092-105.

Birgbauer, E., Cowan, C. A., Sretavan, D. W., and Henkemeyer, M. (2000). Kinase independent function of EphB receptors in retinal axon pathfinding to the optic disc from dorsal but not ventral retina. Development *127*, 1231-41.

Brown, A., Yates, P.A., Burrola, P., Ortuño, D., Vaidya, A., Jessell, T.M., Pfaff, S.L., O'Leary, D.D.M., and Lemke, G. (2000). Topographic mapping from the retina to the midbrain is controlled by relative but not absolute levels of EphA receptor signaling. Cell *102*, 77-88.

Certel, S.J., Clyne, P..J, Carlson, J.R., and Johnson WA. (2000). Regulation of central neuron synaptic targeting by the drosophila POU protein, acj6. Development *127*, 2395-405.

Cohen, D.R., Cheng, C.W., Cheng, S.H., and Hui, C.C. (2000). Expression of two novel mouse Iroquois homeobox genes during neurogenesis. Mechanisms of Development. *91*, 317-321.

Dawid, I.B., Breen, J.J., and Toyama, R. (1998). LIM domains: multiple roles as adapters and functional modifiers in protein interactions. Trends in Genetics *14*, 156-162.

Deiner, M. S., Kennedy, T. E., Fazeli, A., Serafini, T., Tessier-Lavigne, M., and Sretavan, D. W. (1997). Netrin-1 and DCC mediate axon guidance locally at the optic disc: loss of function leads to optic nerve hypoplasia. Neuron *19*, 575-89.

Dräger, U. C. (1985). Birth dates of retinal ganglion cells giving rise to the crossed and uncrossed optic projections in the mouse. Proceedings of the Royal Society of London. Series B: Biological Sciences *224*, 57-77.

Duggan, A., Ma, C., and Chalfie, M. (1998). Regulation of touch receptor differentiation by the Caenorhabditis elegans mec-3 and unc-86 genes. Development *125*, 4107-19.

Erkman, L., McEvilly, R. J., Luo, L., Ryan, A. K., Hooshmand, F., O''Connell, S. M., Keithley, E. M., Rapaport, D. H., Ryan, A. F., and Rosenfeld, M. G. (1996). Role of transcription factors Brn-3.1 and Brn-3.2 in auditory and visual system development. Nature *381*, 603-6.

Erskine, L., Williams, S. E., Brose, K., Kidd, T., Rachel, R. A., Goodman, C. S., Tessier-Lavigne, M., Mason, C. A. (2000). Retinal ganglion cell axon guidance in the mouse optic chiasm: expression and function of Robos and Slits. J Neurosci. *20*, 4975-4982

Feldheim, D. A., Kim, Y. I., Bergemann, A. D., Frisén, J., Barbacid, M., and Flanagan, J. G. (2000). Genetic analysis of ephrin-A2 and ephrin-A5 shows their requirement in multiple aspects of retinocollicular mapping. Neuron *25*, 563-74.

Frisén, J., Holmberg, J., and Barbacid, M. (1999). Ephrins and their Eph receptors: multitalented directors of embryonic development. EMBO Journal *18*, 5159-65.

Frisén, J., Yates, P. A., McLaughlin, T., Friedman, G. C., O'Leary, D. D. M., and Barbacid, M. (1998). Ephrin-A5 (AL-1/RAGS) is essential for proper retinal axon guidance and topographic mapping in the mammalian visual system. Neuron *20*, 235-43.

Gan, L., Wang, S. W., Huang, Z., and Klein, W. H. (1999). POU domain factor Brn-3b is essential for retinal ganglion cell differentiation and survival but not for initial cell fate specification. Developmental Biology *210*, 469-80.

Gan, L., Xiang, M., Zhou, L., Wagner, D. S., Klein, W. H., and Nathans, J. (1996). POU domain factor Brn-3b is required for the development of a large set of retinal ganglion cells. Proceedings of the National Academy of Sciences of the United States of America *93*, 3920-5.

Garel, S., Marín, F., Mattéi, M. G., Vesque, C., Vincent, A., and Charnay, P. (1997). Family of Ebf/Olf-1-related genes potentially involved in neuronal differentiation and regional specification in the central nervous system. Developmental Dynamics *210*, 191-205.

Grillenzoni, N., van Helden, J., Dambly-Chaudière, C., and Ghysen, A. (1998). The iroquois complex controls the somatotopy of Drosophila notum mechanosensory projections. Development *125*, 3563-9.

Halfter, W., Deiss, S., and Schwarz, U. (1985). The formation of the axonal pattern in the embryonic avian retina. Journal of Comparative Neurology *232*, 466-80.

Hallonet, M., Hollemann, T., Pieler, T., and Gruss, P. (1999). Vax1, a novel homeobox-containing gene, directs development of the basal forebrain and visual system. Genes and Development *13*, 3106-14.

Holt, C.E. (1989). A single-cell analysis of early retinal ganglion cell differentiation in Xenopus: from soma to axon tip. Journal of Neuroscience *9*, 3123-45.

Homburger, S. A., and Fekete, D. M. (1996). High efficiency gene transfer into the embryonic chicken CNS using B-subgroup retroviruses. Developmental Dynamics *206*, 112-20.

Huang, E. J., Zang, K., Schmidt, A., Saulys, A., Xiang, M., and Reichardt, L. F. (1999). POU domain factor Brn-3a controls the differentiation and survival of trigeminal neurons by regulating Trk receptor expression. Development *126*, 2869-82.

Hubank, M., & Schatz, D.G. (1994). Identifying differences in mRNA expression by representational difference analysis of cDNA. Nucleic Acids Research *22*, 5640-5648.

Kikuchi, Y., Segawa, H., Tokumoto, M., Tsubokawa, T., Hotta, Y., Uyemura, K., and Okamoto, H. (1997). Ocular and cerebellar defects in Zebrafish induced by the overexpression of the LIM domains of the Islet-3 LIM/Homeodomain protein. Neuron *18*, 369-382.

Kirby, M.A., Wilson, P.D. and Fischer, T.M. (1988). Development of the optic nerve of the opossum (Didelphis virginiana). Developmental Brain Research *44*, 37-48.

Lisitsyn, N. A., Segre, J. A., Kusumi, K., Lisitsyn, N. M., Nadeau, J. H., Frankel, W. N., Wigler, M. H., and Lander, E. S. (1994). Direct isolation of polymorphic markers linked to a trait by genetically directed representational difference analysis. Nature Genetics *6*, 57-63.

Lundquist, E. A., Herman, R. K., Shaw, J. E., and Bargmann, C. I. (1998). UNC-115, a conserved protein with predicted LIM and actin-binding domains, mediates axon guidance in C. elegans. Neuron *21*, 385-92.

Marcus, R. C., and Mason, C. A. (1995). The first retinal axon growth in the mouse optic chiasm: axon patterning and the cellular environment. Journal of Neuroscience *15*, 6389-402.

Marcus, R. C., Shimamura, K., Sretavan, D., Lai, E., Rubenstein, J. L., and Mason, C. A. (1999). Domains of regulatory gene expression and the developing optic chiasm: correspondence with retinal axon paths and candidate signaling cells. Journal of Comparative Neurology *403*, 346-58.

McEvilly, R. J., Erkman, L., Luo, L., Sawchenko, P. E., Ryan, A. F., and Rosenfeld, M. G. (1996). Requirement for Brn-3.0 in differentiation and survival of sensory and motor neurons. Nature *384*, 574-7.

McEvilly, R. J., and Rosenfeld, M. G. (1999). The role of POU domain proteins in the regulation of mammalian pituitary and nervous system development. Progress in Nucleic Acid Research and Molecular Biology *63*, 223-55.

McLoon, S.C., and Lund, R.D. (1982). Transient retinofugal pathways in the developing chick. Experimenatal Brain Research *45*, 277-284

Morris, M. E., Viswanathan, N., Kuhlman, S., Davis, F. C., and Weitz, C. J. (1998). A screen for genes induced in the suprachiasmatic nucleus by light. Science *279*, 1544-7.

Naeve, G. S., Ramakrishnan, M., Kramer, R., Hevroni, D., Citri, Y., and Theill, L. E. (1997). Neuritin: a gene induced by neural activity and neurotrophins that promotes neuritogenesis. Proceedings of the National Academy of Sciences of the United States of America *94*, 2648-53.

Nakamura, H., and O'Leary, D. D. M. (1989). Inaccuracies in initial growth and arborization of chick retinotectal axons followed by course corrections and axon remodeling to develop topographic order. Journal of Neuroscience *9*, 3776-3795.

Niclou, S.P., Jia, L., and Raper, JA. (2000). Slit2 is a repellent for retinal ganglion cell axons. Journal of Neuroscience *20*, 4962-74.

Niwa, H., Harrison, L. C., DeAizpurua, H. J., and Cram, D. S. (1997). Identification of pancreatic beta cell-related genes by representational difference analysis. Endocrinology *138*, 1419-26.

O'Keefe, D.D., Thor, S., and Thomas, J.B. (1998). Function and specificity of LIM domains in Drosophila nervous system and wing development. Development *125*, 3915-3923.

O'Leary, D.D.M., Gerfen, C.R., and Cowan, W.M. (1983). The development and restriction of the ipsilateral retinofugal projection in the chick. Developmental Brain Research *312*, 93-109.

O'Leary, D. D. M., and Wilkinson, D. G. (1999). Eph receptors and ephrins in neural development. Current Opinion in Neurobiology *9*, 65-73.

O'Leary, D. D. M., Yates, P. A., and McLaughlin, T. (1999). Molecular development of sensory maps: representing sights and smells in the brain. Cell *96*, 255-69.

Prasad, B. C., Ye, B., Zackhary, R., Schrader, K., Seydoux, G., and Reed, R. R. (1998). unc-3, a gene required for axonal guidance in Caenorhabditis elegans, encodes a member of the O/E family of transcription factors. Development *125*, 1561-8.

Ringstedt, T., Braisted, J.E., Brose, K., Goodman, C., Kidd, T., Tessier-Lavigne, M., O'Leary, D.D.M. (2000). Slit inhibition of retinal axon growth and its role in retinal axon pathfinding and innervation patterns within the diencephalon Journal of Neuroscience *20*, 4983-4991.

Roof, D. J., Hayes, A., Adamian, M., Chishti, A. H., and Li, T. (1997). Molecular characterization of abLIM, a novel actin-binding and double zinc finger protein. Journal of Cell Biology *138*, 575-88.

Ryan, A. K., and Rosenfeld, M. G. (1997). POU domain family values: flexibility, partnerships, and developmental codes. Genes and Development *11*, 1207-25.

Seeger, M. A., and Beattie, C. E. (1999). Attraction versus repulsion: modular receptors make the difference in axon guidance. Cell *97*, 821-4.

Simmons, D. M., Voss, J. W., Ingraham, H. A., Holloway, J. M., Broide, R. S., Rosenfeld, M. G., and Swanson, L. W. (1990). Pituitary cell phenotypes involve cell-specific Pit-1 mRNA translation and synergistic interactions with other classes of transcription factors. Genes and Development *4*, 695-711.

Simon, D. K., and O'Leary, D. D. M. (1992). Development of topographic order in the mammalian retinocollicular projection. Journal of Neuroscience *12*, 1212-32.

Simon, D.K., Prusky, G.T., O'Leary, D.D.M., and Constantine-Paton, M. (1992). NMDA receptor antagonists disrupt the development of a mammalian neural map. Proc. Natl. Acad. Sci. USA, *89*,10593-10597.

Simon, D.K., Roskies, A.L., O'Leary, D.D.M. (1994). Plasticity in the development of topographic order in the mammalian retinocollicular projection. Developmental Biology *162*, 384-393.

Sornson, M. W., Wu, W., Dasen, J. S., Flynn, S. E., Norman, D. J., O'Connell, S. M., Gukovsky, I., Carrière, C., Ryan, A. K., Miller, A. P., Zuo, L., Gleiberman, A. S., Andersen, B., Beamer, W. G., and Rosenfeld, M. G. (1996). Pituitary lineage determination by the Prophet of Pit-1 homeodomain factor defective in Ames dwarfism. Nature *384*, 327-33.

Sretavan, D. W., and Kruger, K. (1998). Randomized retinal ganglion cell axon routing at the optic chiasm of GAP-43-deficient mice: association with midline recrossing and lack of normal ipsilateral axon turning. Journal of Neuroscience *18*, 10502-13.

Sze, J. Y., Liu, Y., and Ruvkun, G. (1997). VP16-activation of the C. elegans neural specification transcription factor UNC-86 suppresses mutations in downstream genes and causes defects in neural migration and axon outgrowth. Development *124*, 1159-68.

Tear, G. (1999). Neuronal guidance. A genetic perspective. Trends in Genetics *15*, 113-8.

Thanos, S., and Bonhoeffer, F. (1984). Development of the transient ipsilateral retinotectal projection in the chick embryo: a numerical fluorescence-microscopic analysis. Journal of Comparative Neurology. *224*, 407-414.

Torres, M., Gómez-Pardo, E., and Gruss, P. (1996). Pax2 contributes to inner ear patterning and optic nerve trajectory. Development *122*, 3381-91.

Tuttle, R., Braisted, J. E., Richards, L. J., O'Leary, D. D. M. (1998). Retinal axon guidance by region specific cues in the diencephalon. Development *125*, 791-801.

Wang, S. S., Tsai, R. Y. L., and Reed, R. R. (1997). The characterization of the Olf-1/EBF-like HLH transcription factor family: implications in olfactory gene regulation and neuronal development. Journal of Neuroscience *17*, 4149-58.

Wilkinson, D. G., and Nieto, M. A. (1993). Detection of messenger RNA by in situ hybridization to tissue sections and whole mounts. Methods in Enzymology *225*, 361-73.

Williams, R. W., Bastiani, M. J., Lia, B., and Chalupa, L. M. (1986). Growth cones, dying axons, and developmental fluctuations in the fiber population of the cat's optic nerve. Journal of Comparative Neurology *246*, 32-69.

Williams, R. W., Strom, R. C., Rice, D. S., and Goldowitz, D. (1996). Genetic and environmental control of variation in retinal ganglion cell number in mice. Journal of Neuroscience *16*, 7193-205.

Xiang, M. (1998). Requirement for Brn-3b in early differentiation of postmitotic retinal ganglion cell precursors. Developmental Biology *197*, 155-69.

Xiang, M., Gan, L., Li, D., Chen, Z. Y., Zhou, L., O''Malley, B. W., Jr., Klein, W., and Nathans, J. (1997). Essential role of POU-domain factor Brn-3c in auditory and vestibular hair cell development. Proceedings of the National Academy of Sciences of the United States of America *94*, 9445-50.

Xiang, M., Gan, L., Zhou, L., Klein, W. H., and Nathans, J. (1996). Targeted deletion of the mouse POU domain gene Brn-3a causes selective loss of neurons in the brainstem and

trigeminal ganglion, uncoordinated limb movement, and impaired suckling. Proceedings of the National Academy of Sciences of the United States of America *93*, 11950-5.

Xue, D., Finney, M., Ruvkun, G., and Chalfie, M. (1992). Regulation of the mec-3 gene by the C.elegans homeoproteins UNC-86 and MEC-3. Embo Journal *11*, 4969-79.

Zhu, Q., and Julien, J. P. (1999). A key role for GAP-43 in the retinotectal topographic organization. Experimental Neurology *155*, 228-42.

GenBank Accession Numbers

The GenBank accession numbers for the 3'UTR RDA product and the LIM domain of m-abLIM are, AF316037, and AF316038, respectively.

Figure Legends

Figure 1. RGC axon pathfinding defects in *Brn3.2*$^{-/-}$ mice.

(A and B) RGCs were retrogradely labeled in wild type (A) and *Brn3.2*$^{-/-}$ (B) mice by multiple injections of DiI extending across the medial-lateral axis of the rostral SC at P0 (inset). Fewer DiI labeled RGCs were found in retinal wholemounts of *Brn-3.2*$^{-/-}$ mice (B), as compared to wild type (A), indicating that fewer RGC axons have entered the SC in the mutant mice at this stage. SC, superior colliculus; d, dorsal; n, nasal; t, temporal; v, ventral.

(C) Comparison of estimated number of optic nerve axons between wild type and *Brn-3.2*$^{-/-}$ mice from embryonic day (E) 12.5 to adult. Axon counts were performed using electron micrographs of optic nerve cross sections at the indicated developmental stages.

(D and E) Axon guidance errors within E14.5 retina of *Brn-3.2* $^{-/-}$ mice revealed by small focal injections of DiI in mid-retina of wild type (D) and mutant (E) littermates. Note the wave-like appearance and aberrant trajectories (arrowhead) of some RGCs in the mutant retina (E). Cell bodies appear as bright spots, and are not all in the same focal plan.

Figure 2. Defective pathfinding of RGC axons in *Brn3.2*$^{-/-}$ mice at multiple locations in their pathway.

(A-D) RGC axon projections at the optic chiasm. In the wild type (A), DiI injection in P0 retina shows that most RGC axons extend through the ipsilateral optic nerve (ion), cross the midline (arrowhead), and enter the contralateral optic tract (cot). In *Brn-3.2*$^{-/-}$ mice (B-D) axon guidance at the midline is severely affected. Some RGC axons aberrantly project into the ipsilateral optic tract (iot, B), the contralateral optic nerve (con, B), or dorsally at the midline into the hypothalamus (arrow, C). Furthermore, in the mutant, a proportion of RGC axons do not extend past the optic chiasm (arrow, D). Photographs B-D are taken from different mutant mice.

(E and F) Montages showing the trajectories of axons from P1 wild type (E) and *Brn-3.2*$^{-/-}$ (F) retina, traced from the optic nerve (on) to the superior colliculus (SC). Focal injections of DiI were placed in nasal (n) – ventral (v) wild type retina (inset, E) and nasal – dorsal (d) mutant retina (inset, F). Note that in the mutant (F), a smaller proportion of axons found at the optic chiasm (ch) reach the SC, and some axons exhibit pathfinding defects at the chiasm (open arrowhead). Furthermore, some RGC axons in *Brn3.2*$^{-/-}$ mice stall at the dorsal diencephalon and fail to reach the SC (arrow). The rostral border of the SC is indicated with an arrowhead. t, temporal.

(G) Montage showing the dorsal midbrain of a P1 *Brn3.2*$^{-/-}$ mouse injected with DiI in nasal – dorsal retina (injection site is similar in size and location to that shown in panel F, inset).

Many RGC axons stop their extension at the dorsal diencephalon. Note that in the mutant, most RGC axons originating from dorsal retina aberrantly enter the SC from its medial aspect (arrow), rather its lateral aspect as in wild type. C, caudal; L, lateral; M, medial; SC, superior colliculus.

Figure 3. Aberrant topographic mapping of RGC axons in *Brn-3.2*$^{-/-}$ mice.
(A and B) Dorsal view of the SC after focal injection of DiI in the temporal (t) - dorsal (d) retina (insets) at P14. A dense termination zone (TZ) is present in the topographically correct site in rostral-lateral SC in the wild type (A). In the mutant (B), a similar injection reveals a lack of topography and no dense arborizations. A single RGC axon (open arrowhead) aberrantly elaborates an extensive arbor covering a substantial portion of the SC (arrows). Arrowhead indicates the rostral border of the SC. L, lateral; M, medial; n, nasal; v, ventral.
(C and D) Wholemounts of P14 wild type (C) and *Brn-3.2*$^{-/-}$ (D) retina after focal injection of DiI in rostral-medial superior colliculus (insets). In the wild type (C), most DiI labeled RGCs are found in the correct position (arrow). However, in the mutant (D), DiI labeled RGCs are more or less uniformly distributed, indicating a lack of topography in the retinocollicular projection. C, caudal; d, dorsal; L, lateral; n, nasal; t, temporal; v, ventral.

Figure 4. Expression patterns of molecular markers and morphology of the retina, optic chiasm and superior colliculus of wild type and *Brn-3.2*$^{-/-}$ mice.
(A-D) Horizontal sections of E15.5 retina were hybridized with *Netrin-1* (A-B) and *DCC* (C-D) riboprobes. Morphology and expression levels of markers are normal in *Brn-3.2*$^{-/-}$ mice (B and D). Arrow marks the optic disk. n, nasal; t, temporal.
(E and F) Expression domain of *Shh* in ventral diencephalon of *Brn-3.2* gene-deleted mice (E) compared to their wild type littermates (F); (ventral view). Wholemeount in situ hybridization was performed on brains of 11.5-day old embryos dissected with the optic nerves attached. Brackets in E and F show the expression domain of Shh. a, anterior; p, posterior; oc, optic cup.
(G and H) Rostrocaudal gradients of Ephrin A2 mRNA in wild type and *Brn-3.2*$^{-/-}$ superior colliculus at P0, as revealed by in situ hybridization of sagittal sections. a, anterior; p, posterior. Scale bar: 200 μm in (A-D); 500 μm in (E and F); 150 μm in (G and H)

Figure 5. Analysis and characterization of representational difference products.
(A) Southern blot analysis of a sample of RDA products for initial assessment of differential expression in the mutant and wild type mice. After cloning of third difference products, the inserts were purified, labeled with ^{32}P and hybridized to Southern blots consisting of 250 ng

of either +/+ and -/- driver. C# 91 and C#70: clones with no matching sequences in the databases.

(B) Classification of genes according to their homolgy to sequences published in the databases. The degree of identity at the nucleotide level is indicated. Five genes particularly relevant to axon pathfinding were tested for differential expression by Southern blot and/or in situ hybridization analysis. ND, not done.

(C) Amino acid dentities between human and mouse abLIM and unc-115. Lim domains are indicated by brackets. *C. Elegans* lim #1,2 and 3 best align with abLIM lim# 1, 3, and 4, respectively. Note the conservation in the linker regions between mouse and human proteins.

(D) Schematic diagram of unc-115, human abLIM proteins and the bicistronic construct abLIM$_{DN}$-IRES-EGFP encompassing the LIM domain including all 4 LIM motifs of abLIM.

(E-H) In situ hybridization of sagittal sections of wild type E15.5 mouse midbrain (E), spinal cord (F), dorsal root ganglia (G), and thymus (H). a, anterior; p, posterior; drg, dorsal root ganglia; th, thymus; h, heart. Scale bar = 500 μm.

Figure 6. Differential expression of *Irx6*, *Olf-1*, *Olf-2*, *m-abLIM*, and *neuritin* in vivo.

(A-J) Riboprobes transcribed from plasmids containing the RDA inserts were hybridized to sagittal sections of retina from wild type and mutant littermates at E15.5. Note more subtle decrease in the levels of *Olf-2* mRNA in the *Brn-3.2*$^{-/-}$ retina (H), as compared to a dramatic loss of message levels for the other candidates analyzed (F,G,I,J). ICL, inner cell layer; pe, pigmented epithelium. Scale bar = 200 μm.

Figure 7. Temporal pattern of expression of *Brn-3.2*, *Irx6* and *m-abLIM* in wild type mouse embryos.

(A-L) Adjacent sections of E12.5, E13.5 , E15.5 and E17.5 mouse retina were hybridized to *Brn-3.2 Irx6*, and *m-abLIM* riboprobes. Note the sequence of initial detectable expression of *Irx6* and *abLIM* during development. ICL, inner cell layer; pe, pigmented epithelium. Scale bar = 200 μm.

Figure 8. RGC pathfinding defects in chick retinas transfected with Expression of abLIM$_{DN}$.

(A-C) Wholemounted retina of E10 chick embryos transfected with RCAS-EGFP (A) or RCAS-abLIM$_{DN}$-IRES-EGFP (B and C). Retinal ganglion cells (RGC) and RGC axons labeled with EGFP are clearly visible and appear white. The optic fissure is not shown, but is located to the lower left of each panel.

(A) Axons from RGCs expressing EGFP pathfind directly to the optic fissure and have straight parallel trajectories. The transfected cell bodies in this example are not shown, but are located to the upper right of the panel.

(B-C) RGCs expressing abLIM$_{DN}$-IRES-EGFP (arrow) extend axons which, in contrast to controls, have a wave-like trajectory and appear to be more highly fasciculated. (C) In the most severe cases, several fascicles have very aberrant trajectories and make significant turns away from the optic fissure (arrowhead).

(D and E) Views of wholemounts of the ventral dienencephalon showing the optic chiasm in E10 chick embryos transfected in the right retina with either RCAS-EGFP (D) or RCAS-abLIM$_{DN}$-IRES-EGFP (E). Anterior is towards the bottom. In the control RCAS-EGFP transfected case, (D) a large fascicle extends from the retina, through the ipsilateral optic nerve (ion), across the chiasm (ch), and into the contralateral optic tract (cot). No axons are visible in the ipsilateral optic tract (iot, outlined) or the contralateral optic nerve (con, outlined). In the RCAS-abLIM$_{DN}$-IRES-EGFP transfected case, (E) RGC axons course through the ipsilateral optic nerve (ion), cross the chiasm (ch), and enter the contralateral optic tract (cot). In addition, a substantial number of RGC axons aberrantly enter the ipsilateral optic tract (iot, arrow) as well as the contralateral optic nerve (con, arrowhead). There are no labeled cells in the contralateral (left) eye (not shown).

(F) Wholemounted left retina of an E10 chick embryo transfected with RCAS-abLIM$_{DN}$-IRES-EGFP in the right retina. No labeled cell bodies are present in the left retina. RGC axons originating in the right retina, contralateral to the retina shown, extend a large fascicle across the optic chiasm and aberrantly into the contralateral optic nerve. The fascicle enters the left eye at the optic fissure (arrow). The RGC axons originating in the right retina extend for several millimeters within the left retina where they end in growth cones (not shown). Scale bar = 500 μm.

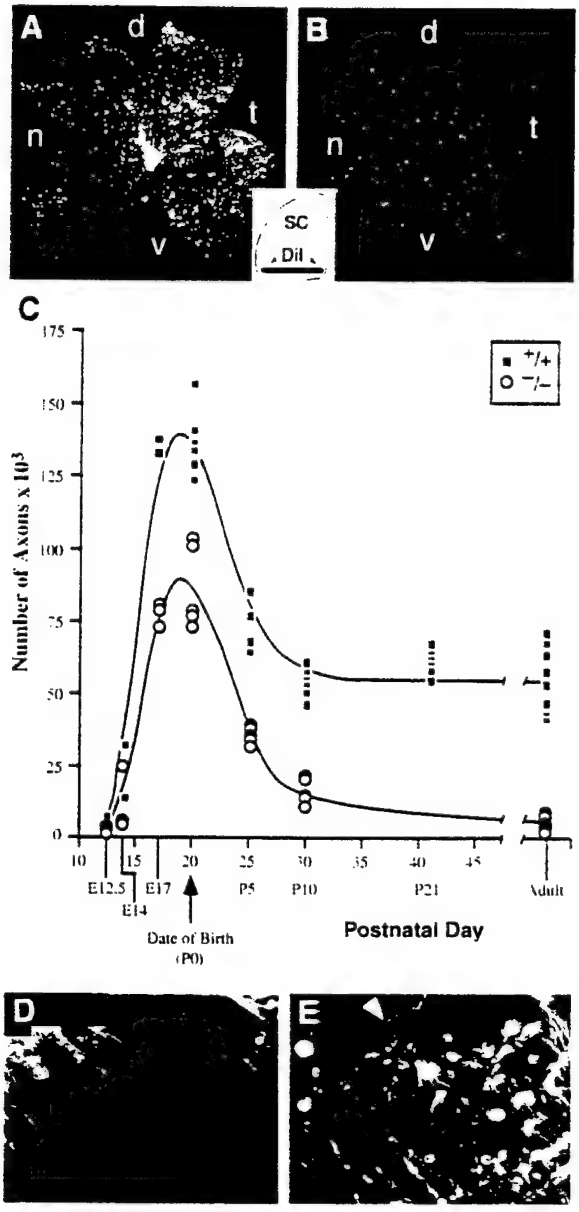
A
d
t
n
v
SC
DiI
B
d
t
n
v
C
+/+
−/−
Number of Axons x 10³
175
150
125
100
75
50
25
0
10
15
20
25
30
35
40
45
E12.5
E14
E17
P5
P10
P21
Adult
Date of Birth
(P0)
Postnatal Day
D
E

Fig. 1

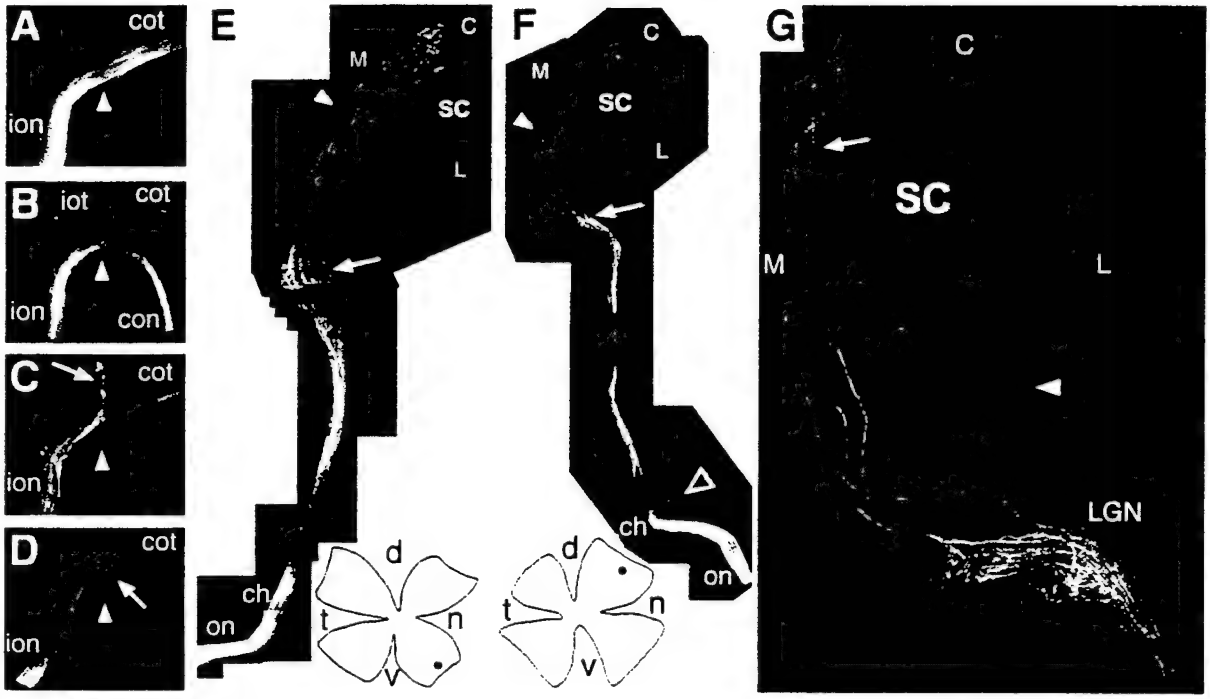
A
cot
ion
B
iot
cot
ion
con
C
cot
ion
D
cot
ion
E
C
M
SC
L
ch
on
d
t
n
v
F
C
M
SC
L
ch
on
d
t
n
v
G
C
SC
M
L
LGN

Fig. 2

A
TZ
M
L
B
M
L
D
d
n
t
v
C
d
n
t
v

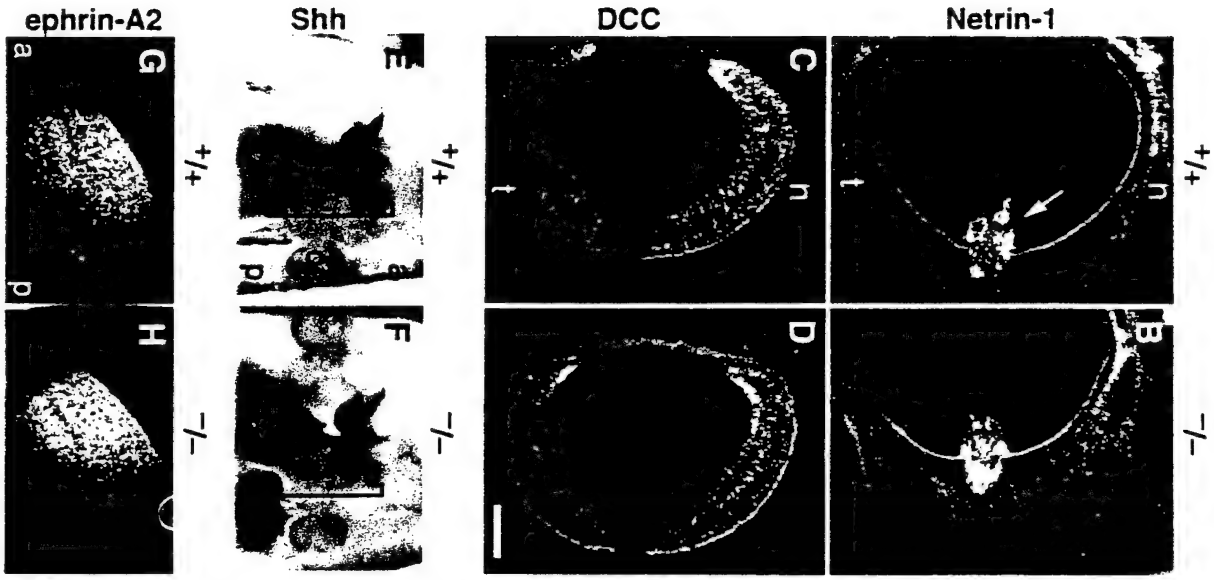

Fig. 4

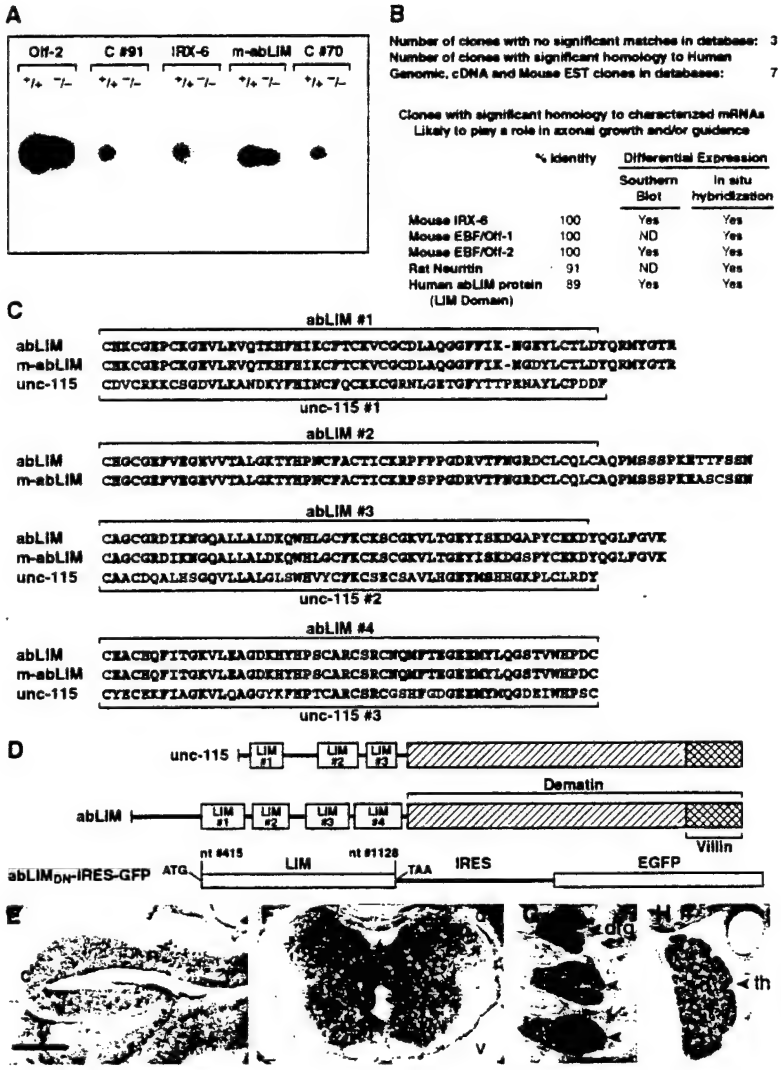
A
Off-2
C #91
IRX-6
m-abLIM
C #70
+/+ −/−
B
Number of clones with no significant matches in database: 3
Number of clones with significant homology to Human Genomic, cDNA and Mouse EST clones in databases: 7
Clones with significant homology to characterized mRNAs Likely to play a role in axonal growth and/or guidance
% identity
Differential Expression
Southern Blot
In situ hybridization
Mouse IRX-6 100 Yes Yes
Mouse EBF/Olf-1 100 ND Yes
Mouse EBF/Olf-2 100 Yes Yes
Rat Neurtin 91 ND Yes
Human abLIM protein (LIM Domain) 89 Yes Yes
C
abLIM #1
abLIM CHKCGEPCKGEVLEVQTKHFHIECFTCEVCGCDLAQGGFFIK-NGEYLCTLDYQRMYGTR
m-abLIM CHKCGEPCKGEVLEVQTKHFHIECFTCKVCGCDLAQGGFFIK-NGDYLCTLDYQRMYGTR
unc-115 CDVCRKKCSGDVLKANDKYFHINCFQCKKCGRNLGETGFYTTPRNAYLCPDDF
unc-115 #1
abLIM #2
abLIM CHGCGKFVEGEVVTALGKTYHPHCFACTICKRPFPPGDRVTFNGRDCLCQLCAQPMSSSPKETTFSEN
m-abLIM CHGCGEFVEGEVVTALGKTYHPHCFACTICKRPSPPGDRVTFNGRDCLCQLCAQPMSSSPKEASCSEN
abLIM #3
abLIM CAGCGRDIKNGQALLALDKQWHLGCFKCKSCGKVLTGEYISKDGAPYCKKDYQGLFGVK
m-abLIM CAGCGRDIKNGQALLALDKQWHLGCFKCKSCGKVLTGEYISKDGSPYCKKDYQGLFGVK
unc-115 CAACDQALESGQVLLALGLSWHVYCFKCSECSAVLHGEYMSHHGKPLCLRDY
unc-115 #2
abLIM #4
abLIM CHACHQFITGKVLEAGDKHYHPSCARCSRCHQPFTGEEMYLQGSTVWHPDC
m-abLIM CHACHQFITGKVLEAGDKHYHPSCARCSRCHQPFTGEEMYLQGSTVWHPDC
unc-115 CYECKKFIAGKVLQAGGYKFHPTCARCSRCGSHFGDGEEMYMQGDEIWHPSC
unc-115 #3
D
unc-115
LIM #1
LIM #2
LIM #3
abLIM
LIM #4
Dematin
Villin
abLIM$_{DN}$-IRES-GFP
nt #415
nt #1128
ATG
LIM
TAA
IRES
EGFP
E
F
G
H
dg
th
v

Fig. 5

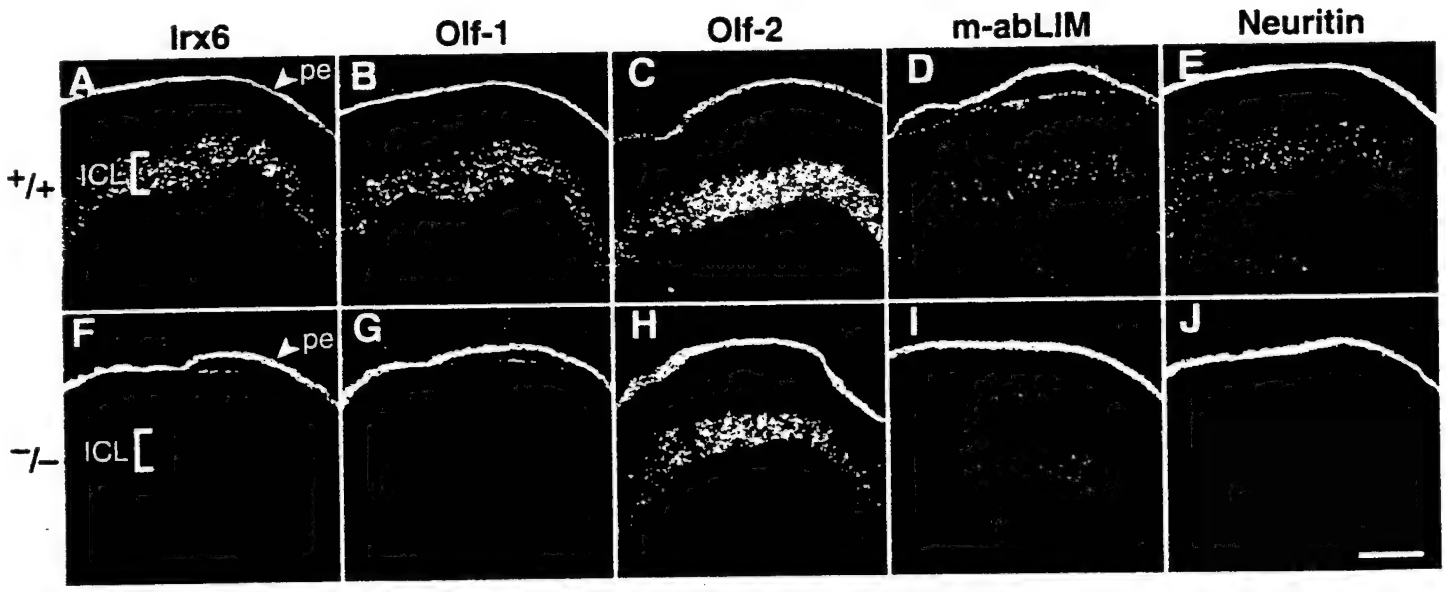

Fig. 6

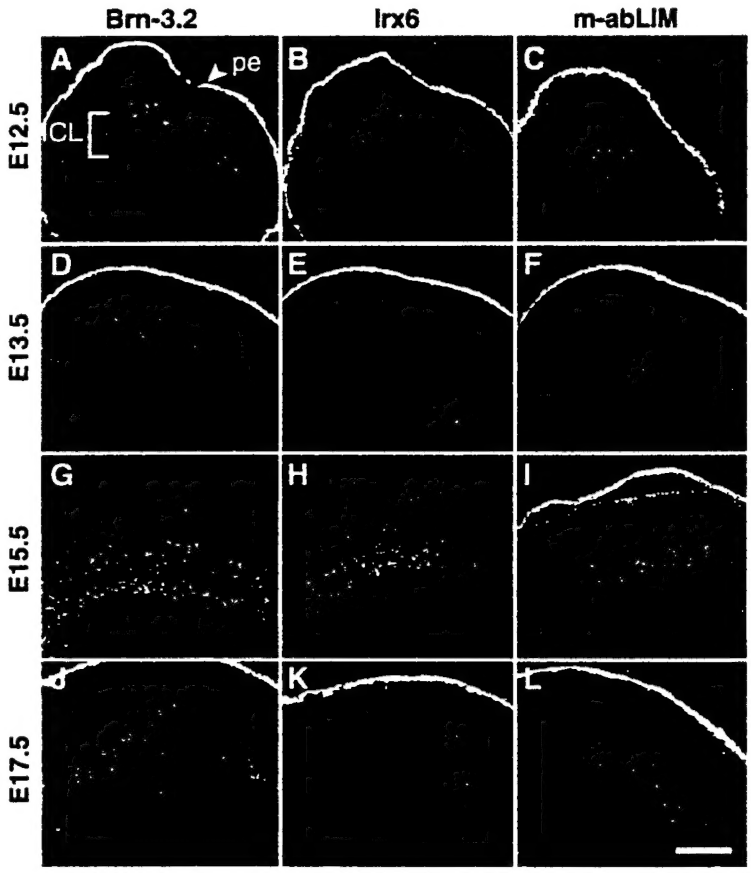

Fig. 7

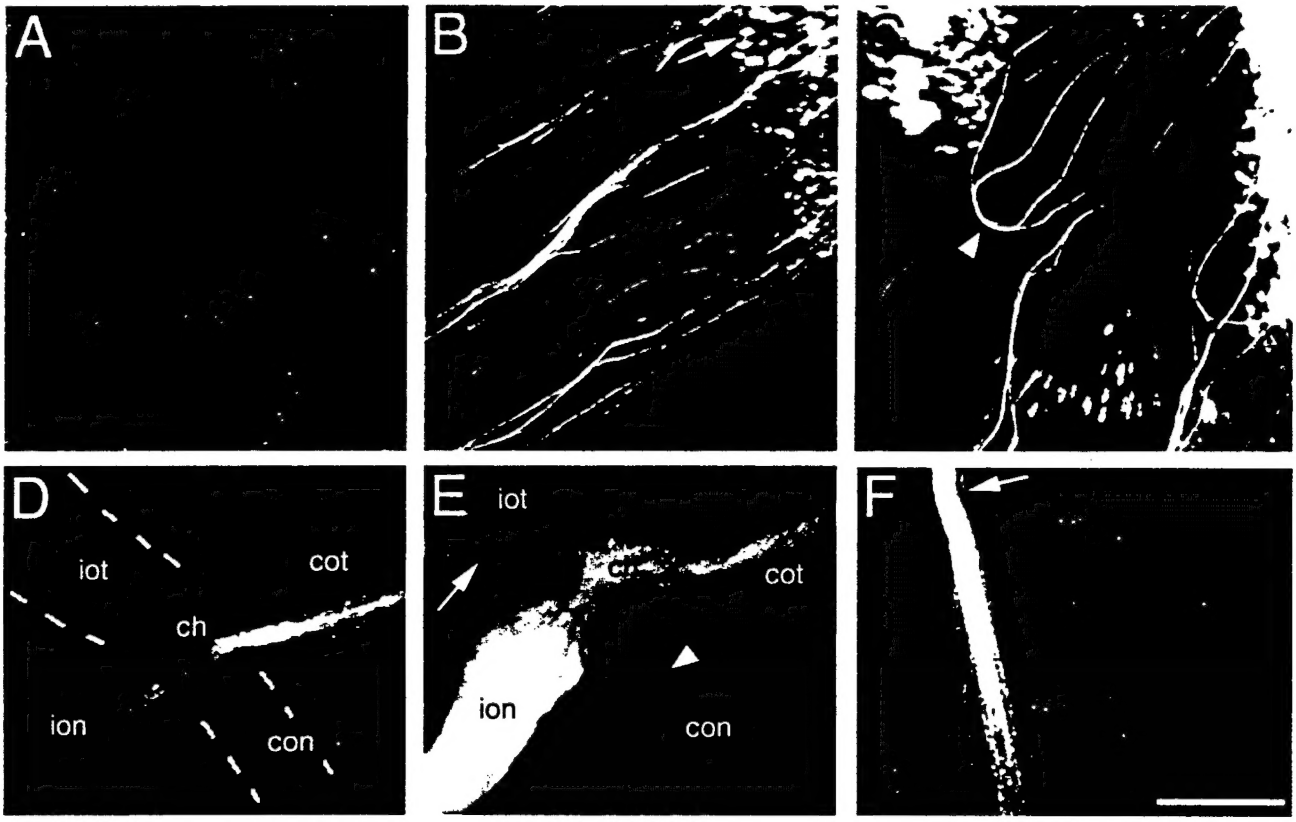

Fig. 8

BIBLIOGRAPHY

Determinants of coactivator LXXLL motif specificity in nuclear receptor transcriptional activation. McInerney E.M., Rose D.W., Flynn S.E., Westin S., Mullen T.M., Krones A., Inostroza J., Torchia J., Nolte R.T., Assa-Munt N., Milburn M.V., Glass C.K., Rosenfeld M.G. ***Genes & Development.*** 12:3357-68 (1998).

Bermingham J.R., Shumas S., Whisenhut T.R., O'Connell S.M., Rosenfeld M.G. and Scherer S.S. A modification of representational difference analysis applied to the isolation of forskolin-regulated genes from Schwann cells. ***J. Neurosci Res.*** (in press).

Erkman, L., P.A. Yates, T. McLaughlin, R.J. McEvilly, T. Whisenhunt, S.M. O'Connell, A.L. Krones, M.A. Kirby, D.H. Rapaport, J.R. Bermingham, D.D.M. O'Leary, and M.G. Rosenfeld. Cell autonomous regulation of axon pathfinding in the vertebrate visual system by a Brn-3-2-dependent transcriptional program. ***Neuron*** (in press).

PERSONNEL ON PROJECT

Sung Hee Baek – Postdoctoral Fellow

John Bermingham – Postdoctoral Fellow

Catherine Carriere – Postdoctoral Fellow

Chrissa Kioussi – Assistant Project Scientist

Forrest Liu – Staff Research Associate

Robert McEvilly – Assistant Project Scientist

Wei Zhang – Postdoctoral Fellow